Axial anomaly and fluctuation effects in the inhomogeneous chiral phase

Ryo Yoshiike
Department of Physics, Kyoto University

January 26, 2018

Abstract

One of the most interesting problems in nuclear physics is understanding the QCD phase diagram in the temperature-density plane. There have been discussed the various phases. Recently, from the studies of the effective models, it was suggested that there exists the inhomogeneous chiral phase, where the order parameter described by the quark condensates might depend on the position. In this thesis, we focus on one of the inhomogeneous configurations of the quark condensates, called dual chiral density wave (DCDW). In the presence of an external magnetic field, it is known that DCDW is drastically enhanced. Then the energy spectrum of the lowest Landau level becomes asymmetric about zero and gives rise to the anomalous quark number. This phenomenon is closely related to axial anomaly. The main goal of this thesis is to see the various peculiar properties brought by axial anomaly and the fluctuation effects by using the Nambu-Jona-Lasinio model. First, we study the response of quark matter in the DCDW phase to the weak external magnetic field. We see that the spectral asymmetry also gives rise to the spontaneous magnetization. This mechanism may be one of candidates for the origin of the strong magnetic field in pulsars and/or magnetars. Secondly, we consider the effect of the change of the current quark mass on the DCDW phase in the QCD phase diagram, and discuss the properties of the phase transition using the generalized Ginzburg-Landau expansion. The strong external magnetic field extends this phase over the low chemical potential region even if the current quark mass is finite. This implies that the existence of this phase can be explored by the lattice QCD simulation. Thirdly, in 1+1 dimensions, we shall discuss axial anomaly and nesting from two different points of view: one is the inhomogeneous chiral phase transition and the other is the Fulde-Ferrel-Larkin-Ovchinnikov (FFLO) state in superconductivity, which are closely related to each other by way of duality. It is shown that axial anomaly leads to a particular kind of the FFLO state within the two dimensional Nambu-Jona Lasinio model, where axial anomaly is manifested in a different mode. Nesting is a driving mechanism for both phenomena, but its realization has different features. We reconsider the effect of nesting in the context of duality. Fourthly, we consider the effect of fluctuations on the inhomogeneous chiral phase since above studies is based on the mean-field approximation. In the absence of the magnetic field, the effect of fluctuations is discussed around the phase boundary between the inhomogeneous chiral phase and the chiral-restored phase. It is argued that a singular behavior in the thermodynamic quantities should have phenomenological implications for the inhomogeneous chiral transition. In the presence of the magnetic field, the inhomogeneous chiral phase becomes stable against the fluctuations of the Nambu-Goldstone modes compared to the case of the absence of the magnetic field.

Contents

Chapter 1

Introduction

Among the four interactions existing in nature, the fundamental theory for describing the strong interaction is called quantum chromodynamics (QCD) [1, 2, 3]. QCD is the SU(3) gauge theory, and the Lagrangian renders,

$$\mathcal{L} = \overline{\psi}\left(i\not{D} - m\right)\psi - \frac{1}{4}F^a_{\mu\nu}F^{\mu\nu}_a. \tag{1.0.1}$$

Although the Lagrangian is very simple, it is known that rich phenomena appear in QCD, for example, color confinement, spontaneous breaking of chiral symmetry, color superconductivity and quark-gluon plasma (QGP). Nowadays it is one of the most important problems in nuclear physics to understand the QCD phase diagram in the temperature (T)-density plane [4]. The QCD phase diagram is also very important from a phenomenological point of view. The QGP phase appearing in the high T region is considered to be realized in heavy ion collision experiments [5]. On the other hand, neutron stars can be considered as an realistic object of quark matter in the low T and the high chemical potential (μ) regions [6, 7]. Even though the radius is about 10 km by observation, ones with the mass up to twice the solar mass have been observed [8, 9]. The equations of state for neutron stars have been extensively studied from the QCD phase diagram [10, 11].

As an analytical study of QCD, a perturbative method can be considered. However, from the non-Abelian nature of the SU(3) gauge theory, the gluonic coupling constant increases and the perturbative calculation fails in the low energy region while QCD has asymptotic freedom in the high energy limit [2, 3]. As a method to analyze QCD non-perturbatively, the lattice QCD has been developed [12, 13]. In the high density region, however, there arises a difficulty in numerical calculation called the sign problem [14, 15], and the calculation does not work well there. For this reason, analysis of high density regions has been carried out using various effective models rather than directly calculating QCD Lagrangian. As one of the effective models, the Nambu-Jona-Lasinio (NJL) model [16] is well known when considering effective theory of low energy, focusing on chiral symmetry. Chiral symmetry is spontaneously broken in the vacuum, and it is thought that chiral symmetry is restored at high T or high density region. The NJL model is an effective model to describe the chiral phase transition in the finite T or finite density region [17, 18].

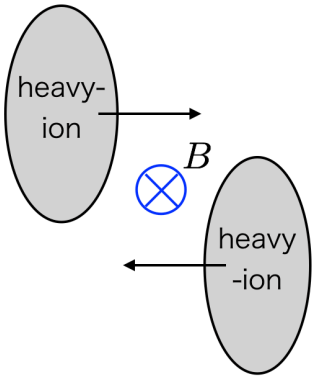

Figure 1.1: Schematic picture of the noncentral heavy-ion collision in the center-of-mass system. The charged currents make the vertical magnetic field to the transverse plane of the collision.

Research on QCD in the magnetic field is also one of the subjects which has become very interesting in recent years in experiments, observation and theory. In the noncentral heavy-ion collision, it is expected that the two charged currents make the magnetic field $B \sim 10^{19}$G [19]. Fig. 1.1 schematically shows that the heavy-ions are regarded as the charged currents, which make the magnetic field in the noncentral collision. Therefore the analysis of the behavior of quark matter in the magnetic field is essential to understand the experimental data. Furthermore, neutron stars called magnetars have a magnetic field of about 10^{15}G at the surface [20, 21]. Therefore the influence on the internal structure due to the magnetic field can not be ignored. Also from the theoretical viewpoint, some phenomena have been actively discussed; magnetic catalysis gives rise to the enhancement of chiral symmetry breaking when B is applied [22, 23, 24]. Magnetic inhibition [25, 26] makes chiral symmetry breaking weaker at high T. The chiral magnetic effect (CME) induces the electric current flows in quark matter in a strong magnetic field [27].

Recently, analysis of the effective models have suggested the possible existence of a new phase called the inhomogeneous chiral phase (iCP) around the conventional chiral phase transition line [28, 29, 30, 31]. From the analysis based on the Schwinger-Dyson equation within QCD, it has been also shown that there is a region of iCP [32]. In iCP, the chiral condensates, which are the order parameters characterizing the chiral phase transition have spatially modulating structures. As the form of the inhomogeneous condensates, we often use the two kinds of the one-dimensional modulation,

$$\Delta(z)e^{i\theta(z)} \equiv \langle\bar{\psi}\psi\rangle + i\langle\bar{\psi}i\gamma^5\tau_3\psi\rangle \sim \begin{cases} \frac{2m\sqrt{\nu}}{1+\sqrt{\nu}}\mathrm{sn}\left(\frac{2mz}{1+\sqrt{\nu}}\right), \\ me^{iqz}. \end{cases} \tag{1.0.2}$$

The upper form, called real kink crystal (RKC), is real and only Δ oscillates. For the lower one, called dual chiral density wave (DCDW), the phase θ spatially changes but the amplitude Δ is constant.

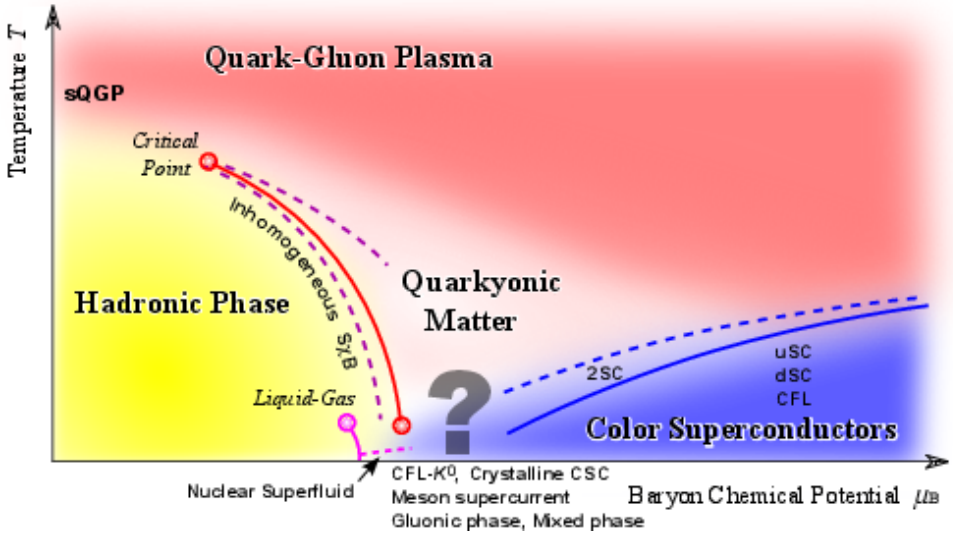

Figure 1.2: QCD phase diagram in the T-μ plane. (The figure is taken from Ref. [4].)

The systems with the nonuniform order paramters have been studied for a long time in the condensed matter physics; spin density wave [33, 34] and charge density wave [35] in low dimensional matter, and the FFLO state of type-II superconductivity [36, 37, 38] are some examples. Also in QCD, the nonuniform structure in the color superconducting phase [39] or in the quarkionic phase [40] have been proposed. iCP, which is the subject of this paper, shows many similar features with these nonuniform systems.

So far, various analyses about iCP has been done, for example, with the current mass [41], in the 3-flavor system [42], in the system that breaks isospin symmetry [43], with the vector type interaction [44] and in the presence of the magnetic field [45, 46]. In particular, the properties of iCP drastically change due to chiral anomaly when external magnetic field is applied. The effect of the magnetic field has been first discussed by Frolov et al. for the DCDW phase [45]. They have found that the spatial direction of the wavevector $\boldsymbol{q}$ is favored to be parallel to the magnetic field, and the domain of the DCDW phase is much extended in the QCD phase diagram. In Ref. [46], these features arises from some topological effect through spectral asymmetry of the quark energy; quarks exhibit an interesting feature in the presence of the magnetic field and the energy spectrum becomes asymmetric about zero. Such spectral asymmetry gives rise to the anomalous particle number [47, 48], which is closely related axial anomaly [46, 49].

In the following, we explain the motivation of our works. First, we would like to elucidate the magnetic properties inherent in iCP, especially DCDW, and their phenomenological implications. Since iCP appears in the middle to high density region of the QCD phase diagram, it is expected that quark matter exists in iCP inside of neutron stars. Then magnetic field becomes important. Although it is known from the observation that magnetars have the huge magnetic field $\sim \mathcal{O}(10^{15})$G at the surface [20, 21], there is no clear theory explaining the origin of this magnetic field. As a candidate of the origin, amplification of the magnetic field

by the dynamo mechanism, magnetorotational instability or the hypothesis of the fossil magnetic field has been proposed so far from the macroscopic point of view. Although numerical simulations have been actively performed, no definite conclusions have been obtained. On the other hand, spontaneous magnetization due to the spin alignment of quarks is considered by analogy of electron gas from the microscopic theory [46]. However, the region where the spontaneous magnetization appears is limited to the low density compared to the inner of neutron star. As another mechanism, it has been proposed that axial anomaly acting on the parallel layer of the pion domain wall produces magnetization in nuclear matter [49, 50]. We study magnetic properties of the DCDW phase to reveal *spontaneous magnetization* in the DCDW phase to suggest a new microscopic origin of the strong magnetic field in neutron stars [51].

Next, we inquire into the observability of iCP by way of the lattice QCD simulations. Theoretically the lattice QCD simulations have been done for the deconfinement transition or the chiral phase transition under the magnetic field with various strength. The QCD phase diagram in the finite μ region has been explored by the lattice QCD simulation, but its availability is severely restricted due to the sign problem. Some methods to overcome the sign problem have been proposed: for example the Taylor expansion method [52, 53], the reweighting method [54, 55, 56, 57], the canonical approach [58, 59, 60, 61], the analysis of Lee-Yang zero in QCD [62, 63, 64] and the analytic continuation method from imaginary chemical potentials [65, 66, 67, 68, 69]. However, these methods are limited in the high T region, $\mu/T < 1$ region. As recent approaches to evade the sign problem, the complex Langevin method [70, 71, 72] and Lefschetz-thimble path-integral method [73, 74, 75] have been studied. These methods are not limited about the applicable region in principle, while they have not been applied on QCD yet. In the external magnetic field, the DCDW phase is remarkably developed in the low μ region except for $\mu = 0$. Therefore it seems that we can get a direct observation of DCDW by a lattice QCD simulations. However, the effect of the current mass should be also considered to discuss a realistic case. It is known that the current mass disfavor the appearance of iCP without the magnetic field [28, 41]. Once the current mass is turned on, a competition arises between the positive effect on the DCDW phase by the magnetic field and the negative effect by the current mass. If the DCDW phase with the current mass develops in the low μ region, we may have a chance to observe this phase by the lattice QCD simulation [76].

Secondly, we would like to clarify the mechanism leading to iCP in terms of many-body dynamics. At the same time, we point out the common basic concepts with condensed matter physics. It is known that nesting plays an important role for the appearance of iCP [29]. Moreover, axial anomaly also plays an important role in some situations, e.g. in the presence of the magnetic field. We shall figure out the characteristic roles of axial anomaly and nesting and their interplay in the context of iCP. We consider iCP in 1+1 dimensions by using the effective models to clearly see their interplay. Manifestation of nesting or axial anomaly should be a common feature of iCP in any dimension, since these concepts are based on geometry of the Fermi surface and chiral symmetry itself. We utilize the duality transformation for this purpose, which is available in 1+1 dimensions. Thies has pointed out that there is a duality relation between chiral transition and a kind of superconductivity

[77, 78]. Then μ can be regarded as an effective magnetic field. It is well known in condensed matter physics that the Bardeen-Cooper-Schrieffer (BCS) state changes to the another state, called the Fulde-Ferrell-Larkin-Ovchinnikov (FFLO) state, beyond the lower critical field, where the the Cooper pair condensate is spatially modulating [36, 37, 38, 79, 80, 81, 82]. Thus inhomogeneous chiral transition at finite density is mapped into the problem of the FFLO state in a kind of superconductivity [83].

Finally, we would like to elucidate the effects of the fluctuations on the mean-field around the transition point as well as inside iCP. Although so far most discussions have been restricted to the mean-field level, we need the analysis beyond the mean-field level to know iCP in the more realistic situation. Recent studies focus on the stability of iCP against such fluctuations [84, 85]. According to the studies, the NG modes have the spatially anisotropic dispersion relation. However, if we consider the similar NG mode in the presence of the magnetic field, the isotropy of the system is already violated by the magnetic field. Therefore it is expected that stability of the iCP changes. Furthermore we focus on another interesting aspect of the fluctuations near the phase boundary. A general theory for the inhomogeneous phase transition has been first presented by Brazovskii [86] at finite T. A similar issue has been discussed by Dyugaev [87] at $T = 0$ in the context of pion condensation. They have taken into account the interactions among the fluctuations beyond the Gaussian approximation. One of the remarkable findings is the change of the order of the phase transition stemming from the fluctuation effects; the second-order phase transition within the MFA is changed to the first-order one (sometimes termed the *fluctuation-induced first-order phase transition*). For the inhomogeneous chiral transition, a heuristic argument about the fluctuation-induced first-order phase transition is presented [88]. Therefore we study the nature of the inhomogeneous phase transition around the R-boundary by looking into both quantum and thermal fluctuations of quark-antiquark pairs or quark particle-hole pairs in the chiral-restored phase.

In the following, the outline of this thesis is shown. In Chapter 2, we briefly survey the studies about the inhomogeneous chiral phase up to now. In Chapter 3, we discuss the magnetic properties of quark matter in the DCDW phase and show the possibility of spontaneous magnetization within the two-flavor NJL model. In Chapter 4, we describe the region of the DCDW phase by the generalized Ginzburg-Landau expansion [89] when the both effect of the magnetic field and the current quark mass are considered. In Chapter 5, we discuss the interplay of nesting or anomaly between iCP and the FFLO state in superconductivity by utilizing the duality relation in 1+1 dimensions. In Chapter 6, we first show the stability of the DCDW phase in the presence of the magnetic field. Next, the change of the order of the phase transition due to the thermal or temperature fluctuation effect is discussed in the absence of the magnetic field. Finally in Chapter 7, we summarize some conclusions of this thesis.

Chapter 2

Brief survey about the inhomogeneous chiral phase

2.1 Case of the absence of the magnetic field

In this section, we review the method to obtain a general structure of the chiral condensate that allows spatial modulation by using the $1+1$ dimensional Nambu-Jona-Lasinio model (NJL_2 model) within the mean-field approximation (MFA) [90, 30]. From the Marmin-Wagner-Coleman (MWC) theorem (for detail see Appendix A), the structure in $1+1$ dimensions is unstable due to the fluctuations. However, the contribution of the quark loop representing the effect of the fluctuation takes a factor of $1/N_c$ compared with the contribution of the tree level. Therefore, when considering in the limit of large N_c, it becomes possible to avoid the MWC theorem. Next, we review Ref. [29]: whether or not the dual chiral density wave (DCDW) phase survives within the $1+3$ dimensional NJL model.

2.1.1 1+1 dimensions

When there is a spatially modulating order parameter, the simplest way to find its form is to construct an effective potential while leaving the unknown order parameter $\Delta(x)$ and solve a gap equation,

$$\frac{\delta V(\Delta(x))}{\delta \Delta(x)} = 0. \tag{2.1.1}$$

The concrete form of $\Delta(x)$ can be determined from the gap equation. This method seems simple, but the gap equation cannot be always solved. In this section, first, some assumption about the structure of $\Delta(x)$ is put and we find the eigenfunction by solving the Schrödinger equation using that structure. Next, we check whether the obtained eigenfunction is consistent with the assumed structure of the order parameter. Thus we can finally get the self-consistent solution by repeating the cycle of checking.

The Lagrangian of the NJL_2 model for 1-flavor case renders,

$$\mathcal{L}_{\mathrm{NJL}_2} = \bar{\psi} i \partial\!\!\!/ \psi + G\left[\left(\bar{\psi}\psi\right)^2 + \left(\bar{\psi} i\gamma^5 \psi\right)^2\right], \tag{2.1.2}$$

where the γ matrices are represented by the Pauli matrices, $\gamma^0 = \sigma^1, \gamma^1 = -i\sigma^2, \gamma^5 = \sigma^3$. Using MFA, the Lagrangian can be,

$$\mathcal{L}_{\mathrm{MF}} = \bar{\psi}\left[\, i\,\partial\!\!\!/ - (\sigma + i\gamma^5\pi)\right]\psi - \frac{\sigma^2+\pi^2}{4G}, \tag{2.1.3}$$

where σ and π represent the mean fields, $\sigma \equiv -2G\langle\bar{\psi}\psi\rangle, \pi \equiv -2G\langle\bar{\psi} i\gamma^5\psi\rangle$. Furthermore σ and π are order parameters about chiral symmetry and can have spatial modulation. In the following, we redefine the order parameters as,

$$\Delta(x) \equiv \sigma(x) - i\pi(x). \tag{2.1.4}$$

Using the new order parameter $\Delta(x)$, the effective potential within MFA can be rewritten as,

$$V(\Delta(x)) = \frac{1}{4G\mathcal{V}}\int d^2x|\Delta(x)|^2 + \frac{iN_c}{\mathcal{V}}\mathrm{lnDet}\left[i\partial\!\!\!/ - \frac{1}{2}(1-\gamma^5)\Delta(x) - \frac{1}{2}(1+\gamma^5)\Delta^*(x)\right], \tag{2.1.5}$$

where $\mathcal{V}$ denotes the space-time volume. From the Lagrangian, the Schrödinger equation can be obtained as,

$$H\psi = E\psi, \tag{2.1.6}$$

where the Hamiltonian takes the form,

$$\begin{aligned} H &\equiv -i\gamma^5\frac{d}{dx} + \gamma^0\left(\frac{1}{2}(1-\gamma^5)\Delta(x) - \frac{1}{2}(1+\gamma^5)\Delta^*(x)\right) \\ &= \begin{pmatrix} -i\frac{d}{dx} & \Delta(x) \\ \Delta^*(x) & i\frac{d}{dx} \end{pmatrix}. \end{aligned} \tag{2.1.7}$$

The differential equation with this structure is known as the Bogoliubov-de Gennes equation which has been discussed in the context of superconductivity [91, 92]. On the other hand, the gap equation is obtained from the variation of Eq. (2.1.5) about $\Delta^*(x)$,

$$\Delta(x) = -2iGN_c\frac{\delta}{\delta\Delta^*(x)}\mathrm{lnDet}\left[i\partial\!\!\!/ - \frac{1}{2}(1-\gamma^5)\Delta(x) - \frac{1}{2}(1+\gamma^5)\Delta^*(x)\right]. \tag{2.1.8}$$

To make the gap equation possible to solve with some assumption, we use the diagonal resolvant and transform the gap equation into the form of nonlinear Schrödinger equation (NLSE) obtained in Ref. [90]. NLSE takes the form,

$$\Delta'' - 2|\Delta|^2\Delta + i\left(b(E) - 2E\right)\Delta' - 2\left(a(E) - E\,b(E)\right)\Delta = 0, \tag{2.1.9}$$

where the prime stands for the spatial differential. We can then get the general modulating structure of $\Delta(x)$ by solving NLSE.

The general solution of NLSE has been obtained in Ref. [90] and takes the form,

$$\Delta(x) = -me^{iqx}\, A\, \frac{\sigma(mA\, x + i\boldsymbol{K'} - i\theta/2)}{\sigma(mA\, x + i\boldsymbol{K'})\sigma(i\theta/2)}\, \exp\left[imA\, x\, (-i\, \zeta(i\theta/2) + i\, \mathrm{ns}(i\theta/2)) + i\, \theta\eta_3/2\right], \tag{2.1.10}$$

where,

$$A \;\; = \;\; A(\theta,\nu) \equiv -2i\, \mathrm{sc}\,(i\theta/4)\, \mathrm{nd}\,(i\theta/4)\,. \tag{2.1.11}$$

$\mathrm{ns} = 1/\mathrm{sn}, \mathrm{sc} = \mathrm{sn}/\mathrm{cn}, \mathrm{nd} = 1/\mathrm{dn}$ are the Jacobi's elliptic functions with modulus ν and σ, ζ are the Weierstrass's sigma and zeta function. $K(\nu), K'(\nu) \equiv K(1-\nu)$ denotes the complete elliptic integral, $K(\nu) \equiv \int_0^{\pi/2} dt/\sqrt{1-\nu \sin^2 t}$. Furthermore there are four free parameters, $m, q, \nu \in [0,1], \theta \in [0, 4K'(\nu)]$. $\Delta(x)$ has the both modulations of the amplitude and phase and the period of the amplitude reads, $L = \frac{2K(\nu)}{mA}$. The two limits of the general solution (2.1.10) have been discussed in the most studies so far. One is the limit, $\theta = 0$ or $\theta = 4K(\nu)$, called chiral spiral. The chiral spiral condensate takes the form, $\Delta(x) = me^{iqx}$: the similar condensate is called DCDW in the 1+3 dimensions [29]. The other is the limit, $q = 0$ and $\theta = 2K'(\nu)$, called real kink crystal (RKC). The RKC condensate takes the form, $\Delta(x) = \frac{2m\sqrt{\nu}}{1+\sqrt{\nu}} \mathrm{sn}\left(\frac{2mx}{1+\sqrt{\nu}}\right)$.

By solving the BdG equation (2.1.6) with Eq. (2.1.10), the eigenfunctions has been obtained in Ref. [90]. We can see inversely that $\Delta(x) \equiv \sigma(x) - i\pi(x)$ reproduces Eq. (2.1.10) by using the eigenfunctions. Therefore we can conclude that the general solution (2.1.10) is the self-consistent solution.

Next, we would like to see the thermodynamic properties of the obtained self-consistent solution [90]. The thermodynamic potential is explicitly calculated for a given solution and the T-μ phase diagram is obtained by determining the free parameters, which make the thermodynamic potential minimum. We show the analysis of the case of only chiral spiral; in the case of the general solution (2.1.10), the details of the calculation has been given in Ref. [30]. Actually, within the present model, it is known that the solution of the chiral spiral type is the most energetically favored [30]. In the following, all dimensionful quantities are regarded as the dimensionless quantities scaled by the magnitude of the gap function Δ at $T = \mu = 0$. According to Ref. [30], the spectral function for the chiral spiral renders,

$$\rho(E) = \frac{1}{\pi} \frac{|E - q/2|}{\sqrt{(E-q/2)^2 - m^2}}, \tag{2.1.12}$$

where the energy spectrum opens the gap of $2m$ centered on $E = q/2$. Using the spectral function, the thermodynamic potential is obtained as,

$$\Psi[\Delta(x) = m\, e^{iqx}; T, \mu] = m^2 \hat{\Psi} + \frac{m^2}{2\pi} \ln m + \frac{m^2 \hat{\mu}^2}{2\pi} - \frac{\mu^2}{2\pi}, \tag{2.1.13}$$

where $\hat{\Psi}$ takes the form,

$$\hat{\Psi} = -\frac{1}{4\pi} - \frac{\hat{T}}{\pi}\int_1^\infty dE \frac{E}{\sqrt{E^2-1}} \ln[(1+e^{-\hat{\beta}(E-\hat{\mu})})(1+e^{-\hat{\beta}(E+\hat{\mu})})], \tag{2.1.14}$$

and $\hat{\mu} = \frac{\mu - q/2}{m}$, $\hat{\beta} = \frac{1}{\hat{T}} = m\beta$. Next we consider the stationary condition for q. Because the dependence of q is included only through $\hat{\mu}$, the stationary condition is obtained as,

$$\begin{aligned} 0 =& \frac{\partial \Psi}{\partial q} \\ =& \frac{m}{2}\left(-\frac{\partial \hat{\Psi}}{\partial \hat{\mu}} - \frac{\hat{\mu}}{\pi}\right). \end{aligned} \tag{2.1.15}$$

At the zero temperature, the solution, $q = 2\mu$, can be obtained form Eq. (2.1.15), for $\hat{\Psi} = -\frac{1}{4\pi}$. It means that the center of the gap always takes the value of μ. At the finite T, analytical calculations can not be performed, but it is confirmed that the same relation holds from the result of numerical calculation. Furthermore the quark number density can be evaluated in the same way,

$$\begin{aligned} n \equiv& -\frac{\partial \Psi}{\partial \mu} \\ =& \frac{q}{2\pi}\left(= \frac{\mu}{\pi}\right), \end{aligned} \tag{2.1.16}$$

which does not depend on the magnitude of the energy gap, m.

Next we consider the stationary condition for m. Substituting $q = 2\mu$, the thermodynamic potential (2.1.13) takes the form,

$$\Psi[\Delta(x) = me^{iqx}; T, \mu] = \frac{m^2}{4\pi}(\ln m - 1) - \frac{2mT}{\pi}\int_1^\infty dE \frac{E}{\sqrt{E^2-1}} \ln(1+e^{-\hat{\beta}E}) - \frac{\mu^2}{2\pi}, \tag{2.1.17}$$

which does not depend on μ. Therefore m should be determined independent of μ. The stationary condition takes the form,

$$\begin{aligned} 0 \equiv& \frac{\partial \Psi}{\partial m} \\ =& \frac{m}{\pi}\ln m - \frac{2T}{\pi}\int_1^\infty dE \frac{E}{\sqrt{E^2-1}} \ln(1+e^{-\hat{\beta}E}) + \frac{2m}{\pi}\int_1^\infty dE \frac{E^2}{\sqrt{E^2-1}} \frac{1}{1+e^{-\hat{\beta}E}}. \end{aligned} \tag{2.1.18}$$

At $T = 0$, the solution, $m = 1$, can be obtained. Next we would like to know the critical temperature (T_c), where m vanishes. Since it is sufficient to consider the lowest order of m near T_c, Eq. (2.1.18) can be recast into,

$$0 = \ln \pi T - \gamma - \frac{14\zeta'(-2)m^2}{4T^2}, \tag{2.1.19}$$

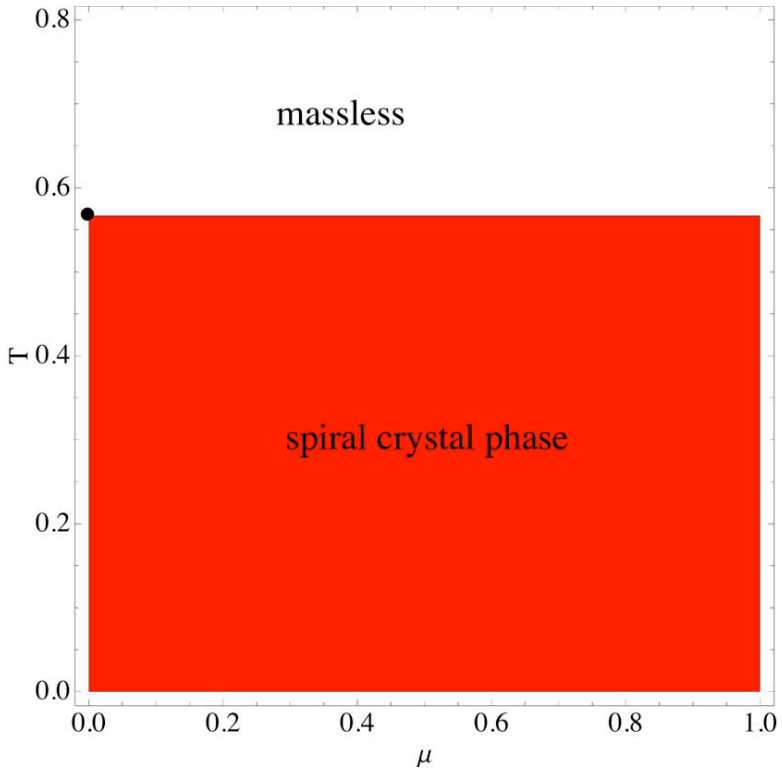

Figure 2.1: The phase diagram in the T-μ plane within the NJL$_2$ model. (The figure is taken from Ref. [90].)

where ζ denotes the zeta function. Therefore the critical temperature can be given as $T_c = e^\gamma/\pi$ because m vanishes at $T = T_c$. The phase transition occurs at $T = T_c$ and the chiral symmetry is restored at a higher T than T_c. On the other hand, by expanding with $\delta T = T_c - T$, the T dependence of m just below T_c can be obtained as,

$$m(T) \simeq \sqrt{\frac{2T_c(T_c - T)}{-7\zeta(-2)}} \simeq 3.06\sqrt{T_c(T_c - T)}. \tag{2.1.20}$$

Furthermore it is also confirmed that m decreases monotonically as increasing T from the numerical calculation. Fig. 2.1 summarizes the above results in the phase diagram in the $T - \mu$ plane. From the figure, the phase region does not depend on μ, and it is shown that chiral symmetry is restored at $T = e^\gamma/\pi \simeq 0.5669$.

2.1.2 1+3 dimensions

In this section, we would like to consider the 1+3 dimensional NJL model. Solving the gap equations in the spatial three dimensions as described in the previous section brings further difficulties, so we use the solution obtained from the NJL$_2$ model as the ansatz in the 1+3

dimensions. In particular, we focus on the thermodynamic properties in the case of only the DCDW type structure [29].

The Lagrangian of the NJL model for the two-flavor case within MFA renders,

$$\mathcal{L}_{\rm MF} = \bar{\psi}\left[\, i\,\partial\!\!\!/ - m\big(\cos(\boldsymbol{q}\cdot\boldsymbol{r}) + i\gamma_5\tau_3\sin(\boldsymbol{q}\cdot\boldsymbol{r})\big)\right]\psi - \frac{m^2}{4G}, \tag{2.1.21}$$

and the effective potential does,

$$V(\sigma,\pi) = \frac{m^2}{4G} + \frac{iN_cN_f}{\mathcal{V}}\mathrm{lnDet}\left[i\partial\!\!\!/ - m\big(\cos(\boldsymbol{q}\cdot\boldsymbol{r}) + i\gamma_5\tau_3\sin(\boldsymbol{q}\cdot\boldsymbol{r})\big)\right], \tag{2.1.22}$$

where we assume the DCDW type condensate, $\sigma = m\cos(\boldsymbol{q}\cdot\boldsymbol{r}), \pi_3 = m\sin(\boldsymbol{q}\cdot\boldsymbol{r})$, and impose that the system is the eigenstate of the electric charge, $\pi_{1,2} = 0$. Since the three-dimensional space is isotropic, q vector is considered along any direction. Taking the direction of q vector along the z direction, we can put as $\boldsymbol{q}\cdot\boldsymbol{r} \to qz$. Before the energy spectrum and thermodynamic potential are calculated, for convenience of calculation we introduce the specific chiral transformation called the Weinberg transformation,

$$\psi(\boldsymbol{r}) \to \psi'(\boldsymbol{r}) = e^{-i\gamma_5\tau_3 qz/2}\psi(\boldsymbol{r}). \tag{2.1.23}$$

After the transformation, the Lagrangian can be rewritten as,

$$\mathcal{L}_{\rm MF} = \bar{\psi}'\left[\, i\,\partial\!\!\!/ - m + \frac{1}{2}\tau_3\gamma_5 q\right]\psi' - \frac{m^2}{4G}. \tag{2.1.24}$$

The energy spectrum is given by solving the eigenvalue equation of the Hamiltonian obtained from the Lagrangian and takes the form,

$$E_\pm(\boldsymbol{p}) = \sqrt{E_0(\boldsymbol{p})^2 + q^2/4 \pm \sqrt{(p_z q)^2 + m^2q^2}}, \tag{2.1.25}$$

where $E_0(p) = (m^2 + |\boldsymbol{p}|^2)^{1/2}$ and $\pm E_\pm(\boldsymbol{p})$ denotes the positive(negative) energy spectrum. Fig. 2.2 shows the energy spectrum for $p_\perp = \sqrt{p_x^2 + p_y^2} = 0$.

Once the energy spectrum is obtained, we can calculate the thermodynamic potential. First, at the zero temperature, the thermodynamic potential renders,

$$\Omega = \Omega_{\rm fer} + \Omega_{\rm vac} + \frac{m^2}{4G}, \tag{2.1.26}$$

where,

$$\Omega_{\rm vac} \equiv -N_fN_c\int\frac{\mathrm{d}^3p}{(2\pi)^3}\sum_{s=\pm}E_s(\boldsymbol{p}), \tag{2.1.27}$$

$$\Omega_{\rm fer} \equiv N_fN_c\int\frac{\mathrm{d}^3p}{(2\pi)^3}\sum_{s=\pm}\left(E_s(\boldsymbol{p}) - \mu\right)\theta\left(\mu - E_s(\boldsymbol{p})\right). \tag{2.1.28}$$

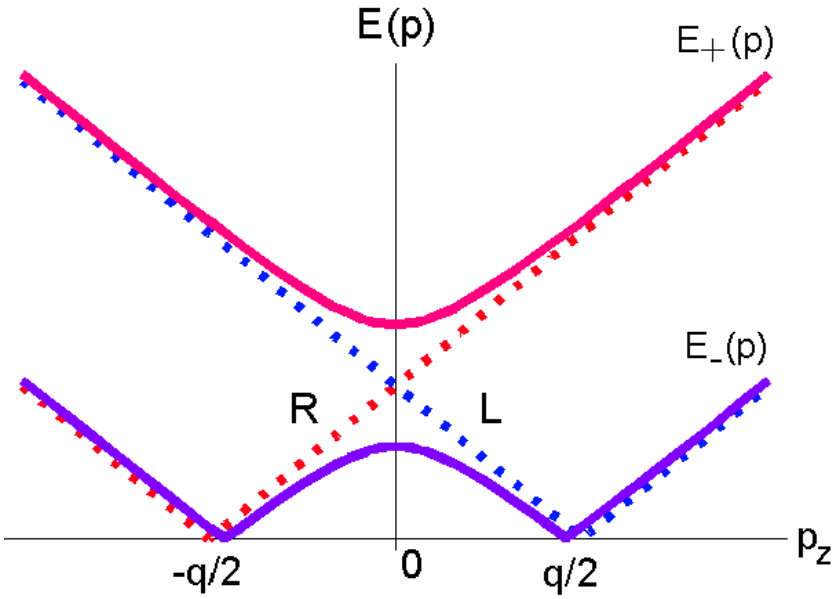

Figure 2.2: The energy spectrum fixed as $p_\perp = 0$. The dotted line represents the case of $m = 0$, and R(L) represents the energy spectrum of the right-(left-)handed particle. (The figure is taken from Ref. [29])

$\Omega_{\rm vac}$ represents the contribution of the Dirac sea and $\Omega_{\rm fer}$ does the contribution of the Fermi sea. Since $\Omega_{\rm vac}$ has the ultraviolet divergence, the proper time regularization (PTR) is applied (for detail see the Appendix B). The regularized $\Omega_{\rm vac}$ takes the form,

$$\Omega_{\rm vac} = \frac{N_f N_c}{8\pi^{3/2}} \int \frac{dp_z}{2\pi} \int_{1/\Lambda^2}^{\infty} \frac{d\tau}{\tau^{5/2}} \left[e^{-\tau\left(\sqrt{p_z^2+m^2}+q/2\right)^2} + e^{-\tau\left(\sqrt{p_z^2+m^2}-q/2\right)^2} \right], \tag{2.1.29}$$

where the cutoff Λ is introduced and the constant term, which does not depend on m, q is dropped. To analyze the phase transition between the usual spontaneous symmetry breaking (SSB) phase and the DCDW phase, we consider the expansion with respect of q. Since the thermodynamic potential (2.1.26) is obviously even function of q, the thermodynamic potential includes only the even-order term for q and renders,

$$\Omega = \Omega_0 + \frac{1}{2}(\beta_{\rm fer} + \beta_{\rm vac})q^2 + O(q^4), \tag{2.1.30}$$

where,

$$\beta_{\rm fer} \equiv \frac{\partial^2 \Omega_{\rm fer}}{\partial q^2}|_{q\to 0} = -N_f N_c \frac{m^2}{\pi^2} H(\mu/m), \tag{2.1.31}$$

$$\beta_{\rm vac} \equiv \frac{\partial^2 \Omega_{\rm vac}}{\partial q^2}|_{q\to 0} = N_f N_c \frac{\Lambda^2}{2\pi^2} J(m^2/\Lambda^2), \tag{2.1.32}$$

and $J(x) = x\int_x^\infty {\rm d}\tau \exp(-\tau)/\tau, H(x) = \ln(x+\sqrt{x^2-1})$. From Eq. (2.1.31), (2.1.32), it can be seen that $\beta_{\rm fer} < 0$ and $\beta_{\rm vac} > 0$. In order to minimize the thermodynamic potential at

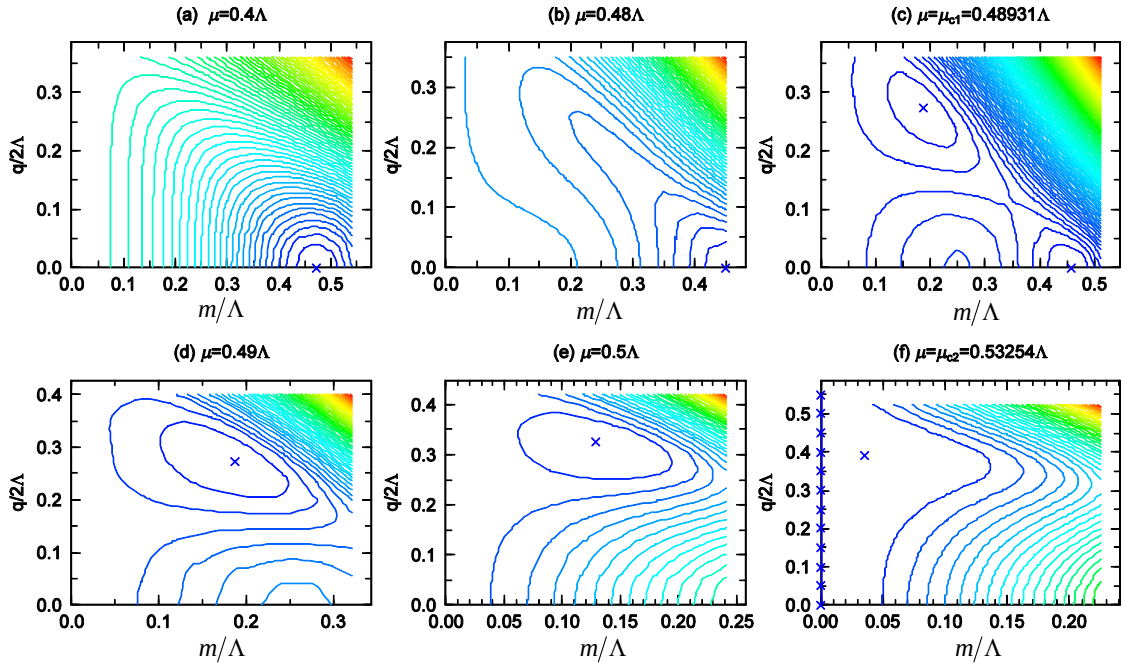

Figure 2.3: The contour map indicating m, q dependence of the thermodynamic potential for each μ. (The figures are taken from Ref. [29].)

$q \neq 0$, it is necessary for the second order coefficient of q to be negative. Therefore the contribution from Fermi sea promotes the phase transition to the DCDW phase. Since $H(x)$ is a monotonically increasing function, it is expected that the contribution from Fermi sea increases as μ increases and the phase transition to the DCDW phase occurs. In the present calculation, $\beta_{\rm tot}$ can be negative when $\mu/\Lambda > 0.38$.

Next, the contour map of the thermodynamic potential, for fixed μ is presented as the function of the order parameters m, q in Fig. 2.3. From that figure, when $\mu < \mu_{c1}$, there is the minimum point at $m \neq 0, q = 0$, where the usual SSB phase is realized. When $\mu_{c1} < \mu < \mu_{c2}$, there is the minimum point at $m \neq 0, q \neq 0$ and the DCDW phase is realized. When $\mu > \mu_{c2}$, the minimum point is located on $m = 0$ and chiral symmetry restored phase is realized. There are two different minima in $\mu = \mu_{c1}$, which indicate that the phase transition from the homogeneously broken phase to the DCDW phase is the first order. On the other hand, the minimum point at $m = 0$ and the minimum point at $m \neq 0$ are very close in $\mu = \mu_{c2}$, which implies the phase transition from the DCDW phase to the restored phase is the second order or the weakly first order.

Fig. 2.4 shows the μ dependence of the order parameters which make the thermodynamic potential minimum. Certainly the order parameters have discontinuities at $\mu = \mu_{c1}$ and it is confirmed that the first order phase transition occurs.

Finally, we consider the phase diagram extended to finite T. The thermodynamic poten-

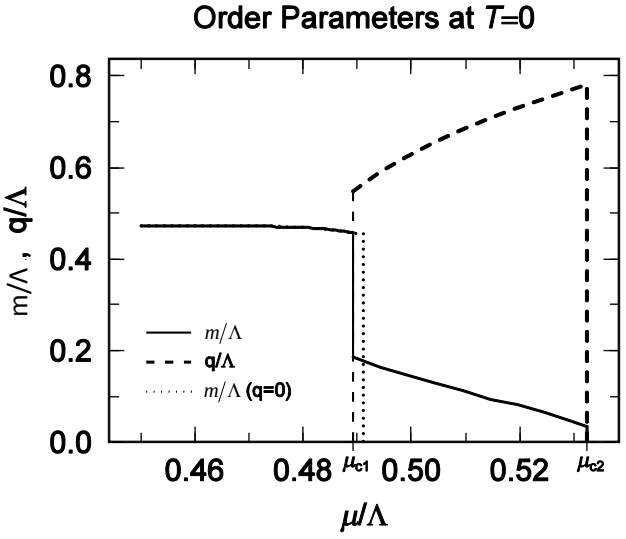

Figure 2.4: The μ dependence of the order parameters m, q. On μ_{c1}, the first order phase transition from the usual SSB phase to the DCDW phase occurs. On μ_{c2}, the second order phase transition from the DCDW phase to the restored phase takes place. (The figure is taken from Ref. [29].)

tial is calculated as

$$\begin{aligned}\Omega_\beta(\mu, T; q, m) &= -\frac{T}{V}\ln Z(\mu, T; q, m) \\ &= -N_f N_c \int \frac{d^3\boldsymbol{p}}{(2\pi)^3} \sum_{s=\pm} \left\{ T \ln \left[e^{-\beta(E_s(\boldsymbol{p})-\mu)} + 1 \right] \left[e^{-\beta(E_s(\boldsymbol{p})+\mu)} + 1 \right] + E_s(\boldsymbol{p}) \right\} + \frac{m^2}{4G}\end{aligned} \tag{2.1.33}$$

At each T and μ, we can determine the realized phase from the value of the order parameters m, q which minimizes this thermodynamic potential. Fig. 2.5 shows the phase diagram in the T-μ plane. From the figure, it is found that when T increases, the region of the DCDW phase becomes narrower and moves to the lower density. Finally, the DCDW phase disappears at the critical point, called the Lifshitz point (LP), $T_{\rm LP}/\Lambda \simeq 0.14$, $\mu_{\rm LP}/\Lambda \simeq 0.4$.

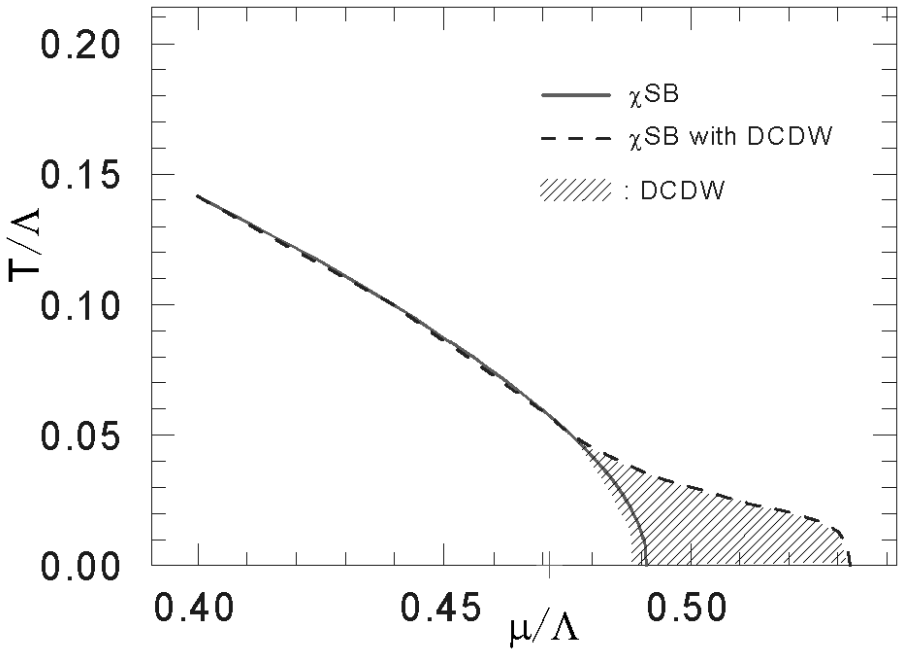

Figure 2.5: The phase diagram in T-μ plane within 1+3 dimensional NJL model. (The figure is taken from Ref. [29])

2.1.3 Nesting effect

In this section, the analogy of the nesting effect is considered as the physical reason for appearance of the DCDW phase. The nesting effect has been proposed for a long time in the context of the condensed matter physics, and it explains the existence of periodic structures such as the charge density wave (CDW) [35, 93] and the spin density wave (SDW) [33, 34] by the overlap of the Fermi surfaces.

First of all, in the 1+1 dimensional electron system, we consider the periodic potential as,

$$V_q(x) = A(e^{iqx} + e^{-iqx}). \tag{2.1.34}$$

With the potential, the energy spectrum of electrons takes the form,

$$E_q^{\pm}(k) = \frac{1}{2}\left[\epsilon_k + \epsilon_{k-q} \pm \sqrt{(\epsilon_k - \epsilon_{k-q})^2 + 4A^2}\right], \tag{2.1.35}$$

where ϵ_k denotes the free one-particle energy spectrum, $\epsilon_k = \frac{k^2}{2m_e}$. The energy spectrum is shown in Fig. 2.6. It is found that whenever particles occupy the states in the lower spectrum, $E_q^-(k)$, the total energy decreases compared with the one in the case of $q = 0$. The total energy reduction takes place due to opening a gap at the Fermi energy regardless of the magnitude of the interaction and the details of the model. In the case of $T = 0$, the total energy takes the minimum value when the chemical potential is located at the center of the

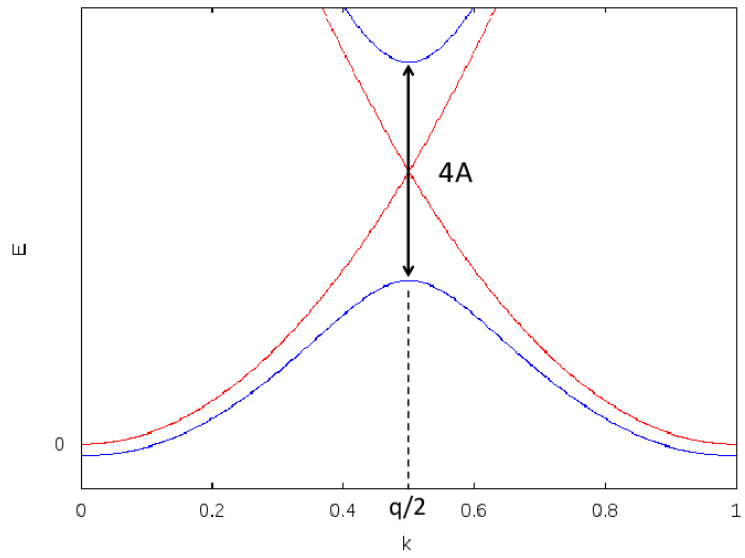

Figure 2.6: The energy spectrums with or without the interaction. $E_q^{\pm}(k)$ is described by the blue line. ϵ_k and ϵ_{k-q} are represented by the red line. In this figure, we set $q = 1$.

gap and the all states of $E_q^-(k)$ are occupied. This situation is realized when $q = 2k_F$, where k_F denotes the Fermi momentum of the free electrons. In CDW and SDW, the periodic structure appears as the mean field. The existence of the mean field with the wave number q indicates that the particle-hole pair with the relative momentum of q are coupled.

The nesting effect is strongly related to the geometry of the Fermi surface. If the particle-hole pair with the relative momentum q is always located on the Fermi surface, the pair can generate the condensate with the wave number q without any excitation energy. On the other hand, some excitation energy is taken to generate the condensate by the particle-hole pair which is not on the Fermi surface. In 1+1 dimensions, the particle-hole pair with the relative momentum $q = 2k_F$ can be always on the Fermi surface as shown in the left schematic figure in Fig. 2.7. In other words, when the Fermi surface is translated by momentum q, the Fermi surface exactly overlaps with itself. The exact overlap is called the perfect nesting. However, in the 1+3 dimensions, the particle-hole pairs with the same relative momentum $\boldsymbol{q}$ are not always located on the Fermi surface as shown in the right schematic figure in Fig. 2.7. In other words, the overlap of the Fermi surface is not perfect and the situation is called imperfect nesting.

Therefore, in the 1+3 dimensions, it depends on the detail of the model whether the inhomogeneous phase is energetically favored. It has been known that SDW may develop in the free electron gas system if the interaction is sufficiently strong [33]. When we compare the kinetic and interaction energy between the state where the Fermi spheres are in contact with each other at one point and that where the Fermi spheres slightly overlap each other, it can be seen that the Fermi sphere overlapping decreases the total energy. That is, the case of $q < 2k_F$ is more stable than $q = 2k_F$. In addition, CDW is actually observed in the

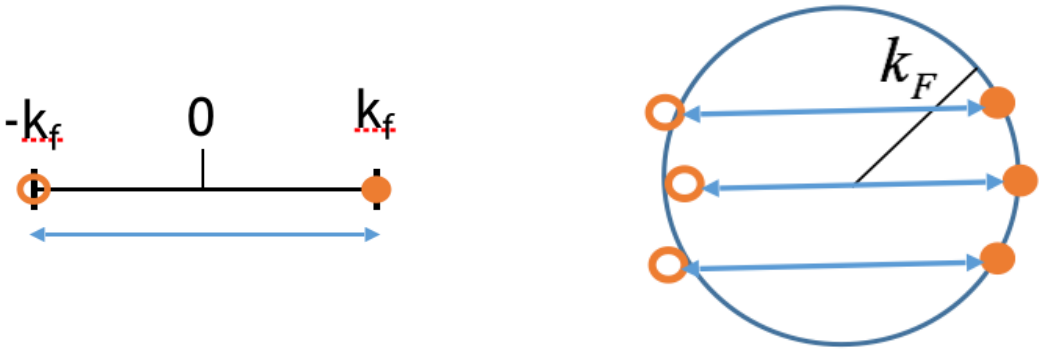

Figure 2.7: The schematic pictures of the Fermi surface and the particle-hole pair with the relative momentum $\boldsymbol{q}$. The left picture shows the Fermi surface in the 1+1 dimensions. When the relative momentum is taken $q = 2k_F$, the particle-hole pair is located on the Fermi surface. The right picture shows the Fermi surface in the 1+3 dimensions. Even if the relative momentum is taken any value, all the particle-hole pairs are not always placed on the Fermi surface.

pseudo-two dimensional compounds with the layered crystal structure [12].

Next we consider the case of the DCDW phase. In the 1+1 dimensions, the nesting relations, $q = 2\mu$, seems to always hold as shown in the previous section. However, the relation is given rise to by axial anomaly (the details are discussed in Chapter 4). On the other hand, the nesting relation can not be derived in the 1+3 dimensions. However, at the critical chemical potential, μ_{c1}, in Fig. 2.4, it can be seen that the relation, $q < 2k_F$, is realized.

2.2 Case of the presence of the magnetic field

In this section, we review how the appearance of iCP changes by analyzing the thermodynamic potential when a magnetic field is applied as an external field [45]. We also introduce the method of calculating anomaly due to the energy spectrum asymmetry about zero [47, 48, 94].

2.2.1 DCDW phase within the NJL model in the external magnetic field

First, we consider only the case of the structure of the inhomogeneous condensate limited to the DCDW type [45]. In this section, the two-flavor NJL model is used in the presence of the external magnetic field. Within MFA, the Lagrangian takes the form,

$$\mathcal{L}_{\rm MF} = \bar{\psi}\left[\, i\not{D} - m\big(\cos(qz) + i\gamma_5\tau_3\sin(qz)\big)\right]\psi - \frac{m^2}{4G}, \tag{2.2.1}$$

where D denotes the covariant derivative, $D_\mu = \partial_\mu + iQA_\mu$ and Q represents the electric charge matrix, $Q = \mathrm{diag}\left(\frac{2}{3}e, -\frac{1}{3}e\right), e > 0$, in the flavor space. We assume that the magnetic field is constant in the z direction and take the Landau gauge, $A^\mu = (0, 0, Bx, 0)$. Applying the Weinberg transformation, the Lagrangian can be rewritten as,

$$\mathcal{L}_{\mathrm{MF}} = \bar{\psi}' \left[i \not{D} - m + \frac{1}{2}\tau_3\gamma_5 q \right] \psi' - \frac{m^2}{4G}. \tag{2.2.2}$$

The thermodynamic potential can be calculated from that Lagrangian.

First of all, we consider the one-flavor case, but as we can see, the two-flavor case can be analyzed using the 1-flavor result. The Hamiltonian takes the form,

$$H = \boldsymbol{\alpha} \cdot \hat{\boldsymbol{P}} + \gamma^0 m - \frac{1}{2}\Sigma_3 q \tag{2.2.3}$$

where $\hat{\boldsymbol{P}} = -i\boldsymbol{D}, \Sigma_3 = \frac{i}{2}[\gamma_1, \gamma_2]$. The eigenfunction of that Hamiltonian can be obtained as,

$$\Psi_{n,p_z,p_y}(x, y, z) = \frac{1}{\sqrt{2\pi}} e^{ip_z z} \frac{1}{\sqrt{2\pi}} e^{ip_y y} \begin{pmatrix} c_1\, u_{n-1}(\xi) \\ ic_2\, u_n(\xi) \\ c_3\, u_{n-1}(\xi) \\ ic_4\, u_n(\xi) \end{pmatrix} (eB)^{1/4}, \tag{2.2.4}$$

where $\xi \equiv \sqrt{eB}x + \frac{p_y}{\sqrt{eB}}$. $u_n(\xi)$ is defined as,

$$u_n(\xi) \equiv \left(\frac{1}{2^n n! \pi^{1/2}} \right)^{1/2} e^{-\frac{\xi^2}{2}} H_n(\xi) \tag{2.2.5}$$

$$u_{-1}(\xi) \equiv 0 \tag{2.2.6}$$

where $H_n(\xi)$ denotes the Hermite polynomial. p_y specifies the center, $x_0 = -\frac{p_y}{eB}$, in the x direction of the wave function. Therefore if considering the finite system $\mathcal{V} = L_t \times L_x L_y L_z$, the range of p_y is limited to $-eBL_x < p_y < 0$ for $0 < x_0 < L_x$. The eigenspinor takes the form,

$$\begin{pmatrix} c_1 \\ c_2 \\ c_3 \\ c_4 \end{pmatrix} = \frac{1}{2\sqrt{2}} \begin{pmatrix} -\zeta B(P - \epsilon\zeta Q) \\ -A(P + \epsilon\zeta Q) \\ A(P - \epsilon\zeta Q) \\ -\zeta B(P + \epsilon\zeta Q) \end{pmatrix}, \tag{2.2.7}$$

where $A = \sqrt{1 + \frac{m}{\Pi}}, B = \sqrt{1 - \frac{m}{\Pi}}, P = \sqrt{1 - \frac{p_\perp}{E}}, Q = \sqrt{1 + \frac{p_\perp}{E}}, \Pi = \zeta\sqrt{m^2 + p^2}$ and we put $\zeta = \epsilon$ at $n = 0$. Furthermore, the energy spectrum can be obtained as,

$$E^{\mathrm{hLL}}_{n,\zeta,\epsilon,p_z} = \epsilon\sqrt{\left(\zeta\sqrt{m^2 + p_z^2} + q/2\right)^2 + 2|eB|n}, \quad n = 1, 2, \ldots, \tag{2.2.8}$$

$$E^{\mathrm{LLL}}_{\epsilon,p_z} = \epsilon\sqrt{m^2 + p_z^2} + q/2, \quad n = 0, \tag{2.2.9}$$

where n denotes the Landau levels and $\zeta = \pm 1$ represents the spin degree of freedom. It is important that the lowest Landau level(LLL), $n = 0$, is asymmetric about zero although all higher Landau levels(hLLs), $n \geq 1$, are symmetric. In above calculation, we have assumed that the direction of the magnetic field and $\boldsymbol{q}$ are the same. If we consider the slightly shift of the direction of $\boldsymbol{q}$ as $\boldsymbol{q} = (0, 0, q) \to \boldsymbol{q} = (q_\perp, 0, q)$, the change of the energy is estimated within the perturbation theory and the change is always positive [45]. Therefore we use the assumption of $\boldsymbol{q}$ parallel to the magnetic field in the following.

Next we would like to analyze the thermodynamic properties. For the two-flavor case, the effective potential renders,

$$V(m,q) = \frac{m^2}{4G} + \frac{i}{\mathcal{V}}\mathrm{Tr}_{\mathrm{D,f,c}}\mathrm{Ln}\left[i\not{D} - m + \frac{1}{2}\gamma_5\tau_3 q\right] \tag{2.2.10}$$

Multiplying the d-quark sector by $1 = [\det(\gamma_2\gamma_3)]^2$, it can be rewritten as,

$$V(m,q) = \frac{m^2}{4G} + \tilde{V}(m,q)|_{e\to\frac{2}{3}e} + \tilde{V}(m,q)|_{e\to\frac{1}{3}e}, \tag{2.2.11}$$

where $\tilde{V}(m,q)$ denotes the effective potential for the one-flavor case,

$$\tilde{V}(m,q) \equiv \frac{iN_c}{\mathcal{V}}\mathrm{Tr}_{\mathrm{D}}\mathrm{Ln}\left[i\gamma^\mu(\partial_\mu + ieA_\mu) - m + \frac{1}{2}\gamma_5 q\right]. \tag{2.2.12}$$

Therefore, it can be seen that the result of the one-flavor case can be easily extended to the two-flavor case. In the following, we show the calculation of the 1-flavor case. Since the eigenstates and the energy spectrum have been obtained, the effective potential can be calculated as,

$$\tilde{V} = \frac{iN_c}{2}\frac{eB}{(2\pi)^2}\int\frac{dp_0}{2\pi}\int dp_z\left\{\sum_\epsilon \ln\left[-p_0^2 + (E^{\mathrm{LLL}}_{\epsilon,p_z})^2\right] + \sum_{n\zeta\epsilon}\ln\left[-p_0^2 + (E^{\mathrm{hLL}}_{n,\zeta,\epsilon,p_z})^2\right]\right\}. \tag{2.2.13}$$

By extending that effective potential to the case of the finite T and density, the thermodynamic potential can be obtained as,

$$\Omega = \Omega_{\mathrm{v}} + \Omega_\mu + \Omega_T + \frac{m^2}{4G}, \tag{2.2.14}$$

where,

$$\Omega_{\mathrm{v}} = -\frac{N_c}{2}\frac{eB}{(2\pi)^2}\int dp_z\left(\sum_\epsilon |E^{\mathrm{LLL}}_{\epsilon,p_z}| + \sum_{n\zeta\epsilon}|E^{\mathrm{hLL}}_{n,\zeta,\epsilon,p_z}|\right), \tag{2.2.15}$$

$$\Omega_\mu = -\frac{N_c}{2}\frac{eB}{(2\pi)^2}\int dp_z\left[\sum_\epsilon\left(|E^{\mathrm{LLL}}_{\epsilon,p_z} - \mu| - |E^{\mathrm{LLL}}_{\epsilon,p_z}|\right) + \sum_{n\zeta\epsilon}\left(|E^{\mathrm{hLL}}_{n,\zeta,\epsilon,p_z} - \mu| - |E^{\mathrm{hLL}}_{n,\zeta,\epsilon,p_z}|\right)\right], \tag{2.2.16}$$

$$\Omega_T = -\frac{N_c}{\beta}\frac{eB}{(2\pi)^2}\int dp_z\left[\sum_\epsilon \ln\left(1 + e^{-\beta|E^{\mathrm{LLL}}_{\epsilon,p_z} - \mu|}\right) + \sum_{n\zeta\epsilon}\ln\left(1 + e^{-\beta|E^{\mathrm{hLL}}_{n,\zeta,\epsilon,p_z} - \mu|}\right)\right]. \tag{2.2.17}$$

Since $\Omega_{\rm v}$ has the UV divergence, PTR is applied in the same way in Eq. (2.1.29). The regularized $\Omega_{\rm v}$ then takes the form,

$$\Omega_{\rm v} \to \frac{N_c}{4\sqrt{\pi}} \frac{eB}{(2\pi)^2} \int dp \int_{1/\Lambda^2}^{\infty} \frac{ds}{s^{3/2}} \left(\sum_{\epsilon} e^{-s(E^{\rm LLL}_{\epsilon,p_z})^2} + \sum_{n\zeta\epsilon} e^{-s(E^{\rm hLL}_{n,\zeta,\epsilon,p_z})^2} \right), \tag{2.2.18}$$

where the cutoff parameter Λ is introduced. It is confirmed that if the magnetic field is set to be zero, it is reduced to Eq. (2.1.29). Though Ω_μ is finite, the part of LLL in Ω_μ ($\Omega_\mu^{\rm LLL}$) is ill-defined. In this section, to definitely calculate $\Omega_\mu^{\rm LLL}$, we introduce the regulator l as the upper limit of the energy, which preserves the gauge invariance. $\Omega_\mu^{\rm LLL}$ with l is written as,

$$\Omega_\mu^{\rm LLL} = \lim_{l\to\infty} -\frac{N_c}{2} \frac{eB}{(2\pi)^2} \int dp_z \sum_{\epsilon} \left(|E^{\rm LLL}_{\epsilon,p_z} - \mu| - |E^{\rm LLL}_{\epsilon,p_z}| \right) \theta(l - |E^{\rm LLL}_{\epsilon,p_z}|). \tag{2.2.19}$$

Note that, if we consider l as the upper limit of the momentum, which violates the gauge invariance, $\Omega_\mu^{\rm LLL}$ is shifted by a finite value, $2\mu q$, compared to Eq. (2.2.19) [45]. However, in this case, the thermodynamic potential still depends on q when $m = 0$. In other words, it is physically incorrect that it depends on the phase of the condensate despite of the zero amplitude. Therefore we use l as the upper limit of the energy in the following analysis. On the other hand, taking into account $E^{\rm hLL}_{n,\zeta,\epsilon=+1,p_z} = -E^{\rm hLL}_{n,\zeta,\epsilon=-1,p_z}$, the part of hLLs in Ω_μ ($\Omega_\mu^{\rm hLL}$) can be calculated as,

$$\begin{aligned}
\Omega_\mu^{\rm hLL} =& -\frac{N_c}{2} \frac{eB}{(2\pi)^2} \int dp_z \sum_{n,\zeta,\epsilon} \left(|E^{\rm hLL}_{n,\zeta,\epsilon,p_z} - \mu| - |E^{\rm hLL}_{n,\zeta,\epsilon,p_z}| \right) \\
=& -N_c \frac{eB}{(2\pi)^2} \int dp_z \sum_{n,\zeta} \left(\mu - E^{\rm hLL}_{n,\zeta,\epsilon=+1,p_z} \right) \theta(\mu - E^{\rm hLL}_{n,\zeta,\epsilon=+1,p_z}).
\end{aligned} \tag{2.2.20}$$

Since thermodynamic potential in obtained, the phase diagram of $T = 0$ can be calculated. In this calculation, the value of the coupling constant is assumed to be $G\Lambda^2 = 6$. All the values in the following figures are regarded as dimensionless by the cutoff parameter Λ. Furthermore, $\sqrt{eH}$ in the figure is the same as $\sqrt{eB}$. First, when the magnetic field vanishes, there are four phases A, B, C and D, which are the restored phase, the usual SSB phase with the vanishing density, the usual SSB phase with the finite density and the DCDW phase, respectively. Fig. 2.8 shows the phase diagram in the $\mu - \sqrt{eB}$ plane. As we can see, the B and C phases become the DCDW phase even if a tiny magnetic field is switched on in the finite μ region.

Fig. 2.9 shows the change of the order parameters m, q when μ is fixed and the magnetic field is changed. When $\mu = 0$, even if the magnetic field is applied, $q = 0$ remains vanishing. It indicates the the usual SSB phase remains. Furthermore, we can see that magnetic catalysis that m increases as the magnetic field increases. When $\mu = 0.3$, q rises from zero as soon as the magnetic field is switched on; that is, if the magnetic field is applied even a little, the B phase changes to the DCDW phase. When $\mu = 0.5$, the transition from the DCDW phase to the C phase should be seen from the zero magnetic field, but the order parameter is oscillating due to the de Haas-van Alphen effect [95]. Therefore it makes difficult to

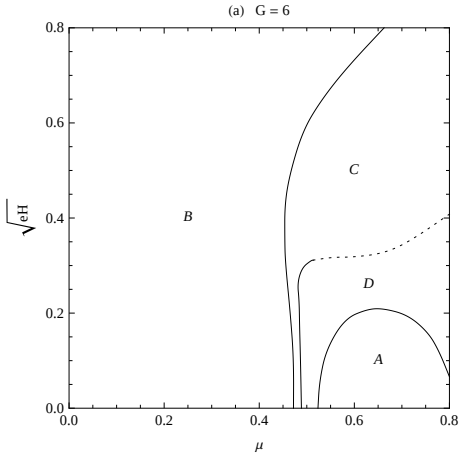

Figure 2.8: The phase diagram on the $\mu - \sqrt{eB}$ plane at $T = 0$. When the magnetic field vanishes, A, B, C, and D represents the restored phase, the usual SSB phase with the vanishing density, the usual SSB phase with the finite density and the DCDW phase, respectively. It is described how the region of the phases changes when the magnetic field is applied. In the B and C phases, the condensate has the wave number q when $\mu \neq 0$ and $B \neq 0$. (The figure is taken from Ref. [45].)

distinguish the phase transition point. By the same reason, the boundary of the C and D phases is partially dotted in Fig. 2.8. Furthermore when $\mu = 0.5$, the transition from the restored phase (A) to the D phase can be seen.

Finally, Fig. 2.10 shows the change in the order parameters when the magnetic field is fixed and μ is changed. When $\sqrt{eB} = 0$, the phase transition is similar to the previous one (Fig. 2.4). When $\sqrt{eB} = 0.15$, we can see that the B and C phases become the DCDW phase. As the magnetic field increases as $\sqrt{eB} = 0.3, 0.5$, q in the B phase sharply increases and approaches to $\mu = q/2$.

In conclusion, the phase which is the usual SSB phase in the absence of the magnetic field becomes the DCDW phase except for $\mu = 0$ when the magnetic field is switched on. Furthermore the region of the DCDW phase also spreads. These results indicate that the magnetic field works to grow the DCDW phase. Although we have analyzed only the DCDW type condensate, it is known that the DCDW phase also appears in the case of considering hybrid chiral condensate, which has the both features of DCDW and RKC if the magnetic field becomes stronger [96].

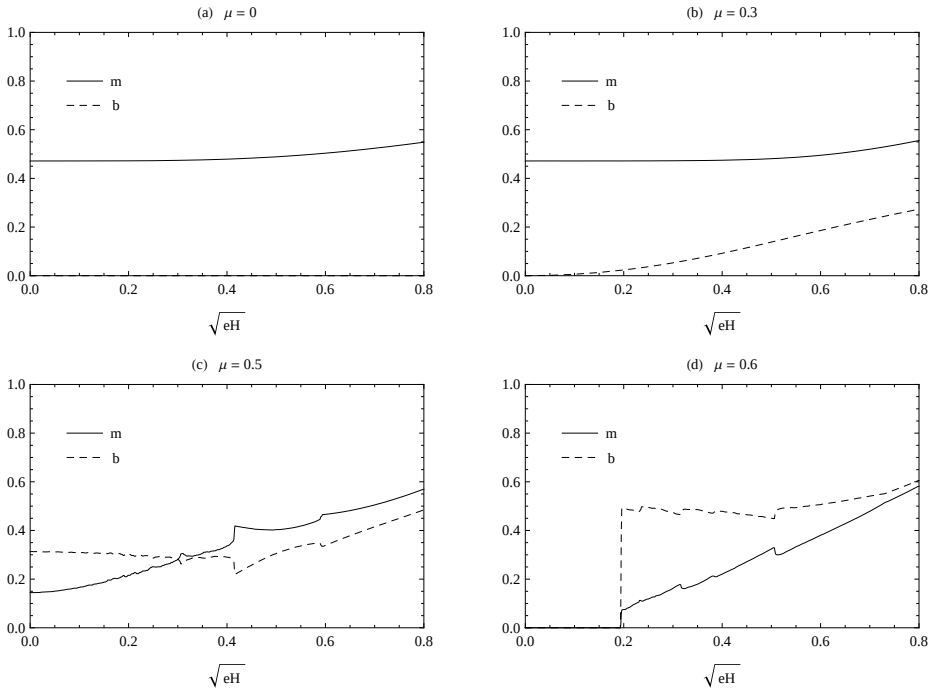

Figure 2.9: The dependence of the magnetic field in the order parameters m, q at each μ and $T = 0$. (The figures are taken from Ref. [45].)

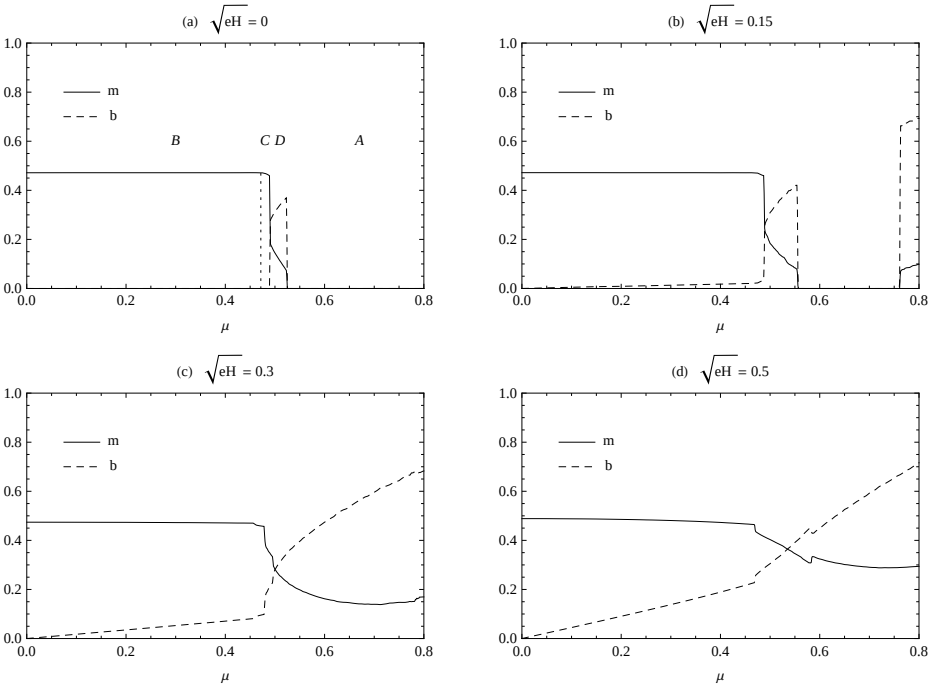

Figure 2.10: The μ dependence of order parameters m, q at each magnetic field and $T = 0$. (The figures are taken from Ref. [45].)

2.2.2 Anomaly due to the asymmetric energy spectrum

As seen in the previous section, LLL becomes positive / negative asymmetric in the DCDW phase with the magnetic field. In the case of such an asymmetric spectrum, it is known that an anomalous term appears in the particle number [47, 48]. In this section, we review the calculation method of particle number and discuss the relationship with chiral anomaly.

Generally, the fermion field expanded by the eigenfunction of the energy renders,

$$\psi(\boldsymbol{r}) = \sum_k b_k \phi_k^{(+)}(\boldsymbol{r}) + \sum_{k'} d_{k'}^\dagger \phi_{k'}^{(-)}(\boldsymbol{r}), \tag{2.2.21}$$

where $\phi_k^{(+)}$, b_k denotes the eigenfunction of the positive energy and the annihilation operator of the particles and $\phi_{k'}^{(-)}, d_{k'}^\dagger$ does the eigenfunction of the negative energy and the creation operator of the anti-particles. The all eigenfunctions is regarded to be normalized already. The eigenvalue of the energy is represented as λ_k ($H\phi_k = \lambda_k \phi_k$). At zero temperature, if the particle number is defined antisymmetric so as to avoid the divergence, it can be written as,

$$\begin{aligned} N =& \frac{1}{2}\int d\boldsymbol{r} \langle [\psi^\dagger(\boldsymbol{r}), \psi(\boldsymbol{r})] \rangle \\ =& \sum_k \langle b_k^\dagger b_k \rangle - \sum_{k'} \langle d_{k'}^\dagger d_{k'} \rangle - \frac{1}{2}\int d\boldsymbol{r} \left(\sum_k \phi_k^{(+)\dagger} \phi_k^{(+)} - \sum_{k'} \phi_{k'}^{(-)\dagger} \phi_{k'}^{(-)} \right) \\ =& N_{\mathrm{nom}} - \frac{1}{2}\sum_{k,k'} \mathrm{sign}(\lambda_{k,k'}), \end{aligned} \tag{2.2.22}$$

where N_{nom} represents the ordinary particle number in the quantum field theory, which means the number of particles minus the number of anti-particles. The second term represents the anomalous particle number given by the difference in the number of the eigenstates of the positive and negative energies when the energy spectrum is asymmetric [47, 48]. Recall that such anomalous particle number is an important concept in the context of the chiral bag model, which is one of the models describing nucleon [97, 98].

Next, we discuss the anomalous particle number in the DCDW phase with the magnetic field [94]. From Eq. (2.2.14), the thermodynamic potential at zero temperature renders,

$$\Omega = \Omega_{\mathrm{v}} + \Omega_\mu + \frac{m^2}{4G}. \tag{2.2.23}$$

From Eq. (2.2.16), the contribution of the density, Ω_μ, can be calculated as,

$$\begin{aligned} \Omega_\mu =& \frac{eB}{(2\pi)^2}\int dp \left[\sum_\epsilon (E_{\epsilon,p}^{\mathrm{LLL}} - \mu)\theta(E_{\epsilon,p}^{\mathrm{LLL}})\theta(\mu - E_{\epsilon,p}^{\mathrm{LLL}}) + \sum_{n\zeta\epsilon} (E_{n,\zeta,\epsilon,p}^{\mathrm{hLL}} - \mu)\theta(E_{n,\zeta,\epsilon,p}^{\mathrm{hLL}})\theta(\mu - E_{n,\zeta,\epsilon,p}^{\mathrm{hLL}}) \right] \\ &+ \frac{1}{2}\frac{eB}{(2\pi)^2}\int dp\ \mu \sum_\epsilon \mathrm{sign}(E_{\epsilon,p}^{\mathrm{LLL}}). \end{aligned} \tag{2.2.24}$$

Therefore the quark number density at $T = 0$ can be obtained as,

$$\begin{aligned} n \equiv & -\frac{\partial \Omega}{\partial \mu} \\ =& \frac{eB}{(2\pi)^2}\int dp \left[\sum_{\epsilon} \theta(E^{\rm LLL}_{\epsilon,p})\theta(\mu - E^{\rm LLL}_{\epsilon,p}) + \sum_{n\zeta\epsilon} \theta(E^{\rm hLL}_{n,\zeta,\epsilon,p})\theta(\mu - E^{\rm hLL}_{n,\zeta,\epsilon,p})\right] \\ & - \frac{1}{2}\frac{eB}{(2\pi)^2}\int dp \sum_{\epsilon} {\rm sign}(E^{\rm LLL}_{\epsilon,p}), \end{aligned} \tag{2.2.25}$$

where the first term denotes the number of states between from $E = 0$ to $E = \mu$, which means the number of particles in the usual sense ($N_{\rm nom}$). On the other hand, the second term represents the anomalous particle number given by the difference in the number of eigenstates of the positive and negative energies[1]. In the present model, only LLL is asymmetric about zero. Since the second term is ill-defined, we should evaluate it after introducing some proper regulator. In this section, we introduce the quantity,

$$\eta_H \equiv \frac{eB}{2\pi}\int \frac{dp}{2\pi} \sum_{\epsilon} {\rm sign}(E^{\rm LLL}_{\epsilon,p}), \tag{2.2.26}$$

and,

$$\eta_H = \lim_{s\to+0} \eta_H(s) = \lim_{s\to+0} \frac{eB}{2\pi}\int \frac{dp}{2\pi} \sum_{\epsilon} {\rm sign}(E^{\rm LLL}_{\epsilon,p}) |E^{\rm LLL}_{\epsilon,p}|^{-s}, \tag{2.2.27}$$

where η_H denotes the topological quantity called η-invariant by Atiyah-Patodi-Singer [48]. It is important to introduce the regularization about the energy, which does not violate the gauge invariance[2]. When $m > q/2$, that quantity can be calculated as,

$$\begin{aligned} \eta_H(s) =& \frac{eB}{2\pi}\int \frac{dp}{2\pi} \sum_{\epsilon=\pm} {\rm sign}\left(E^{\rm LLL}_{\epsilon,p}\right) \int_0^\infty d\omega \frac{\omega^{s-1}}{\Gamma(s)} e^{-\omega |E^{\rm LLL}_{\epsilon,p}|} \\ =& -\frac{eB}{\pi\Gamma(s)}\int \frac{dp}{2\pi} \int_0^\infty d\omega \omega^{s-1} e^{-\omega\sqrt{m^2+p^2}} \sinh\left(\frac{q\omega}{2}\right) \\ =& -\frac{2^{s-2} eBq m^{-s}}{\pi^2\Gamma(s)} \Gamma\left(1+\frac{s}{2}\right)\Gamma\left(\frac{s}{2}\right) {}_2F_1\left(1+\frac{s}{2}, \frac{s}{2}, \frac{3}{2}, \frac{q^2}{4m^2}\right) \\ \to & -\frac{eBq}{2\pi^2} \quad (s \to +0), \end{aligned} \tag{2.2.28}$$

where ${}_2F_1$ denotes the Gauss's hypergeometric function. When $m < q/2$, a part of the eigenvalues counted as the negative energy at $m > q/2$ changes the eigenvalue of the positive

[1] In the two-flavor case, the anomalous particle number should be the summation of the contribution of u and d-quarks in the same way of the thermodynamic potential (2.2.11).

[2] If we introduce the regularization about the momentum, anomalous particle number loses the gauge invariance.

energy. The number of the eigenvalues that change to positive from negative can be easily counted as,

$$\begin{aligned}\Delta\eta =&\frac{eB}{2\pi}\int_0^\infty \frac{dp}{2\pi}\theta\left(-\sqrt{m^2+p^2}+\frac{q}{2}\right)\\ =&\frac{eB}{2\pi^2}\sqrt{\frac{q^2}{4}-m^2}.\end{aligned} \tag{2.2.29}$$

Therefore the η-invariant at $m < q/2$ can be obtained asd,

$$\begin{aligned}\eta_H =&-\frac{eBq}{2\pi^2}+2\Delta\eta\\ =&-\frac{eBq}{2\pi^2}+\frac{eB}{\pi^2}\sqrt{\frac{q^2}{4}-m^2}.\end{aligned} \tag{2.2.30}$$

However, as we see above, the first term represents the topological part that appears by correctly evaluating the subtraction of the divergence with including the regulator s, and the second term is not topological quantity which can be calculated without the regulator.

In the previous we consider the calculation assuming DCDW, but the similar calculation can be done with the more general condensate [94]. Here, we consider the more general condensate,

$$\Delta(\boldsymbol{r}) = \sigma(\boldsymbol{r}) + i\pi^3(\boldsymbol{r}) = m(\boldsymbol{r})e^{i\theta(\boldsymbol{r})}. \tag{2.2.31}$$

In that case, the Lagrangian of the NJL model within MFA takes the form,

$$\mathcal{L}_{\rm MF} =\bar{\psi}\left[i\not{D}-\frac{1}{2}(1+\gamma^5)\Delta(\boldsymbol{r})-\frac{1}{2}(1-\gamma^5)\Delta^*(\boldsymbol{r})\right]\psi-\frac{|\Delta|^2}{4G}, \tag{2.2.32}$$

where the 1-flavor case is considered for simplicity. Therefore the eigenvalue equation about the energy can be obtained as,

$$H(\Delta)\phi_k = E_k(\Delta)\phi_k, \tag{2.2.33}$$

where the Hamiltonian renders,

$$H = \boldsymbol{\alpha}\cdot(-i\boldsymbol{\nabla}+e\boldsymbol{A})+\gamma^0\left[\frac{1}{2}(1+\gamma^5)\Delta(\boldsymbol{r})+\frac{1}{2}(1-\gamma^5)\Delta^*(\boldsymbol{r})\right] \tag{2.2.34}$$

where $\boldsymbol{\alpha} = \gamma_0\boldsymbol{\gamma}$ and the Landau gauge is taken, $A^\mu = (0, 0, Bx, 0)$. After the CT transformation, $\psi \to i\gamma^5\gamma^0\psi^*$, the energy spectrum transforms as, $E_k(\Delta) \to -E_k(\Delta^*)$. It means that as long as $\Delta(\boldsymbol{r})$ is real, the positive and negative symmetry of the spectrum is preserved. Since we are interested in the case where the spectrum is asymmetric, pay attention only to the phase of $\Delta(\boldsymbol{r})$, and the amplitude is fixed at constant, $m(\boldsymbol{r}) \to m$, in the following. After the Weinberg transformation, $\psi(\boldsymbol{r}) \to \psi'(\boldsymbol{r}) = e^{-i\gamma_5\theta(\boldsymbol{r})/2}\psi(\boldsymbol{r})$, the Hamiltonian can be rewritten as,

$$H = \quad \boldsymbol{\alpha}\cdot(-i\boldsymbol{\nabla}+\boldsymbol{A})+\gamma^0 m-\gamma_5\boldsymbol{\gamma}\cdot\boldsymbol{\nabla}\theta(\boldsymbol{r})/2. \tag{2.2.35}$$

Since the energy spectrum can not be analytically obtained from that Hamiltonian, we represent η-invariant as the general form,

$$\eta_H = \lim_{s\to+0} \sum_k \mathrm{sign}(E_k)|E_k|^{-s}. \tag{2.2.36}$$

Using the Mellin transformation, η-invariant can be calculated as,

$$\begin{aligned}\eta_H &= \lim_{s\to+0} \frac{1}{\pi}\cos\left(s\frac{\pi}{2}\right)\sum_k \int_0^\infty d\omega\omega^{-s}\frac{E_k}{E_k^2+\omega^2} \\ &= \lim_{s\to+0} \frac{1}{\pi}\cos\left(s\frac{\pi}{2}\right)\int_0^\infty d\omega\omega^{-s}\int d^3\boldsymbol{r}\ \mathrm{tr}\left[\langle\boldsymbol{r}|\frac{1}{H-i\omega}|\boldsymbol{r}\rangle + c.c.\right].\end{aligned} \tag{2.2.37}$$

From the Hamiltonian (2.2.35), we can perform the derivative expansion of the integrand,

$$\begin{aligned}\langle\boldsymbol{r}|\frac{1}{H-i\omega}|\boldsymbol{r}\rangle =& -\langle\boldsymbol{r}|\gamma_0\frac{1}{S_A^{-1}(i\omega,\boldsymbol{r})+\gamma_5\boldsymbol{\gamma}\cdot\boldsymbol{\nabla}\theta(\boldsymbol{r})/2}|\boldsymbol{r}\rangle \\ =& -\int\frac{d^3\boldsymbol{p}}{(2\pi)^3}\gamma_0\tilde{S}_A(i\omega,\boldsymbol{p}) + \int\frac{d^3\boldsymbol{p}}{(2\pi)^3}\gamma_0\tilde{S}_A(i\omega,\boldsymbol{p})\frac{1}{2}\gamma_5\boldsymbol{\gamma}\cdot\boldsymbol{\nabla}\theta(\boldsymbol{r})\tilde{S}_A(i\omega,\boldsymbol{p})+\cdots,\end{aligned} \tag{2.2.38}$$

where S_A denotes the propagator, $S_A(i\omega,\boldsymbol{r}) = \frac{1}{i\omega\gamma_0+\boldsymbol{\gamma}\cdot(-i\boldsymbol{\nabla}+e\boldsymbol{A})-m}$. According to Ref. [99], the propagator by the momentum representation can be obtained as,

$$\tilde{S}_A(k) = i\exp\left[\frac{\boldsymbol{k}_\perp^2}{|eB|}\right]\sum_{n=0}^\infty\frac{(-1)^n}{k_0^2-k_3^2-m^2-2|eB|n}D_n, \tag{2.2.39}$$

where

$$\begin{aligned}D_n \equiv&(\gamma_0k_0-\gamma_3k_3+m)\left[\big(1-i\gamma_1\gamma_2\mathrm{sign}(eB)\big)L_n^0\left(\frac{2\boldsymbol{k}_\perp^2}{|eB|}\right)-\big(1+i\gamma_1\gamma_2\mathrm{sign}(eB)\big)L_n^0\left(\frac{2\boldsymbol{k}_\perp^2}{|eB|}\right)\right] \\ &+4\boldsymbol{\gamma}_\perp\cdot\boldsymbol{k}_\perp L_{n-1}^1\left(\frac{2\boldsymbol{k}_\perp^2}{|eB|}\right).\end{aligned} \tag{2.2.40}$$

From these equations, η_H can be calculated as,

$$\begin{aligned}\eta_H &= \lim_{s\to+0}\frac{1}{\pi}\cos\left(s\frac{\pi}{2}\right)\int_0^\infty d\omega\omega^{-s}\int d^3\boldsymbol{r}\frac{-eB}{2\pi}\frac{m^2}{(m^2+\omega^2)^{3/2}}\partial_z\theta(\boldsymbol{r}) \\ &= -\frac{eB}{2\pi^2}\int d^3\boldsymbol{r}\partial_z\theta(\boldsymbol{r}),\end{aligned} \tag{2.2.41}$$

It can be seen that if $\theta(\boldsymbol{r}) = qz$ is substituted, the case of DCDW (2.2.28) is reproduced. Note that the expansion parameter of the derivative expansion is $\nabla\theta(\boldsymbol{r})/m$, and it can not be applied in the case of $m < q/2$.

In the above calculation the magnetic field is taken in the z direction, but if it is taken in an arbitrary direction, the η-invariant can be calculated as,

$$\eta_H = -\frac{1}{2\pi^2}\int d^3\boldsymbol{r}\ e\boldsymbol{B}\cdot\boldsymbol{\nabla}\theta(\boldsymbol{r}). \tag{2.2.42}$$

Since that quantity means the anomalous particle number, the thermodynamic potential should have the anomalous term,

$$\Omega_{\rm anom} = -\frac{\mu}{4\pi^2 V}\int d^3\boldsymbol{r}\ e\boldsymbol{B}\cdot\boldsymbol{\nabla}\theta(\boldsymbol{r}), \tag{2.2.43}$$

which shows that the DCDW phase is most favorable when $\boldsymbol{q}//\boldsymbol{B}$.

Next, we review the calculation of chiral anomaly using the chiral perturbation theory [49] and see that its result is equivalent to the anomalous contribution derived from the asymmetry of the energy spectrum. In the QCD Lagrangian, when chiral limit is taken, the axial-vector current is classically preserved, $\partial^\mu(\bar{\psi}\gamma_\mu\gamma_5\psi) = 0$. However, including the quantum effects such as the quark loops the axial-vector current is not conserved. Specifically, the quark loops allow the decay process, $\pi^0 \to 2\gamma$, through the triangle diagram. Chiral anomaly is brought about by such diagram.

On the other hand, the chiral perturbation theory is one of the low energy effective theories of QCD described by the degree of freedom of Nambu-Goldstone bosons, where the quark degree of freedom is integrated out [100]. If we construct the Lagrangian of the chiral perturbation theory from the original QCD Lagrangian, symmetry must be preserved: the quantum effect of the quark loop can not be considered and $\pi^0 \to 2\gamma$ decay can not be described. Therefore, we should add a term that explicitly breaks the chiral symmetry called the Wess-Zumino-Witten (WZW) term [101, 102], to incorporate the effect of the chiral anomaly. The Lagrangian in the chiral perturbation theory renders,

$$\mathcal{L} = \frac{f_\pi^2}{4}\ {\rm tr}\left[D_\mu\Sigma^\dagger D^\mu\Sigma\right], \tag{2.2.44}$$

where the covariant derivative is represented as,

$$D_\mu\Sigma = \partial_\mu\Sigma + ieA_\mu[Q,\Sigma], \tag{2.2.45}$$

and A_μ denotes the electromagnetic field applied as the external field and $Q = {\rm diag}(2/3, -1/3)$.

In the two-flavor case, Σ is represented by the σ and π mesons as,

$$\Sigma = \frac{1}{f_\pi}(\sigma + i\tau^a\pi^a), \tag{2.2.46}$$

where $f_\pi^2 = \sigma^2 + \pi^a\pi^a$. The symmetries of the Lagrangian are global $SU_L(2)\times SU_R(2)$ and local $U_{\rm EM}(1)$. Next, we define $L_\mu \equiv \Sigma\partial_\mu\Sigma^\dagger, R_\mu \equiv \partial_\mu\Sigma^\dagger\Sigma$ to introduce the WZW term. Assuming that μ is finite, we consider the fictious gauge field, $A_\mu^B = (\mu, 0, 0, 0)$, coupling with

the baryon current. Using these quantities, the WZW term can be obtained as [103],

$$S_{\rm WZW}[\Sigma, A_\mu, A_\mu^B] = S_{\rm WZW}[0] + \frac{N_c\epsilon^{\mu\nu\alpha\beta}}{48\pi^2}\int d^4x\Big(eA_\mu {\rm tr}\left[QL_\nu L_\alpha L_\beta + QR_\nu R_\alpha R_\beta\right] \\ - ie^2F_{\mu\nu}A_\alpha {\rm tr}\left[Q^2L_\beta + Q^2R_\beta + \frac{1}{2}Q\Sigma Q\partial_\beta\Sigma^\dagger - \frac{1}{2}Q\Sigma^\dagger Q\partial_\beta\Sigma\right]\Big) - \int d^4x A_\mu^B j_B^\mu. \tag{2.2.47}$$

The first term represents the WZW term without the gauge field,

$$S_{\rm WZW}[0] = \frac{iN_c}{240\pi^2}\int d^5x\,\epsilon^{ijklm}{\rm tr}[L_iL_jL_kL_lL_m], \tag{2.2.48}$$

which vanishes in the two-flavor case. The second term denotes the term added when there is the electromagnetic field, and the third term represents the term added when there is μ. Note that, Σ does not transform under the $U_B(1)$ transformation since mesons do not have the baryon number. However, A_μ^B couple to Σ through the quark loops, which are known as the Goldstone-Wilczek baryon current j_B^μ. Therefore, the WZW term can be obtained as,

$$S_{\rm WZW}[\Sigma, A_\mu, A_\mu^B] = \frac{N_c\epsilon^{\mu\nu\alpha\beta}}{48\pi^2}\int d^4x\, eA_\mu\left(\frac{2}{3f_\pi^4}\epsilon^{abcd}\varphi^a\partial_\nu\varphi^b\partial_\alpha\varphi^c\partial_\beta\varphi^d + \frac{2e}{f_\pi^2}\partial_\nu\left[A_\alpha\left(\varphi^3\partial_\beta\varphi^0 - \varphi^0\partial_\beta\varphi^3\right)\right]\right) \\ - \int d^4x A_\mu^B j_B^\mu, \tag{2.2.49}$$

where $\varphi^0 = \sigma,\ \vec{\varphi} = \vec{\pi}$.

Next we calculate the Goldstone-Wilczek baryon current in the WZW term. It is used by the result obtained from the linear sigma model [102, 104]. The Lagrangian of the linear sigma model takes the form,

$$\mathcal{L} = \bar{\psi}\left(i\not{\partial} + \sigma + i\gamma_5\vec{\tau}\cdot\vec{\pi}\right)\psi, \tag{2.2.50}$$

and we put $\sigma^2+\vec{\pi}^2 = \varphi^a\varphi^a = f_\pi^2$. When the expected value of the baryon current is calculated from that Lagrangian, the contribution of the diagram including the quark loop shown in Fig. 2.11 remains and it can be obtained as,

$$j_B^\mu = \langle\bar{\psi}\gamma^\mu\psi\rangle \\ = -\frac{N_c}{12f_\pi^4}\epsilon^{\mu\nu\alpha\beta}\epsilon^{abcd}\varphi^a\partial_\nu\varphi^b\partial_\alpha\varphi^c\partial_\beta\varphi^d - \frac{eN_c}{4f_\pi^2}\epsilon^{\mu\nu\alpha\beta}\partial_\nu\left[A_\alpha\left(\varphi^3\partial_\beta\varphi^0 - \varphi^0\partial_\beta\varphi^3\right)\right]. \tag{2.2.51}$$

Therefore the WZW term (2.2.49) can be obtained as

$$S_{\rm WZW}[\Sigma, A_\mu, A_\mu^B] = -\int d^4x\left(A_\mu^B + \frac{e}{2}A_\mu\right)j_B^\mu \tag{2.2.52}$$

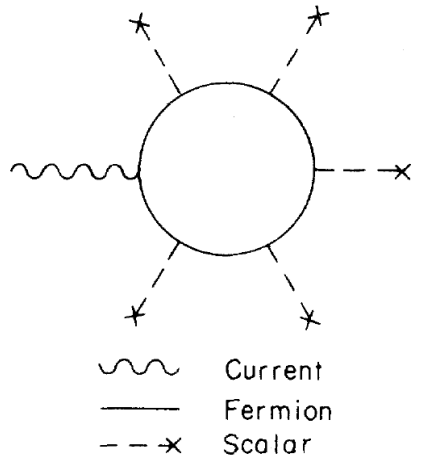

Figure 2.11: The schematic diagram of Eq. (2.2.51). (The figure is taken from Ref. [104].)

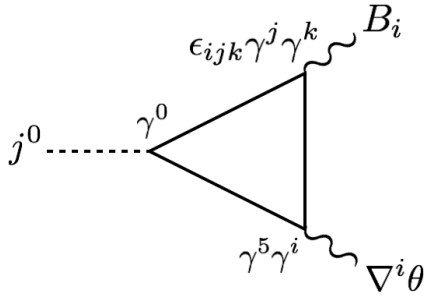

Figure 2.12: The triangle diagram contributing to the anomalous particle number density. The solid line represents the quark propagator.

Now that we consider the general form of the condensate limited to σ, π^3 such as Eq. (2.2.31), $\varphi^a = \big(f_\pi \cos\theta(\boldsymbol{r}), 0, 0, f_\pi \sin\theta(\boldsymbol{r})\big)$. Without the electric field, the WZW term can be reduced as,

$$\begin{aligned} S_{\rm WZW}[\Sigma, A_\mu, A_\mu^B] &= -\frac{eN_c}{4\pi^2}\int d^4x \left(A_\mu^B + \frac{e}{2}A_\mu\right)\epsilon^{\mu\nu\alpha\beta}\partial_\nu(A_\alpha\partial_\beta\theta) \\ &= -\frac{N_c}{4\pi^2}\int d^4x\ \mu e\boldsymbol{B}\cdot\boldsymbol{\nabla}\theta. \end{aligned} \tag{2.2.53}$$

It is confirmed that that term coincides with the anomalous contribution from the spectral asymmetry (2.2.43). Therefore in the case of $|\boldsymbol{\nabla}\theta(\boldsymbol{r})| \ll m$, the anomalous particle number density is also interpreted as the contribution of the triangle diagram as shown in Fig. 2.12. Furthermore in the case of DCDW ($\theta = qz$), we can see that the WZW term corresponds to the topological part of η-invariant (2.2.30).

Chapter 3

Magnetic properties of quark matter in the inhomogeneous chiral phase

In this chapter we analyze the response of quark matter to the weak external magnetic field [51]. In particular, we show the dual chiral density wave (DCDW) phase has spontaneous magnetization by expanding the thermodynamic potential with respect to the magnetic field and discuss the nature of the phase transition.

3.1 Expansion of the thermodynamic potential by the magnetic field

We use the two-flavor Nambu-Jona-Lasinio (NJL) model within the mean-field approximation (MFA). It is sufficient to consider each flavor case because Lagrangian is diagonalized about the flavors. For the DCDW case, the thermodynamic potential in the presence of the magnetic field is already obtained in Eq. (2.2.14), where the external magnetic field is taken to be along the z axis. The energy spectrum is also given in the previous section in Eq. (2.2.9). To investigate the response of quark matter to the weak magnetic field B, the thermodynamic potential is expanded around $B = 0$,

$$\Omega(\mu, T, B\,; m, q) = \Omega^{(0)}(\mu, T\,; m, q) + eB\Omega^{(1)}(\mu, T\,; m, q) + (eB)^2\,\Omega^{(2)}(\mu, T\,; m, q)\cdots, \tag{3.1.1}$$

where e denotes the elementary charge.

First of all, we take the sum over the Landau levels to evaluate the thermodynamic potential because it can not be expanded by the magnetic field before taking the sum. However, the form (2.2.14) is not appropriate to take the summation. So we return to the form before

taking Matsubara sum,

$$\Omega = \frac{m^2}{4G} - T\frac{eBN_c}{4\pi}\int\frac{dp}{2\pi}\sum_k\sum_{n\geq 1,\zeta,\epsilon}\ln[\omega_k^2 + (E^{\rm hLL}_{n\zeta\epsilon} - \mu)^2] \\ - T\frac{eBN_c}{4\pi}\int\frac{dp}{2\pi}\sum_k\sum_{\epsilon}\ln[\omega_k^2 + (E^{\rm LLL}_{\epsilon} - \mu)^2], \tag{3.1.2}$$

where ω_k denotes the Matsubara frequency, $\omega_k = \pi T(2k+1)$. For the calculation of the thermodynamic potential, we must carefully treat the effect of chiral anomaly due to spectral asymmetry of the lowest Landau level (LLL), which gives rise to anomalous particle number proportional to eB as shown in the previous chapter. To correctly evaluate spectral asymmetry, we introduce the regularization about the energy and the thermodynamic potential with the regulator renders,

$$\begin{aligned}\Omega_s &= \frac{m^2}{4G} - T\frac{eBN_c}{4\pi}\int\frac{dp}{2\pi}\sum_k\sum_{\epsilon}\left|E^{\rm LLL}_{\epsilon}\right|^{-s}\ln\left[\omega_k^2 + \left(E^{\rm LLL}_{\epsilon} - \mu\right)^2\right] \\ &\quad - T\frac{eBN_c}{4\pi}\int\frac{dp}{2\pi}\sum_k\sum_{n\geq 1,\zeta}\left(E^{\rm hLL}_{n\zeta\epsilon=+1}\right)^{-s}\ln\left\{\left[\omega_k^2 + (E^{\rm hLL}_{n,\zeta,\epsilon=+1} - \mu)^2\right]\left[\omega_k^2 + (E^{\rm hLL}_{n,\zeta,\epsilon=+1} + \mu)^2\right]\right\} \\ &\equiv \frac{m^2}{4G} + \Omega_s^{\rm LLL} + \Omega_s^{\rm hLL},\end{aligned} \tag{3.1.3}$$

where the second term represents the contribution of LLL and the third term does that of the higher Landau levels (hLLs). Taking the limit of $s \to 0$, the original thermodynamic potential is recovered, $\Omega = \lim_{s\to+0}\Omega_s$. $\Omega_s^{\rm hLL}$ can be calculated as,

$$\begin{aligned}\Omega_s^{\rm hLL} &= -T\frac{eBN_c}{4\pi}\int\frac{dp}{2\pi}\sum_k\sum_{n\geq 1,\zeta}\left(E^{\rm hLL}_{n\zeta\epsilon=+1}\right)^{-s}\ln\Big\{\left[\omega_k + i(E^{\rm hLL}_{n,\zeta,\epsilon=+1} - \mu)\right]\left[\omega_k - i(E^{\rm hLL}_{n,\zeta,\epsilon=+1} - \mu)\right] \\ &\qquad\qquad \times\left[\omega_k + i(E^{\rm hLL}_{n,\zeta,\epsilon=+1} + \mu)\right]\left[\omega_k - i(E^{\rm hLL}_{n,\zeta,\epsilon=+1} + \mu)\right]\Big\} \\ &= -T\frac{eBN_c}{2\pi}\int\frac{dp}{2\pi}\sum_k\sum_{n\geq 1,\zeta}\left(\omega_\zeta^2 + 2eBn\right)^{-s/2}\ln\left[(\omega_k + i\mu)^2 + \omega_\zeta^2 + 2eBn\right],\end{aligned} \tag{3.1.4}$$

where $\omega_\pm \equiv \pm\sqrt{m^2+p^2} + q/2 (= E^{\rm LLL}_{\epsilon=\pm})$. To remove the divergence, we separate the thermodynamic potential as,

$$\begin{aligned}\Omega &= \Omega(q=0,m=0) + \left(\Omega - \Omega(q=0,m=0)\right) \\ &= \Omega(q=0,m=0) + \Delta\Omega.\end{aligned} \tag{3.1.5}$$

$\Omega(q=0,m=0)$ contains divergence, but it is a constant to just shift the energy not dependent on the order parameters. Therefore, $\Delta\Omega$ is analyzed in the following. $\Delta\Omega_s^{\rm LLL}$ and

$\Delta\Omega_s^{\rm hLL}$ render,

$$\Delta\Omega_s^{\rm LLL} = -T\frac{eBN_c}{4\pi^2}\int_0^\infty dp \sum_k \sum_\epsilon \left\{ |\omega_\epsilon|^{-s} \ln\left[\omega_k^2 + (\omega_\epsilon - \mu)^2\right] - p^{-s}\ln\left[\omega_k^2 + (\epsilon p - \mu)^2\right]\right\}, \tag{3.1.6}$$

$$\Delta\Omega_s^{\rm hLL} = -T\frac{eBN_c}{2\pi^2}\int_0^\infty dp \sum_k \sum_{n\geq 1,\zeta} \Bigg\{ \left(\omega_\zeta^2 + 2eBn\right)^{-s/2} \ln\left[(\omega_k + i\mu)^2 + \omega_\zeta^2 + 2eBn\right] - (p^2 + 2eBn)^{-s/2}\ln\left[(\omega_k + i\mu)^2 + p^2 + 2eBn\right]\Bigg\}. \tag{3.1.7}$$

The sum over the Landau levels in $\Delta\Omega_s^{\rm hLL}$ can be separately taken for each sign of ω_k. When $\omega_k > 0$, the sum can be taken as,

$$\begin{aligned}
&- T\frac{eBN_c}{2\pi^2}\int_0^\infty dp \sum_{k=0}^\infty \sum_{n\geq 1,\zeta} \Bigg\{ \left(\omega_\zeta^2 + 2eBn\right)^{-s/2} \ln\left[(\omega_k + i\mu)^2 + \omega_\zeta^2 + 2eBn\right] \\
&\qquad - (p^2 + 2eBn)^{-s/2}\ln\left[(\omega_k + i\mu)^2 + p^2 + 2eBn\right]\Bigg\} \\
&= -T\frac{eBN_c}{2\pi^2}\int_0^\infty dp \sum_{k=0}^\infty \sum_{n\geq 1,\zeta} \frac{1}{\Gamma(s/2)}\int_0^\infty \frac{d\tau}{\tau}\int_0^\infty dx\, x^{s/2-1} e^{-\tau\left[2\mu\omega_k - i\left(\omega_k^2 - \mu^2\right)\right] + 2eB(i\tau - x)n} \\
&\qquad\qquad \times \left[-e^{(i\tau-x)\omega_\zeta^2} + e^{(i\tau-x)p^2}\right] \\
&= -T\frac{eBN_c}{2\pi^2}\int_0^\infty dp \sum_{k=0}^\infty \sum_{\zeta=\pm} \frac{1}{\Gamma(s/2)}\int_0^\infty \frac{d\tau}{\tau}\int_0^\infty dx\, x^{s/2-1} e^{-\tau\left[2\mu\omega_k - i\left(\omega_k^2 - \mu^2\right)\right]} \\
&\qquad\qquad \times \left[-e^{(i\tau-x)\omega_\zeta^2} + e^{(i\tau-x)p^2}\right] \frac{e^{2(i\tau-x)eB}}{1 - e^{2(i\tau-x)eB}} \\
&= -T\frac{N_c}{4\pi^2}\int_0^\infty dp \sum_{k=0}^\infty \sum_{\zeta=\pm} \frac{1}{\Gamma(s/2)}\int_0^\infty \frac{d\tau}{\tau}\int_0^\infty dx\, x^{s/2-1} e^{-\tau\left[2\mu\omega_k - i\left(\omega_k^2 - \mu^2\right)\right]} \left[e^{(i\tau-x)\omega_\zeta^2} - e^{(i\tau-x)p^2}\right] \\
&\qquad\qquad \times \left[\frac{1}{i\tau - x} + eB + \frac{1}{3}(i\tau - x)(eB)^2 + \mathcal{O}\left((eB)^3\right)\right]
\end{aligned} \tag{3.1.8}$$

On the other hand, when $\omega_k < 0$, that can be taken in the similar way as,

$$
\begin{aligned}
&- T\frac{eBN_c}{2\pi^2}\int_0^\infty dp \sum_{k=-1}^{-\infty}\sum_{n\geq 1,\zeta}\Big\{ \left(\omega_\zeta^2 + 2eBn\right)^{-s/2} \ln\left[(\omega_k + i\mu)^2 + \omega_\zeta^2 + 2eBn\right] \\
&\qquad\qquad - (p^2 + 2eBn)^{-s/2} \ln\left[(\omega_k + i\mu)^2 + p^2 + 2eBn\right]\Big\} \\
&= T\frac{N_c}{4\pi^2}\int_0^\infty dp \sum_{k=0}^{\infty}\sum_{\zeta=\pm}\frac{1}{\Gamma(s/2)}\int_0^\infty \frac{d\tau}{\tau}\int_0^\infty dx\, x^{s/2-1} e^{-\tau\left[2\mu\omega_k + i\left(\omega_k^2 - \mu^2\right)\right]}\left[e^{-(i\tau+x)\omega_\zeta^2} - e^{-(i\tau+x)p^2}\right] \\
&\qquad\qquad \times\left[\frac{1}{i\tau + x} - eB + \frac{1}{3}(i\tau + x)(eB)^2 + \mathcal{O}\left((eB)^3\right)\right] \qquad (3.1.9)
\end{aligned}
$$

Now the expansion about eB can be allowed. Therefore when we expand $\Delta\Omega_s$ as $\Delta\Omega_s = \frac{m^2}{4G} + \Delta\Omega_s^{(0)} + \Delta\Omega_s^{(1)} eB + \Delta\Omega_s^{(2)}(eB)^2 + \mathcal{O}\left((eB)^3\right)$, the coefficients can be obtained as,

$$
\begin{aligned}
\Delta\Omega_s^{(0)} &= -\frac{N_c T}{4\pi^2}\int_0^\infty dp \sum_{k=0}^{\infty}\sum_{\zeta=\pm}\frac{1}{\Gamma(s/2)}\int_0^\infty \frac{d\tau}{\tau}\int_0^\infty dx\, x^{s/2-1} e^{-2\tau\mu\omega_k} \\
&\quad\times\left\{\frac{1}{i\tau - x} e^{i\tau\left(\omega_k^2 - \mu^2\right)}\left[e^{(i\tau - x)\omega_\zeta^2} - e^{(i\tau - x)p^2}\right] - \frac{1}{i\tau + x} e^{-i\tau\left(\omega_k^2 - \mu^2\right)}\left[e^{-(i\tau+x)\omega_\zeta^2} - e^{-(i\tau+x)p^2}\right]\right\} \qquad (3.1.10) \\
\Delta\Omega_s^{(1)} &= -\frac{N_c T}{4\pi^2}\int_0^\infty dp \sum_{k=0}^{\infty}\sum_{\zeta=\pm}\frac{1}{\Gamma(s/2)}\int_0^\infty \frac{d\tau}{\tau}\int_0^\infty dx\, x^{s/2-1} e^{-2\tau\mu\omega_k} \\
&\quad\times\left\{e^{i\tau\left(\omega_k^2 - \mu^2\right)}\left[e^{(i\tau - x)\omega_\zeta^2} - e^{(i\tau - x)p^2}\right] + e^{-i\tau\left(\omega_k^2 - \mu^2\right)}\left[e^{-(i\tau+x)\omega_\zeta^2} - e^{-(i\tau+x)p^2}\right]\right\} \\
&\quad - \frac{N_c T}{4\pi^2}\int_0^\infty dp \sum_{k=-\infty}^{\infty}\sum_{\epsilon}\left\{|\omega_\epsilon|^{-s}\ln\left[\omega_k^2 + (\omega_\epsilon - \mu)^2\right] - p^{-s}\ln\left[\omega_k^2 + (\epsilon p - \mu)^2\right]\right\} \\
&\equiv \Delta\Omega_{s,\mathrm{hLL}}^{(1)} + \Delta\Omega_{s,\mathrm{LLL}}^{(1)} \qquad (3.1.11) \\
\Delta\Omega_s^{(2)} &= -\frac{N_c T}{12\pi^2}\int_0^\infty dp \sum_{k=0}^{\infty}\sum_{\zeta=\pm}\frac{1}{\Gamma(s/2)}\int_0^\infty \frac{d\tau}{\tau}\int_0^\infty dx\, x^{s/2-1} e^{-2\tau\mu\omega_k} \\
&\quad\times\left\{(i\tau - x)e^{i\tau\left(\omega_k^2 - \mu^2\right)}\left[e^{(i\tau - x)\omega_\zeta^2} - e^{(i\tau - x)p^2}\right] - (i\tau + x)e^{-i\tau\left(\omega_k^2 - \mu^2\right)}\left[e^{-(i\tau+x)\omega_\zeta^2} - e^{-(i\tau+x)p^2}\right]\right\} \qquad (3.1.12)
\end{aligned}
$$

We can see that LLL contributes only to $\Delta\Omega_s^{(1)}$ because the energy spectrum does not depend on B and the B dependence only emerges through the Landau degeneracy. On the other hand, hLLs contribute to the all order terms of eB [51].

From Eq. (3.1.10), $\Delta\Omega_s^{(0)}$ can be calculated as,

$$\begin{aligned}
\Delta\Omega_s^{(0)} &= -\frac{N_c T}{4\pi^2}\int_0^\infty dp \sum_{k=0}^{\infty}\sum_{\zeta=\pm}\frac{1}{\Gamma(s/2)}\int_0^\infty \frac{d\tau}{\tau}\int_0^\infty dx\, x^{s/2-1}e^{-2\tau\mu\omega_k} \\
&\quad\times\sum_{n=0}^{\infty}\left\{\frac{x^n}{(i\tau)^{n+1}}e^{i\tau\left(\omega_k^2-\mu^2\right)}\left[e^{(i\tau-x)\omega_\zeta^2}-e^{(i\tau-x)p^2}\right]\right. \\
&\qquad\left.-\frac{(-x)^n}{(i\tau)^{n+1}}e^{-i\tau\left(\omega_k^2-\mu^2\right)}\left[e^{-(i\tau+x)\omega_\zeta^2}-e^{-(i\tau+x)p^2}\right]\right\} \\
&= -\frac{N_c T}{4\pi^2}\int_0^\infty dp \sum_{k=0}^{\infty}\sum_{\zeta=\pm}\sum_{n=0}^{\infty}\int_0^\infty \frac{d\tau}{\tau(i\tau)^{n+1}}e^{-2\tau\mu\omega_k}\frac{\Gamma(n+s/2)}{\Gamma(s/2)} \\
&\quad\times\left\{\left|\omega_\zeta\right|^{-2n-s}e^{i\tau\left(\omega_k^2-\mu^2-\omega_\zeta^2\right)}-p^{-2n-s}e^{i\tau\left(\omega_k^2-\mu^2-p^2\right)}\right. \\
&\qquad\left.-(-1)^n\left[\left|\omega_\zeta\right|^{-2n-s}e^{-i\tau\left(\omega_k^2-\mu^2-\omega_\zeta^2\right)}-p^{-2n-s}e^{-i\tau\left(\omega_k^2-\mu^2-p^2\right)}\right]\right\}. \qquad (3.1.13)
\end{aligned}$$

We can see that only term at $n=0$ survives in the limit $s\to 0$ and $\Delta\Omega^{(0)}=\lim_{s\to+0}\Delta\Omega_s^{(0)}$ renders,

$$\Delta\Omega^{(0)} = -\frac{N_c T}{2\pi^2}\int_0^\infty dp\sum_{k=0}^{\infty}\sum_{\zeta=\pm}\int_0^\infty\frac{d\tau}{\tau^2}e^{-2\tau\mu\omega_k}\left\{\sin\left[\tau\left(\omega_k^2-\mu^2-\omega_\zeta^2\right)\right]-\sin\left[\tau\left(\omega_k^2-\mu^2-p^2\right)\right]\right\} \qquad (3.1.14)$$

After some calculation, it is confirmed that $\Delta\Omega^{(0)}$ coincides with the thermodynamic potential in the absence of the magnetic field (2.1.33) except for the irrelevant constant term. Therefore introducing the proper time regularization (PTR) as in the previous chapter, $\Delta\Omega^{(0)}$ takes the form,

$$\Delta\Omega^{(0)} = \Delta\Omega_{\rm vac}^{(0)} + \Delta\Omega_{\mu}^{(0)} + \Delta\Omega_{\rm T}^{(0)}, \qquad (3.1.15)$$

where

$$\Delta\Omega_{\rm vac}^{(0)} \equiv \frac{N_c}{8\pi^{3/2}}\int\frac{dp_z}{2\pi}\int_{1/\Lambda^2}^\infty\frac{d\tau}{\tau^{5/2}}\left[e^{-\tau\left(\sqrt{p_z^2+m^2}+q/2\right)^2}+e^{-\tau\left(\sqrt{p_z^2+m^2}-q/2\right)^2}\right]+\text{const.}, \qquad (3.1.16)$$

$$\Delta\Omega_{\mu}^{(0)} \equiv N_c\int\frac{\mathrm{d}^3\boldsymbol{p}}{(2\pi)^3}\sum_{s=\pm}\left(E_s-\mu\right)\theta\left(\mu-E_s\right)+\text{const.}, \qquad (3.1.17)$$

$$\Delta\Omega_{\rm T}^{(0)} \equiv -N_c T\sum_{s=\pm}\int\frac{d^3\boldsymbol{p}}{(2\pi)^3}\left(\ln\left[1+e^{-\beta|E_s-\mu|}\right]+\ln\left[1+e^{-\beta(E_s+\mu)}\right]\right)+\text{const.}, \qquad (3.1.18)$$

and $E_\pm$ represents the energy spectrum in the absence of the magnetic field, $E_\pm^2\equiv m^2+\boldsymbol{p}^2+q^2/4\pm q\sqrt{p_z^2+m^2}$.

From Eq. (3.1.12), $\Delta\Omega_s^{(2)}$ can be calculated as,

$$\begin{aligned}\Delta\Omega_s^{(2)} = -\frac{N_c T}{12\pi^2}\int_0^\infty dp \sum_{k=0}^{\infty}\sum_{\zeta=\pm}\int_0^\infty \frac{d\tau}{\tau} e^{-2\tau\mu\omega_k}\Bigg\{ &\left(i\tau|\omega_\zeta|^{-s} - \frac{\Gamma(1+s/2)}{\Gamma(s/2)}(\omega_\zeta^2)^{-1-s/2}\right) e^{i\tau\left(\omega_k^2-\mu^2-\omega_\zeta^2\right)} \\ &- \left(i\tau\, p^{-s} - \frac{\Gamma(1+s/2)}{\Gamma(s/2)}p^{-2-s}\right) e^{i\tau\left(\omega_k^2-\mu^2-p^2\right)} \\ &- \left(i\tau|\omega_\zeta|^{-s} + \frac{\Gamma(1+s/2)}{\Gamma(s/2)}(\omega_\zeta^2)^{-1-s/2}\right) e^{-i\tau\left(\omega_k^2-\mu^2-\omega_\zeta^2\right)} \\ &+ \left(i\tau\, p^{-s} + \frac{\Gamma(1+s/2)}{\Gamma(s/2)}p^{-2-s}\right) e^{-i\tau\left(\omega_k^2-\mu^2-p^2\right)}\Bigg\}.\end{aligned} \tag{3.1.19}$$

Therefore $\Delta\Omega^{(2)} = \lim_{s\to+0}\Delta\Omega_s^{(2)}$ renders,

$$\begin{aligned}\Delta\Omega^{(2)} =& \frac{N_c T}{6\pi^2}\int_0^\infty dp \sum_{k=0}^{\infty}\sum_{\zeta=\pm}\int_0^\infty d\tau\, e^{-2\tau\mu\omega_k}\left\{\sin\left[\tau\left(\omega_k^2-\mu^2-\omega_\zeta^2\right)\right] - \sin\left[\tau\left(\omega_k^2-\mu^2-p^2\right)\right]\right\} \\ =& \frac{N_c T}{12\pi}\int\frac{dp}{2\pi}\sum_{k=-\infty}^{\infty}\sum_{\epsilon=\pm}\left[\frac{1}{(\omega_k+i\mu)^2+\omega_\epsilon^2} - \frac{1}{(\omega_k+i\mu)^2+p^2}\right] \\ =& -\frac{1}{12\pi^2}\int_0^\infty dp\Bigg[\frac{1}{2\omega_+}\left(\frac{1}{e^{\beta(\mu+\omega_+)}+1} - \frac{1}{e^{\beta(\mu-\omega_+)}+1}\right) + \frac{1}{2\omega_-}\left(\frac{1}{e^{\beta(\mu+\omega_-)}+1} - \frac{1}{e^{\beta(\mu-\omega_-)}+1}\right) \\ &- \frac{1}{p}\left(\frac{1}{e^{\beta(\mu+p)}+1} - \frac{1}{e^{\beta(\mu-p)}+1}\right)\Bigg].\end{aligned} \tag{3.1.20}$$

It is confirmed that $\Delta\Omega^{(2)}$ does not have the divergence.

3.1.1 Anomaly appearing in $\Delta\Omega^{(1)}$

For the evaluation of $\Delta\Omega_s^{(1)}$, we must carefully treat the limit, $s\to 0$, because $\Delta\Omega_s^{(1)}$ includes the contribution of LLL, which is asymmetric about zero. From Eq. (3.1.11), $\Delta\Omega_{s,\mathrm{hLL}}^{(1)}$ can be

calculated as,

$$\begin{aligned}\Delta\Omega^{(1)}_{s,\mathrm{hLL}} =& -\frac{N_c T}{4\pi^2}\int_0^\infty dp \sum_{k=0}^{\infty}\sum_{\zeta=\pm}\int_0^\infty \frac{d\tau}{\tau}\Big\{ |\omega_\zeta|^{-s}\left[e^{-\tau\left[2\mu\omega_k - i\left(\omega_k^2-\mu^2+\omega_\zeta^2\right)\right]} + e^{-\tau\left[2\mu\omega_k + i\left(\omega_k^2-\mu^2+\omega_\zeta^2\right)\right]}\right] \\ & - p^{-s}\left[e^{-\tau\left[2\mu\omega_k - i\left(\omega_k^2-\mu^2+p^2\right)\right]} + e^{-\tau\left[2\mu\omega_k + i\left(\omega_k^2-\mu^2+p^2\right)\right]}\right]\Big\} \\ =& \frac{N_c T}{4\pi^2}\int_0^\infty dp \sum_{k=-\infty}^{\infty}\sum_{\zeta=\pm}\left\{|\omega_\zeta|^{-s}\ln\left[(\omega_k+i\mu)^2+\omega_\zeta^2\right] - p^{-s}\ln\left[(\omega_k+i\mu)^2+p^2\right]\right\} \\ =& \frac{N_c T}{8\pi^2}\int_0^\infty dp \sum_{k=-\infty}^{\infty}\sum_{\zeta=\pm}|\omega_\zeta|^{-s}\left\{\ln\left[\omega_k^2+(\omega_\zeta+\mu)^2\right]+\ln\left[\omega_k^2+(\omega_\zeta-\mu)^2\right]\right\} \\ & - \frac{N_c T}{4\pi^2}\int_0^\infty dp \sum_{k=-\infty}^{\infty} p^{-s}\left\{\ln\left[\omega_k^2+(p+\mu)^2\right]+\ln\left[\omega_k^2+(p-\mu)^2\right]\right\}. \end{aligned} \tag{3.1.21}$$

We can see that the second term is independent of m, q in $\Delta\Omega^{(1)}_{s,\mathrm{hLL}}$ cancel out the second term in $\Delta\Omega^{(1)}_{s,\mathrm{LLL}}$ (3.1.6). Therefore we drop the constant part in the following. If we sum up the Matsubara frequency, $\Delta\Omega^{(1)}_{s,\mathrm{hLL}}$ can be separated into the vacuum part, density-dependent part and temperature-dependent part, $\Delta\Omega^{(1)}_{s,\mathrm{hLL}} = \Delta\Omega^{(1),\mathrm{vac}}_{s,\mathrm{hLL}} + \Delta\Omega^{(1),\mu}_{s,\mathrm{hLL}} + \Delta\Omega^{(1),T}_{s,\mathrm{hLL}}$,which can be given as,

$$\Delta\Omega^{(1),\mathrm{vac}}_{s,\mathrm{hLL}} = \frac{N_c}{4\pi^2}\int_0^\infty dp \sum_{\zeta=\pm}|\omega_\zeta|^{-s}|\omega_\zeta|, \tag{3.1.22}$$

$$\begin{aligned}\Delta\Omega^{(1),\mu}_{s,\mathrm{hLL}} =& \frac{N_c}{8\pi^2}\int_0^\infty dp \sum_{\zeta=\pm}|\omega_\zeta|^{-s}\left(|\omega_\zeta+\mu|+|\omega_\zeta-\mu|-2|\omega_\zeta|\right) \\ =& \frac{N_c}{4\pi^2}\int_0^\infty dp \sum_{\zeta=\pm}|\omega_\zeta|^{-s}\left[(\omega_\zeta+\mu)\,\theta(-\omega_\zeta)\theta(\omega_\zeta+\mu)+(\mu-\omega_\zeta)\,\theta(\omega_\zeta)\theta(\mu-\omega_\zeta)\right], \end{aligned} \tag{3.1.23}$$

$$\Delta\Omega^{(1),T}_{s,\mathrm{hLL}} = \frac{N_c T}{4\pi^2}\int_0^\infty dp \sum_{\zeta=\pm}|\omega_\zeta|^{-s}\left\{\ln\left(1+e^{-\beta|\omega_\zeta+\mu|}\right)+\ln\left(1+e^{-\beta|\omega_\zeta-\mu|}\right)\right\}. \tag{3.1.24}$$

We find that they are the even functions of q.

$\Delta\Omega^{(1)}_{s,\mathrm{LLL}}$ can be also separated into three parts after the summation about the Matsubara

frequency,

$$\Delta\Omega^{(1),\mathrm{vac}}_{s,\mathrm{LLL}} = -\frac{N_c}{4\pi^2}\int_0^\infty dp \sum_{\zeta=\pm} |\omega_\zeta|^{-s} |\omega_\zeta| \,, \tag{3.1.25}$$

$$\begin{aligned}\Delta\Omega^{(1),\mu}_{s,\mathrm{LLL}} =& -\frac{N_c}{4\pi^2}\int_0^\infty dp \sum_{\zeta=\pm} |\omega_\zeta|^{-s} \left(|\omega_\zeta - \mu| - |\omega_\zeta|\right) \\ =& -\frac{N_c}{2\pi^2}\int_0^\infty dp \sum_{\zeta=\pm} |\omega_\zeta|^{-s} \left(\mu - \omega_\zeta\right)\theta(\omega_\zeta)\theta(\mu-\omega_\zeta) + \frac{\mu N_c}{4\pi}\eta_H(s),\end{aligned} \tag{3.1.26}$$

$$\Delta\Omega^{(1),T}_{s,\mathrm{LLL}} = -\frac{N_c T}{2\pi^2}\int_0^\infty dp \sum_{\zeta=\pm} |\omega_\zeta|^{-s} \ln\left(1+e^{-\beta|\omega_\zeta-\mu|}\right), \tag{3.1.27}$$

where $\eta_H(s)$ is defined as,

$$\eta_H(s) \equiv \int \frac{dp}{2\pi}\sum_\zeta |\omega_\zeta|^{-s}\mathrm{sign}(\omega_\zeta). \tag{3.1.28}$$

We can see that the density dependent term $\Omega^{(1),\mathrm{LLL}}_\mu$ includes the anomalous contribution, $\frac{\mu N_c}{4\pi}\eta_H(s)$, caused by spectral asymmetry. The η-invariant, η_H, can be calculated as in the previous chapter,

$$\begin{aligned}\eta_H \equiv& \lim_{s\to+0}\eta_H(s) \\ =& \begin{cases} -\frac{q}{\pi} & (m > q/2) \\ -\frac{q}{\pi} + \frac{2}{\pi}\sqrt{q^2/4 - m^2} & (m < q/2) \end{cases}.\end{aligned} \tag{3.1.29}$$

When $m > q/2$, this quantity agrees with the contribution of the chiral anomaly represented by the gauged Wess-Zumino-Witten (WZW) term [49]. The gauged WZW term does not depend on m as shown in Eq. (2.2.53) but η_H vanishes in the limit, $m \to 0$.

It can be seen that from Eq. (3.1.22) and (3.1.25) the vacuum parts cancel each other, $\Delta\Omega^{(1),\mathrm{vac}}_{s,\mathrm{hLL}} = -\Delta\Omega^{(1),\mathrm{vac}}_{s,\mathrm{LLL}}$. Thus $\Delta\Omega^{(1)}_s$ does not diverge without any regularization. In this step, we can safely take the limit, $s \to 0$, except for the anomalous contribution because there is no contribution of the ultraviolet region in the residual terms. Therefore $\Delta\Omega^{(1)}$ can be obtained as,

$$\begin{aligned}\Delta\Omega^{(1)} =& \frac{\mu N_c}{4\pi}\eta_H - \frac{N_c}{4\pi}\int\frac{dp_z}{2\pi}\sum_\epsilon\sum_{\tau=\pm1}\tau\left(\mu-\tau\omega_\epsilon\right)\theta(\tau\omega_\epsilon)\theta(\mu-\tau\omega_\epsilon) \\ & - \frac{N_c T}{4\pi}\int\frac{dp_z}{2\pi}\sum_\epsilon\sum_{\tau=\pm1}\tau\ln\left(1+e^{-\beta|\omega_\epsilon-\tau\mu|}\right).\end{aligned} \tag{3.1.30}$$

The first term can be interpreted as the contribution of anomaly and the second and third terms as the contribution of positive-energy valence quarks [51]. Note that the even functions of q in Eq. (3.1.25), (3.1.26), (3.1.27) are completely canceled by the corresponding one in

Eq. (3.1.22), (3.1.23), (3.1.24) to make $\Delta\Omega^{(1)}$ the odd function of q. It vanishes in the limit, $m \to 0$, which behavior may be physically reasonable because there should be no condensate and q should be redundant in this limit. Consequently we can see that $\Delta\Omega^{(1)}$ emerges only when $m \neq 0, q \neq 0$.

3.2 Calculation of the physical quantities

In the previous section, we obtained the expansion of the thermodynamic potential by the magnetic field. Since the order parameters, m and q, still remain as free parameters, they are determined so that the thermodynamic potential is minimized in this section. After that, we calculate spontaneous magnetization and magnetic susceptibility to discuss the magnetism of quark matter in the DCDW phase.

From Eq. (2.2.11), the thermodynamic potential can be expanded for the two-flavor case as,

$$\Delta\Omega = \frac{m^2}{4G} + 2\Delta\Omega^{(0)} + \Delta\Omega^{(1)}eB + \frac{5}{9}\Delta\Omega^{(2)}(eB)^2 + \mathcal{O}\left((eB)^3\right). \tag{3.2.1}$$

In the following, we consider the sufficiently tiny magnetic field and calculate up to the second order of eB. By solving the stationary conditions, $\frac{\partial}{\partial m,q}\Omega(\mu, T, B; m, q) = 0$, the order parameters, $m = m(\mu, T, B)$, $q = q(\mu, T, B)$, are determined for each set of μ, T, B. The stationary conditions renders,

$$0 = \frac{\partial}{\partial m}\left(\frac{m^2}{4G} + 2\Delta\Omega^{(0)} + \Delta\Omega^{(1)}eB + \frac{5}{9}\Delta\Omega^{(2)}(eB)^2\right)\Bigg|_{\substack{m = m_0(\mu,T) + eBm_1(\mu,T) + (eB)^2 m_2(\mu,T) \\ q = q_0(\mu,T) + eBq_1(\mu,T) + (eB)^2 q_2(\mu,T)}}, \tag{3.2.2}$$

$$0 = \frac{\partial}{\partial q}\left(\frac{m^2}{4G} + 2\Delta\Omega^{(0)} + \Delta\Omega^{(1)}eB + \frac{5}{9}\Delta\Omega^{(2)}(eB)^2\right)\Bigg|_{\substack{m = m_0(\mu,T) + eBm_1(\mu,T) + (eB)^2 m_2(\mu,T) \\ q = q_0(\mu,T) + eBq_1(\mu,T) + (eB)^2 q_2(\mu,T)}}, \tag{3.2.3}$$

where the order parameters are also expanded up to the second order about the magnetic field. When those conditions are fully expanded about the magnetic field, we can obtain the six identities to determine $m_{0,1,2}, q_{0,1,2}$. For simplicity, we use the shorthand notation,

$\frac{\partial\Delta\Omega^{(0)}}{\partial m}\big|_{m=m_0,q=q_0} \equiv \partial_m\Delta\tilde{\Omega}^{(0)}$. The six equations are obtained from Eq. (3.2.2) and (3.2.2) as,

$$0 = \frac{m_0}{2G} + 2\,\partial_m\Delta\tilde{\Omega}^{(0)} \tag{3.2.4}$$

$$0 = \frac{m_1}{2G} + 2m_1\,\partial_m^2\Delta\tilde{\Omega}^{(0)} + 2q_1\,\partial_m\partial_q\Delta\tilde{\Omega}^{(0)} + \partial_m\Delta\tilde{\Omega}^{(1)} \tag{3.2.5}$$

$$\begin{aligned} 0 = \frac{m_2}{2G} &+ 2q_2\,\partial_m\partial_q\Delta\tilde{\Omega}^{(0)} + 2m_2\,\partial_m^2\Delta\tilde{\Omega}^{(0)} + m_1^2\,\partial_m^3\Delta\tilde{\Omega}^{(0)} + q_1^2\,\partial_m\partial_q^2\Delta\tilde{\Omega}^{(0)} \\ &+ 2m_1q_1\,\partial_m^2\partial_q\Delta\tilde{\Omega}^{(0)} + m_1\,\partial_m^2\Delta\tilde{\Omega}^{(1)} + q_1\,\partial_m\partial_q\Delta\tilde{\Omega}^{(1)} + \frac{5}{9}\,\partial_m\Delta\tilde{\Omega}^{(2)} \end{aligned} \tag{3.2.6}$$

$$0 = 2\,\partial_q\Delta\tilde{\Omega}^{(0)} \tag{3.2.7}$$

$$0 = 2q_1\,\partial_q^2\Delta\tilde{\Omega}^{(0)} + 2m_1\,\partial_m\partial_q\Delta\tilde{\Omega}^{(0)} + \partial_q\Delta\tilde{\Omega}^{(1)} \tag{3.2.8}$$

$$\begin{aligned} 0 = &2q_2\,\partial_q^2\Delta\tilde{\Omega}^{(0)} + 2m_2\,\partial_m\partial_q\Delta\tilde{\Omega}^{(0)} + q_1^2\,\partial_q^3\Delta\tilde{\Omega}^{(0)} + m_1^2\,\partial_m^2\partial_q\Delta\tilde{\Omega}^{(0)} \\ &+ 2m_1q_1\,\partial_m\partial_q^2\Delta\tilde{\Omega}^{(0)} + q_1\,\partial_q^2\Delta\tilde{\Omega}^{(1)} + m_1\,\partial_m\partial_q\Delta\tilde{\Omega}^{(1)} + \frac{5}{9}\,\partial_q\Delta\tilde{\Omega}^{(2)} \end{aligned} \tag{3.2.9}$$

To determine $m_0(\mu,T), q_0(\mu,T)$, Eq. (3.2.4) and (3.2.7) should be solved numerically. Using the determined m_0, q_0, $m_1(\mu,T)$ and $q_1(\mu,T)$ can be analytically solved as,

$$m_1(\mu,T) = \frac{1}{2}\frac{\partial_m\partial_q\Delta\tilde{\Omega}^{(0)}\cdot\partial_q\Delta\tilde{\Omega}^{(1)} - \partial_q^2\Delta\tilde{\Omega}^{(0)}\cdot\partial_m\Delta\tilde{\Omega}^{(1)}}{\left((4G)^{-1}+\partial_m^2\Delta\tilde{\Omega}^{(0)}\right)\partial_q^2\Delta\tilde{\Omega}^{(0)} - \left(\partial_m\partial_q\Delta\tilde{\Omega}^{(0)}\right)^2} \tag{3.2.10}$$

$$q_1(\mu,T) = \frac{1}{2}\frac{\partial_m\partial_q\Delta\tilde{\Omega}^{(0)}\cdot\partial_m\Delta\tilde{\Omega}^{(1)} - \left((4G)^{-1}+\partial_m^2\Delta\tilde{\Omega}^{(0)}\right)\partial_q\Delta\tilde{\Omega}^{(1)}}{\left((4G)^{-1}+\partial_m^2\Delta\tilde{\Omega}^{(0)}\right)\partial_q^2\Delta\tilde{\Omega}^{(0)} - \left(\partial_m\partial_q\Delta\tilde{\Omega}^{(0)}\right)^2} \tag{3.2.11}$$

In the same way, $m_2(\mu,T), q_2(\mu,T)$ can be obtained. By the above calculations, the order parameters, $m = m(\mu,T,B), q = q(\mu,T,B)$, are determined up to the second order about eB and the minimized thermodynamic potential can be expanded as,

$$\begin{aligned} \Omega_{\min}(\mu,T,B) \equiv&\Omega(\mu,T,B;m,q)|_{m=m(\mu,T,B),\ q=q(\mu,T,B)} \\ =&\Omega(m=0,q=0) + \frac{m_0^2}{4G} + 2\Delta\tilde{\Omega}^{(0)} \\ &+ eB\Delta\tilde{\Omega}^{(1)} + (eB)^2\left\{\frac{5}{9}\Delta\tilde{\Omega}^{(2)} + \frac{1}{2}m_1\partial_m\Delta\tilde{\Omega}^{(1)} + \frac{1}{2}q_1\partial_q\Delta\tilde{\Omega}^{(1)}\right\}, \end{aligned} \tag{3.2.12}$$

which depends on only thermodynamic quantities and $\Omega(m=0,q=0)$ is the even function of eB.

3.2.1 Spontaneous magnetization

The magnetization can be deduced from the thermodynamic potential as,

$$M \equiv -\frac{\partial \Omega_{\min}(\mu, T, B)}{\partial B}, \tag{3.2.13}$$

Taking the limit, $B \to 0$, we find the spontaneous magnetization in the form,

$$M_0 = -e\Delta\Omega^{(1)}(\mu, T; m = m_0, q = q_0), \tag{3.2.14}$$

where m_0 and q_0 are determined by the stationary conditions (3.2.4), (3.2.7) and represent the optimal values for $\Delta\Omega^{(0)}$. In the following, we will figure out the peculiar role of LLL and show that it leads to the spontaneous magnetization.

Note that the spontaneous magnetization takes a special form for some peculiar values of the parameters, m, q, as well as μ, T. At $\mu < m - q/2$ and $T = 0$, where is no valence quark, the magnetization only comes from the gauged WZW term, $M_0 = \frac{\mu N_c q}{4\pi^2}$, argued in Ref. [49]. Unfortunately, such a situation is not realized in the present calculation and there always exist valence quarks in the DCDW phase because the Fermi sphere made by valence quarks is necessary that the DCDW phase becomes favorable due to the nesting effect [29, 34, 93]. On the other hand, when m becomes small compared to μ or T but q still is not small, M_0 is evaluated to be

$$\begin{aligned} M_0 = -e\frac{N_c}{8\pi^2} \sum_{\sigma=\pm 1} \sigma \, \mathrm{Re}\psi \left(\frac{1}{2} + i\frac{q/2 - \sigma\mu}{2\pi T} \right) m^2 \\ + \mathcal{O}\left(m^4\right), \end{aligned} \tag{3.2.15}$$

where ψ is the digamma function. Then, the leading order about m is m^2 by the symmetry, $m \to -m$.

The magnetization is numerically evaluated at $T = 0$ and $T \simeq 30$MeV, for example. In this calculation, we choose $\Lambda = 660$MeV as the cutoff in PTR and $G\Lambda^2 = 6.35$, which reproduce the pion decay constant $f_\pi = 93$MeV and the constituent quark mass $\simeq 330$MeV in the vacuum [23]. Fig. 3.1 shows the μ dependence of the order parameters in the absence of the magnetic field and the spontaneous magnetization M_0. There are three phases, the DCDW phase ($m \neq 0$, $q \neq 0$), the usual spontaneous symmetry breaking (SSB) phase ($m \neq 0$, $q = 0$) and the chiral-restored phase ($m = 0$). We can see that M_0 becomes nonzero only in the DCDW phase and has a discontinuity at the transition point from the usual SSB phase. At this point, the order parameters are also discontinuous, which implies the phase transition is of the first order. On the other hand, near another transition point to the chiral-restored phase, the spontaneous magnetization is proportional to m_0^2. Furthermore, as T increases, the spontaneous magnetization decreases and the region of magnetized phase gets narrower [51].

It can be seen that spontaneous magnetization occurs in the DCDW phase by the analysis so far. Next, we estimate the value of the self-consistent magnetization. Assuming a spherical

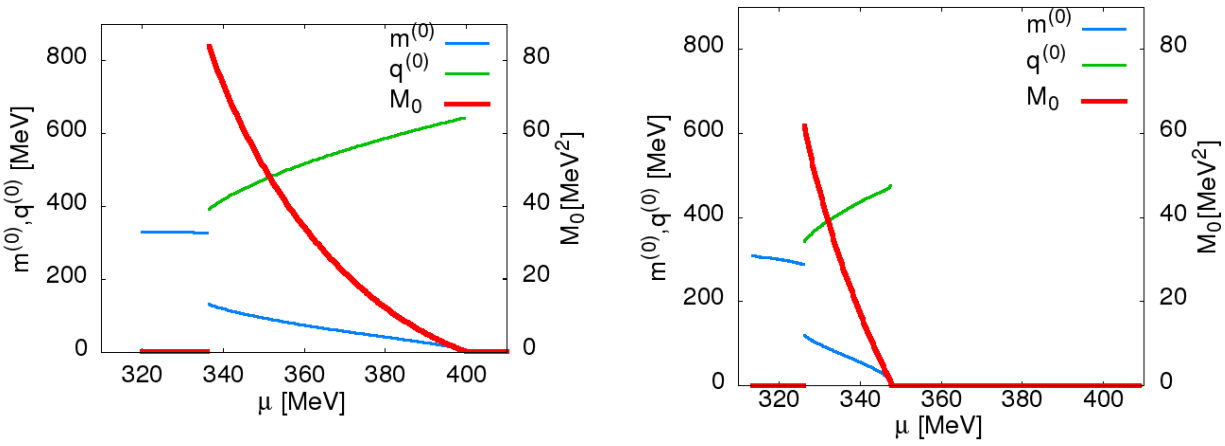

(a) $T = 0$ (b) $T \simeq 30\text{MeV}$

Figure 3.1: The μ dependence of the order parameters and spontaneous magnetization.

quark matter with the constant density, and the magnetic field produced from magnetization, $B = \frac{8\pi}{3}M$, the self-consistent magnetization can be obtained from the self-consistent equation,

$$M = -\frac{\partial \Omega_{\min}}{\partial B}\bigg|_{B=\frac{8\pi}{3}M}. \tag{3.2.16}$$

Strictly speaking, it is necessary to solve the equation of all orders for eB of $\Omega_{\min}$. However we first estimate it by using $\Omega_{\min}$ up to the second order of eB. From Eq. (3.2.12), self-consistent equation (3.2.16) renders,

$$M = -e\Delta\tilde{\Omega}^{(1)} - \frac{8\pi}{3}e^2 M\left\{\frac{10}{9}\Delta\tilde{\Omega}^{(2)} + m_1\partial_m\Delta\tilde{\Omega}^{(1)} + q_1\partial_q\Delta\tilde{\Omega}^{(1)}\right\}. \tag{3.2.17}$$

Therefore the self-consistent magnetization is estimated as,

$$M = \frac{-e\Delta\tilde{\Omega}^{(1)}}{1 + \frac{8\pi}{3}e^2\left[\frac{10}{9}\Delta\tilde{\Omega}^{(2)} + m_1\partial_m\Delta\tilde{\Omega}^{(1)} + q_1\partial_q\Delta\tilde{\Omega}^{(1)}\right]} \tag{3.2.18}$$

Fig, 3.2 shows the μ dependence of M and $\Delta M = M - M_0$ at zero temperature. From the figure, we can see that $\Delta M/M \sim 10^{-3}$, so that the correction is very small. Furthermore if the higher order of the magnetic field is considered in the self-consistent equation (3.2.16), the terms estimated as $\mathcal{O}((\frac{8\pi}{3}eM)^2)$ are added in Eq. (3.2.17). The expansion parameter is obtained as $\frac{8\pi}{3}eM$ divided by μ^2 to make it dimensionless and it is estimated as $\frac{8\pi}{3}\frac{eM}{\mu^2} \sim 10^{-4}$. It is obvious that such corrections due to the second and subsequent terms become even smaller. Therefore, we conclude that the correction to the magnetization by self-consistently estimation can be negligible small.

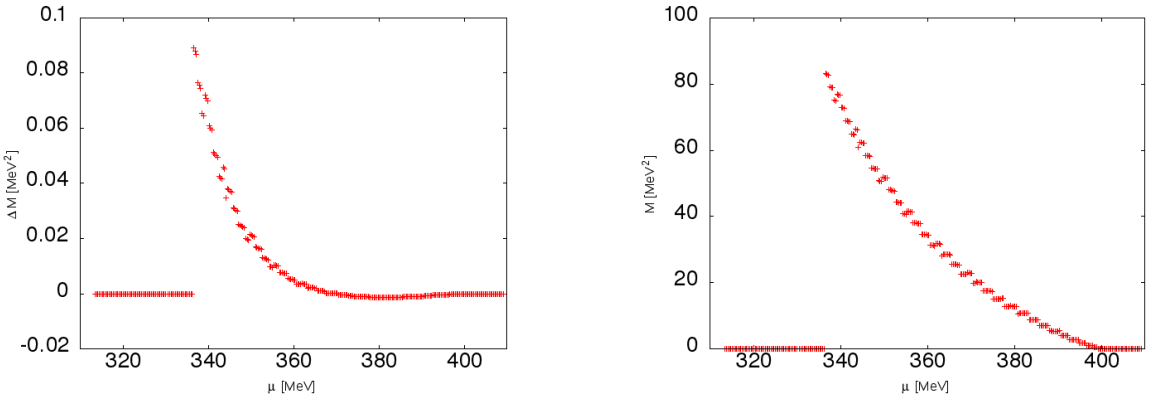

Figure 3.2: The correction to the self-consistent magnetization at $T = 0$. The left panel shows the μ dependence of M_0 and $\Delta M = M - M_0$. The right panel shows the μ dependence of M.

Next, we estimate the magnetic field generated by the spontaneous magnetization. Considering a sphere of the uniform magnetization M_0 again, the magnetic field, $B = \frac{8\pi}{3} M_0$ is produced on the surface. For quark matter with a constant density in the DCDW phase, the magnetic field is estimated $B \sim 10^{16}$G on the surface at $T = 0$, which may be comparable with the observation of magnetars. However, this estimate might be too rough because density is not constant inside neutron stars. Finite shell made of the DCDW phase may be another possible realization. Considering that the DCDW shell gets thin at high T, magnetic field may become much lower than this estimate in hot neutron stars. Actually the spontaneous magnetization vanishes with the disappearance of the DCDW phase at $T \sim 100$MeV. At $T \simeq 30$MeV, which may be a relevant T in newly born neutron stars, the magnetic field remains to be a similar order of magnitude.

In Ref. [29], the expectation value of the magnetic moment, $\langle \bar{\psi}(\boldsymbol{r}) \sigma^{12} \psi(\boldsymbol{r}) \rangle$, is evaluated, which behaves like spin density wave and vanishes after the spatial average. This seems to contradict with the present results. However, we can see that a careful application of the Gordon identity leads to the present results. The external magnetic field minimally couples with the quark field through the covariant derivative, $\int d^4x \, \bar{\psi} Q \gamma^\mu \psi A_\mu$, in the Lagrangian, where Q is the electric charge matrix in the flavor space. According to Ref. [105], this term can be decomposed into the form,

$$\int d^4x \, \bar{\psi} Q \gamma^\mu \psi A_\mu = \frac{B}{2m} \int d^4x \Big[\bar{\chi} Q \sigma^{21} \chi + \bar{\chi} Q 2ix D_2 \chi + \bar{\chi} Q \sigma^{23} i\gamma^5 \tau_3 q \, x \chi \Big], \tag{3.2.19}$$

where the Landau gauge is taken, $\boldsymbol{A} = (0, Bx, 0)$, and χ represents the quark field after the Weinberg transformation, $\chi = e^{i\gamma^5 \tau_3 q z/2} \psi$. Here we have used the modified Gordon decomposition by using the Dirac equation in the presence of DCDW, instead of the free Dirac equation. Consequently, we have the expectation value of the magnetic moment, $\langle \bar{\chi}(\mathbf{r}) \sigma^{\mathbf{12}} \chi(\mathbf{r}) \rangle$, instead of the above one in terms of ψ, which never vanishes after the spatial

average. There appear two contributions in (3.2.19) besides the magnetic moment: the second term can be interpreted as the angular momentum and the third term proportional to q comes from the operator inherent in the DCDW phase. Thus, the magnetization discussed here should be regarded as the statistical average of these operators [51].

Finally, we discuss the spontaneous magnetization at the critical point of the second order phase transition. The expansion of order parameters in Eq. (3.2.2), (3.2.3) is not justified there. From Fig. 3.1, $m_0 = 0, q_0 \neq 0$ at the critical chemical potential (μ_{c2}) where the second order phase transition occurs in the absence of the magnetic field[1]. If the stationary condition for q, $\frac{\partial}{\partial q}\Omega(\mu, T, B; m, q) = 0$, is solved, q can be formally written as,

$$\begin{aligned} q =& q(\mu, T, B; m) \\ =& q^{(0)}(\mu, T; m^2) + eBq^{(1)}(\mu, T; m^2) + (eB)^2 q^{(2)}(\mu; T, m^2), \end{aligned} \tag{3.2.20}$$

which should depend on m^2 due to the Z_2 symmetry about m in the thermodynamic potential. Note that $q^{(0)}$ never vanishes even at μ_c. We substitute $q(\mu, T, B; m)$ into the thermodynamic potential. Because m becomes small near μ_c, the thermodynamic potential can be expanded about m as,

$$\begin{aligned} \Omega(\mu, T, B; q = q(\mu, T, B; m), m) =& \frac{1}{2}\left[\alpha_2^{(0)} + eB\alpha_2^{(1)} + (eB)^2\alpha_2^{(2)}\right] m^2 \\ &+ \frac{1}{4}\left[\alpha_4^{(0)} + eB\alpha_4^{(1)} + (eB)^2\alpha_4^{(2)}\right] m^4 + \cdots, \end{aligned} \tag{3.2.21}$$

where the coefficients are the functions of only μ, T. At μ_{c2}, where α_2 vanishes, the stationary condition on m, $\frac{\partial}{\partial m}\Omega(\mu, T, B; m) = 0$, takes the form,

$$0 = \left[eB\alpha_2' + (eB)^2\alpha_2''\right] m + \left[\alpha_4 + eB\alpha_4' + (eB)^2\alpha_4''\right] m^3. \tag{3.2.22}$$

In order for that equation to hold at the lowest order about the magnetic field, it is necessary to be $m \sim (eB)^{1/2}$. Now we know the dependence of m on the magnetic field at μ_{c2}. Substituting m for the thermodynamic potential (3.2.21), we can obtain the eB dependence of the thermodynamic potential at μ_{c2}, $\Omega_{\min}(\mu_{c2}, T, B) \sim (eB)^2$. Therefore, we can see that M_0 vanishes at μ_{c2} from the definition of spontaneous magnetization (3.2.14). It indicates that M_0 becomes zero at μ_{c2} as shown in Fig. 3.1 and is continuously connected.

3.2.2 Magnetic susceptibility

In this section, we calculate the magnetic susceptibility. The definition of the magnetic susceptibility χ renders [106],

$$\chi \equiv \left.\frac{\partial M}{\partial B}\right|_{B=0} = -\left.\frac{\partial^2 \Omega_{\min}}{\partial B^2}\right|_{B=0} \tag{3.2.23}$$

[1] If $eB \neq 0$, m does not vanish and the phase transition does not still occur.

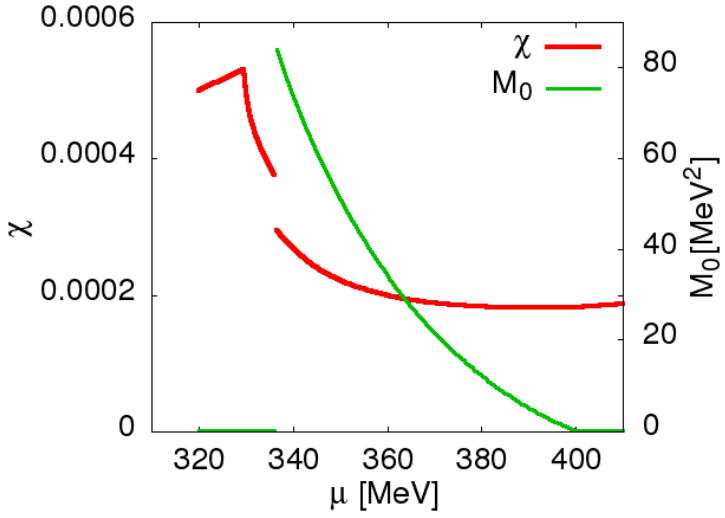

Figure 3.3: The μ dependence of spontaneous magnetization and the magnetic susceptibility at $T = 0$.

From Eq. (3.2.12), χ can be obtained as,

$$\chi = -e^2 \left[\frac{10}{9} \Delta\tilde{\Omega}^{(2)} + m_1 \partial_m \Delta\tilde{\Omega}^{(1)} + q_1 \partial_q \Delta\tilde{\Omega}^{(1)} \right] \tag{3.2.24}$$

In the same way with the calculation of magnetization, we can calculate χ by using the values of the order parameters in Fig. 3.1.

Fig. 3.3 shows the μ dependence of spontaneous magnetization and the magnetic susceptibility at $T = 0$. In the usual SSB phase, the singular point, where the magnetic susceptibility makes a cusp is located at the critical chemical potential where the phase transition from the zero density phase to the finite density phase occurs. At finite T, the phase transition becomes crossover and the singular behavior disappears. Furthermore, it can be seen that the magnetic susceptibility is discontinuous at the critical chemical potential of the first order phase transition from the usual SSB phase to the DCDW phase. However, the magnetic susceptibility does not indicate any singularity at the critical chemical potential of the second order phase transition from the DCDW phase to the chiral-restored phase. This behavior is different from the properties in the system, where spontaneous magnetization is generated by aligning the spins as in the Ising model. In the Ising model, it is known within MFA that the magnetic susceptibility diverges at the critical temperature of the ferromagnetic phase transition. The difference between the magnetic susceptibility in DCDW and the Ising model can be understood by expressing the thermodynamic potential as a function of magnetization by the Legendre transformation. First, we can get the equation, $B = B(\mu, T, M)$, by solving Eq. (3.2.13) for B. Using this relation the Legendre transformation is performed as,

$$G(\mu, T, M) = \left[\Omega_{\min}(\mu, T, B) + MB \right] \Big|_{B=B(\mu,T,M)}. \tag{3.2.25}$$

The partial differential of $G(\mu, T, M)$ by M is calculated as,

$$\begin{aligned}\frac{\partial G}{\partial M} &= \frac{\partial B}{\partial M}\frac{\partial \Omega_{\min}}{\partial B} + B(\mu, T, M) + M\frac{\partial B}{\partial M} \\ &= B(\mu, T, M).\end{aligned} \tag{3.2.26}$$

Therefore the definition of the magnetic susceptibility can be rewritten as,

$$\begin{aligned}\chi &= \left.\frac{\partial M}{\partial B}\right|_{B=0} \\ &= \left.\left(\frac{\partial^2 G}{\partial M^2}\right)^{-1}\right|_{M=M'}\end{aligned} \tag{3.2.27}$$

where M' denotes the value of M satisfying the equation, $\frac{\partial G}{\partial M} = 0$. Thus, we can see that χ is represented as the inverse of the curvature of G at the point where the extremum about M is taken. Since the magnetization is small near the point of the second order phase transition, we consider G expanded by magnetization up to an appropriate order. In the case of the Ising model, G takes the form,

$$G = \alpha_0 + \frac{1}{2}\alpha_2 M^2 + \frac{1}{4}\alpha_4 M^4. \tag{3.2.28}$$

When $\alpha_2 > 0$, the paramagnetic phase ($M = 0$) is realized. At $\alpha_2 = 0$, the phase transition from the paramagnetic phase to the ferromagnetic phase ($M \neq 0$) occurs. At this point, the curvature of G vanishes and the magnetic susceptibility diverges. On the other hand, in the case of the present model, the thermodynamic potential can be formally expanded up to the second order of B as,

$$\Omega_{\min}(\mu, T, B) = \alpha_0(\mu, T) + \alpha_1(\mu, T)B + \frac{1}{2}\alpha_2(\mu, T)B^2. \tag{3.2.29}$$

From Eq. (3.2.29), B is obtained as the function of M, $B(\mu, T, M) = -\frac{1}{\alpha_2}(M + \alpha_1)$. Therefore G renders,

$$G(\mu, T, M) = \alpha_0 - \frac{1}{2\alpha_2}(M + \alpha_1)^2. \tag{3.2.30}$$

Because spontaneous magnetization is obtained as M satisfying $\frac{\partial G}{\partial M} = 0$, the paramagnetic phase is realized for $\alpha_1 = 0$ and the phase transition to the ferromagnetic phase occurs at the point where α_1 becomes finite.

3.3 Massless mode corresponding to magnon

In the ferromagnetic phase where the spins are aligned such as in the Ising model, there appears the Nambu-Goldstone (NG) mode called magnon since the rotational symmetry of

the spin is spontaneously broken [107]. In this section, we discuss whether the similar mode exists in the present model as well. In the absence of the magnetic field, the order parameter $\boldsymbol{q}$ is a vector quantity which can take any direction. On the other hand, in the presence of the magnetic field, $\boldsymbol{q}$ and $\boldsymbol{B}$ can produce the scalar, $\boldsymbol{B}\cdot\boldsymbol{q}$, in the thermodynamic potential. The first order term of the magnetic field gives rise to spontaneous magnetization. The existence of this term can be interpreted as $\boldsymbol{q}$ playing a role of the spin in the DCDW phase, where spontaneous magnetization is generated. In other words, when $\boldsymbol{q}$ has a finite value, one direction is specified and it seems that rotational symmetry is spontaneously broken similar to the case of the spin.

Next we consider whether there is the NG mode caused by the spontaneous breaking of the rotational symmetry, following the argument in Ref. [108]. In the DCDW phase, $\boldsymbol{q}$ appears as the wave number of the inhomogeneous condensate, $\Delta(\boldsymbol{r}) = me^{i\boldsymbol{q}\cdot\boldsymbol{r}}$. The NG mode is the excitation mode which is generated by the local transformation corresponding to the broken symmetry. For example, magnon is the excitation mode which is generated by the local rotation in the spin space. In the DCDW phase, such a transformation is considered to correspond to the rotational transformation of $\boldsymbol{q}$ as,

$$e^{i\boldsymbol{q}\cdot\boldsymbol{r}} \to e^{i(R(\boldsymbol{r})\boldsymbol{q})\cdot\boldsymbol{r}}. \tag{3.3.1}$$

where $R(\boldsymbol{r})$ denotes the local rotation matrix. However, Since that transformation can be rewritten as,

$$e^{i(R(\boldsymbol{r})\boldsymbol{q})\cdot\boldsymbol{r}} = e^{i\boldsymbol{q}\cdot(R^{-1}(\boldsymbol{r})\boldsymbol{r})}, \tag{3.3.2}$$

the degree of freedom to rotate $\boldsymbol{q}$ is the same as the degree of freedom of spatial rotation. Moreover, the elements of the Poincaré group describing the local spatial rotation are represented as,

$$e^{i\theta_j(\boldsymbol{r})\hat{L}_j}, \tag{3.3.3}$$

where $\hat{L}_i$ denotes the generator of the spatial rotation and $\theta_i(\boldsymbol{r})$ represents an arbitrary function which describes the locality of the transformation. Using the generator of the translation $\hat{\boldsymbol{P}}$, $\hat{L}_i$ can be also represented as $\hat{L}_i = \epsilon_{ijk}\, r_j \hat{P}_k$. Note that we regard the spatial coordinates appearing in the above equation as parameters not operators. Thus they are commutative to $\hat{\boldsymbol{P}}$. By regarding so, $e^{i\theta_j(\boldsymbol{r})\hat{L}_j}$ describes the rotational transformation, $e^{i\theta_j(\boldsymbol{r})\hat{L}_j} f(\boldsymbol{r}) \equiv f(R(\theta)\boldsymbol{r})$. On the other hand, the elements of the Poincaré group describing the local translation are represented as,

$$e^{is_j(\boldsymbol{r})\hat{P}_j}, \tag{3.3.4}$$

where $s_i(\boldsymbol{r})$ denotes an arbitrary function which describes the locality of the transformation and $\boldsymbol{r}$ represents just parameter. Therefore we can see that the rotation (3.3.3) can always be represented by the local translation (3.3.4) with the appropriate choice of $s_i(\boldsymbol{r})$ [108, 109, 110]. In other words, the degree of freedom of spatial rotation is the same as the degree of freedom of local spatial translation.

Furthermore, when we consider the local chiral transformation, $\psi \to e^{i\gamma_5\alpha(\boldsymbol{r})}\psi$, the DCDW condensate is also transformed as,

$$me^{i\boldsymbol{q}\cdot\boldsymbol{r}} \to me^{i(\boldsymbol{q}\cdot\boldsymbol{r}-2\alpha(\boldsymbol{r}))}. \tag{3.3.5}$$

On the other hand, by the local translation, $\boldsymbol{r} \to \boldsymbol{r} + \boldsymbol{s}(\boldsymbol{r})$, the DCDW condensate changes as,

$$me^{i\boldsymbol{q}\cdot\boldsymbol{r}} \to me^{i(\boldsymbol{q}\cdot\boldsymbol{r}+\boldsymbol{q}\cdot\boldsymbol{s}(\boldsymbol{r}))}. \tag{3.3.6}$$

Thus, we can see that the local translation can always be represented by a local chiral transformation with proper choice of $\alpha(\boldsymbol{r})$ [84]. In other words, in the case of DCDW, the degree of freedom of the local translation is the same as the degree of freedom of the local chiral transformation. From the above argument, there is only the chiral transformation as the independent degree of freedom of the local transformation and only pions appear as the NG mode. Therefore, it is concluded that there is no excitation mode like magnon in the DCDW phase.

Chapter 4

Axial anomaly vs. symmetry breaking effect

In this chapter, we study the region of the inhomogeneous chiral phase (iCP) around the Lifshitz point (LP) by using the generalized Ginzburg-Landau (GL) expansion [89] with the finite current quark mass [76]. The current mass is small but should be important below the low energy scale of $\mathcal{O}(10^2)$MeV, since it is well-known that pion mass of $\mathcal{O}(10^2)$MeV is generated from the tiny current quark mass of several MeV. Thus it is conceivable that the finite quark mass becomes very important in the vicinity of LP, where the both the wave number and the amplitude of the chiral condensate become very small. For real kink crystal (RKC) the exact solution can be obtained in the massive Gross-Neveu model [111] and the critical point has been demonstrated to be largely shifted [28] to reduce the phase region. For dual chiral density wave (DCDW), although no exact solution is known, the effect of the current mass has been perturbatively discussed in Ref. [112]. They have found that the DCDW phase does not appear for the small coupling constant and the large current mass within the Nambu-Jona-Lasinio (NJL) model, while the DCDW phase appears for the same coupling constant in the chiral limit. However, the discussion may not be sufficient because any deformation of the DCDW form has not been considered. To take into account the deformation, a variational method may work well [41]. Consequently, the effect of the current quark mass is almost similar to the case of RKC: the function form of DCDW is largely deformed near the transition point and accordingly the DCDW region of the phase diagram is reduced.

On the other hand, we know that in the presence of the magnetic field, DCDW phase is remarkably extended in the low μ region except for $\mu = 0$ at $T = 0$ in the chiral limit [45]. The energy spectrum of quarks exhibits the asymmetry, which gives rise to such distinctive enhancement of DCDW [46]. Note that the complex order parameter, $\Delta(\boldsymbol{r})$, is necessary for the energy spectrum to be asymmetric about zero. A peculiar role of the spectral asymmetry can be also seen around the transition point: it induces a new term in the thermodynamic potential, and consequently a new LP should appear on the $\mu = 0$ line in the chiral limit [46].

Therefore once the current mass is turned on, a competition arises between the positive

effect on the DCDW phase by the magnetic field and the negative effect by the current mass.

4.1 Thermodynamic potential with the finite current quark mass

The thermodynamic potential with the current mass is given by the generalized GL expansion near LP, based on the NJL model. The Lagrangian takes the form,

$$\mathcal{L}_{\rm NJL} = \bar{\psi}\left(i\not{D} - m_c\right)\psi + G\left[\left(\bar{\psi}\psi\right)^2 + \left(\bar{\psi}i\gamma^5\tau^a\psi\right)^2\right], \tag{4.1.1}$$

with the covariant derivative, $D_\mu = \partial_\mu + i\mathcal{Q}A_\mu$, where $\mathcal{Q}$ is the electric charge matrix in the flavor space, $\mathcal{Q} = \mathrm{diag}(e_u, e_d)$, and the $SU(2)$ symmetric quark mass, $m_c \equiv m_u = m_d \simeq$ 5MeV. In the presence of the magnetic field, the phase degree of freedom in the order parameter, $\Delta(\boldsymbol{r}) = -2G(\langle\bar{\psi}\psi\rangle + \langle\bar{\psi}i\gamma^5\tau_3\psi\rangle)$, is important to give rise to anomaly as shown in the previous chapters. Therefore we assume the complex order parameter,

$$\Delta(\boldsymbol{r}) = me^{i\theta(z)}, \tag{4.1.2}$$

where the amplitude m is fixed to be constant and plays a role of the dynamical quark mass. The direction of modulation is taken to be parallel to z axis. The deformation of the phase function $\theta(z)$ from DCDW ($\theta(z) = qz$) reflects the effect of the current mass. Then, the Lagrangian within the mean-field approximation (MFA) takes the form,

$$\mathcal{L}_{\rm MF} = \bar{\psi}\left[i\not{D} - m_c - m\left(\cos\theta(z) + i\gamma^5\tau^3\sin\theta(z)\right)\right]\psi - \frac{m^2}{4G}. \tag{4.1.3}$$

Taking the external magnetic field $\boldsymbol{B}$ along the z axis, the thermodynamic potential can be written up to the fourth order about the order parameters and its derivative and the first order in m_c as

$$\begin{aligned}\Omega(\mu,T,B) =& \Omega_0 + \int\frac{d^3\boldsymbol{x}}{V}\Big\{\alpha_1 m\cos\theta + \frac{1}{2}\left(\alpha_2 + \frac{1}{2G}\right)m^2 + \tilde{\alpha}_2 m\,(\sin\theta)' \\ &+ \frac{\alpha_3}{4}\left[4m^3\cos\theta - m\,(\cos\theta)''\right] + \tilde{\alpha}_3 m^2\theta' + \frac{\alpha_4}{4}\left(m^4 - m^2\theta\theta''\right) + 3\tilde{\alpha}_{4a}m^3\,(\sin\theta)' \\ &+ \tilde{\alpha}_{4b}m\,(\sin\theta)'''\Big\},\end{aligned} \tag{4.1.4}$$

with a shorthand notation, $\theta' \equiv \partial\theta/\partial z$, for given μ, T and B [76]. The GL coefficients now

read,

$$\alpha_{2j} = (-1)^j 2N_c \sum_f T \sum_k \frac{|e_f B|}{2\pi} \sum_{n\geq 0} \times \int \frac{dp}{2\pi} \frac{2-\delta_{n,0}}{[(\omega_k + i\mu)^2 + p^2 + 2|e_f B|n]^j}, \tag{4.1.5}$$

$$\alpha_{2j-1} = m_c \alpha_{2j}, \tag{4.1.6}$$

$$\tilde{\alpha}_3 = N_c \sum_f \frac{|e_f B|}{16\pi^3 T} \mathrm{Im}\psi^{(1)}\left(\frac{1}{2} + i\frac{\mu}{2\pi T}\right), \tag{4.1.7}$$

$$\tilde{\alpha}_2 = m_c \tilde{\alpha}_3, \tag{4.1.8}$$

$$\tilde{\alpha}_{4b} = m_c N_c \sum_f \frac{|e_f B|}{1536\pi^5 T^3} \mathrm{Im}\psi^{(3)}\left(\frac{1}{2} + i\frac{\mu}{2\pi T}\right), \tag{4.1.9}$$

where $\omega_k = (2k+1)\pi T$ is the Matsubara frequency and Ω_0 is the constant term independent of the order parameters. The derivation of these equations is somewhat cumbersome and is given in Appendix C. Here $\tilde{\alpha}_{4a}$ cannot be represented as a simple form (see Appendix C for details). Note that the effect of the current quark mass is included in α_{2j-1}, $\tilde{\alpha}_2$, $\tilde{\alpha}_{4a}$ and $\tilde{\alpha}_{4b}$, which are proportional to m_c. The coefficients α_i $(i = 1-4)$ include a ultraviolet divergence and should be properly regularized by applying some regularization scheme. In the present calculation, the Pauli-Villars regularization (PVR) is used[1]. For convenience, we introduce the function I_j and rewrite Eq. (4.1.5),

$$\alpha_{2j} = (-1)^j N_c \sum_f \frac{|e_f B|}{2\pi} I_j(0), \tag{4.1.10}$$

where

$$I_j(\Lambda^2) \equiv 2T \sum_k \sum_{n\geq 0} \int \frac{dp}{2\pi} \frac{2-\delta_{n,0}}{[(\omega_k + i\mu)^2 + E_n^2(\Lambda^2)]^j}, \tag{4.1.11}$$

$$E_n(\Lambda^2) \equiv \sqrt{p^2 + \Lambda^2 + 2|e_f B|n}. \tag{4.1.12}$$

Then, $I_1(0)$ and $I_2(0)$ have the ultraviolet divergence and should be regularized. Taking the

[1]If the vacuum contributions of α_i are regularized by the proper time regularization in the similar way as in the previous chapters, the artificial infrared divergence emerges in all coefficients ($i \geq 4$) as the consequence of the GL expansion. The original thermodynamic potential does not include any infrared divergence and the infrared divergence may be vanished by summing up all order therms in the GL expansion. In the PVR scheme, we automatically evade the difficulty.

sum over the Matsubara frequency,

$$I_1 = \sum_{n\geq 0} \int \frac{dp}{2\pi} \frac{2-\delta_{n,0}}{E_n} \left[1 - f_F(E_n+\mu) - f_F(E_n-\mu)\right], \tag{4.1.13}$$

$$I_2 = \frac{1}{2}\sum_{n\geq 0}(2-\delta_{n,0}) \int \frac{dp}{2\pi} \Bigg\{ \frac{1}{E_n^3}\left[1 - f_F(E_n+\mu) - f_F(E_n-\mu)\right] + \frac{1}{E_n^2}\left[f_F'(E_n+\mu) + f_F'(E_n-\mu)\right] \Bigg\}, \tag{4.1.14}$$

where f_F is the Fermion distribution function. Therefore the diverging vacuum part can be extracted as,

$$I_{1,\mathrm{vac}} = \sum_{n\geq 0} \int \frac{dp}{2\pi} \frac{2-\delta_{n,0}}{E_n}, \tag{4.1.15}$$

$$I_{2,\mathrm{vac}} = \frac{1}{2}\sum_{n\geq 0} \int \frac{dp}{2\pi} \frac{2-\delta_{n,0}}{E_n^3}. \tag{4.1.16}$$

Then, $I_1(0)$ and $I_2(0)$ are regularized as follows,

$$I_{1,\mathrm{vac}}(0) \to I_{1,\mathrm{vac}}(0) - 2I_{1,\mathrm{vac}}(\Lambda^2) + I_{1,\mathrm{vac}}(2\Lambda^2), \tag{4.1.17}$$

$$I_{2,\mathrm{vac}}(0) \to I_{2,\mathrm{vac}}(0) - I_{2,\mathrm{vac}}(\Lambda^2). \tag{4.1.18}$$

Thus, all the divergences in the coefficients can be removed [76].

The total derivative terms in Eq. (4.1.4) are irrelevant for the stationary condition: $\delta\Omega/\delta\theta(z) = 0$. Note here that the $\tilde{\alpha}_3$ term never affects the stationary condition; it plays instead an important role through the thermodynamic potential. From the extremum condition, we find the equation in the sine-Gordon form,

$$\theta'' + \mathrm{sign}(\alpha_1 + m^2\alpha_3) m_\pi^{*2} \sin\theta = 0, \tag{4.1.19}$$

with

$$m_\pi^{*2} \equiv 2\frac{|\alpha_1 + m^2\alpha_3|}{m\alpha_4}, \tag{4.1.20}$$

which is proportional to m_c. The relevant solution to Eq. (4.1.19) can be obtained as,

$$\theta(z) = 2\mathrm{am}\left(\frac{m_\pi^*}{k}z, k\right) + \pi\theta\left(-\alpha_1 - m^2\alpha_3\right), \tag{4.1.21}$$

where "am" is the amplitude function with modulus $k \in [0,1]$. Then, the period (l) and the wave number (Q) of condensates are defined by the relations,

$$l = \frac{2kK(k)}{m_\pi^*},\ Q = \frac{2\pi}{l} = \frac{\pi m_\pi^*}{kK(k)}, \tag{4.1.22}$$

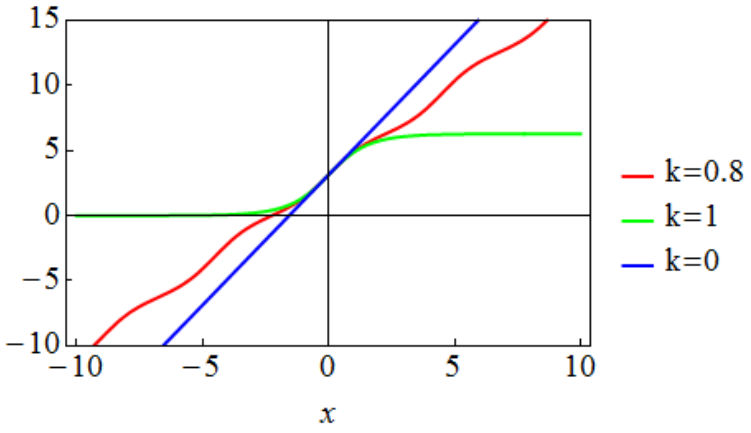

Figure 4.1: Plot of $\pi + 2\mathrm{am}(x,k)$. The red, green and blue line describes the function at $k = 0.8$, 1, 0 respectively. (The figure is taken from Ref. [76].)

where $K(k)$ is the complete elliptic integral of the first kind. There are two order parameters, m and k (or Q): m characterizes the magnitude of spontaneous symmetry breaking (SSB), and k measures a degree of the inhomogeneity. We plot the function: $\pi + 2\mathrm{am}(x,k)$ in Fig. 4.1. When $k = 1$, Eq. (4.1.21) takes the form,

$$\theta(z)|_{k=1} = 4\tan^{-1}\left(e^{m_\pi^* z}\right) - \pi\theta\left(\alpha_1 + m^2\alpha_3\right), \tag{4.1.23}$$

and behaves like a single kink. Accordingly, l diverges and Q vanishes because $K(k \to 1) \to \infty$. Then, we can see that the thermodynamic potential is reduced to the one in the homogeneous phase. On the other hand, when k and m_c simultaneously go to zero and $2m_\pi^*/k \to q$, Eq. (4.1.21) takes the form,

$$\theta(z) \to qz + \pi\theta\left(-\alpha_1 - m^2\alpha_3\right), \tag{4.1.24}$$

and the original DCDW phase is recovered. In the following, we call the phase where $0 < k < 1, m \neq 0$ the *massive DCDW phase* [76].

Then the thermodynamic potential takes the form,

$$\Omega = \Omega_0 - \left|\alpha_1 m + \alpha_3 m^3\right| C_1(k) + \frac{1}{2}\left(\alpha_2 + \frac{1}{2G}\right)m^2 + \tilde{\alpha}_3\sqrt{2\frac{|\alpha_1 + m^2\alpha_3|}{\alpha_4}}m^{3/2}C_3(k) + \frac{\alpha_4}{4}m^4, \tag{4.1.25}$$

with

$$C_1(k) \equiv \frac{2}{k^2} - 1 - \frac{4E(k)}{k^2K(k)}, \tag{4.1.26}$$

$$C_3(k) \equiv \frac{\pi}{kK(k)}, \tag{4.1.27}$$

where $E(k)$ is the complete elliptic integral of the second kind. Note that $\tilde{\alpha}_2, \tilde{\alpha}_{4a}, \tilde{\alpha}_{4b}$ terms vanish by the spatial integral. We can easily observe that Eq. (4.1.25) recovers the thermodynamic potential in the homogeneous phase at $k \to 1$ because $C_1(k \to 1) = 1$ and $C_3(k \to 1) = 0$.

One may also find another possible solution of Eq. (4.1.19),

$$\theta_{\rm os}(z) = 2\cos^{-1}\left[k' \,\mathrm{sn}\left(m_\pi^* z, k'\right)\right] + \pi\theta\left(-\alpha_1 - m^2\alpha_3\right), \tag{4.1.28}$$

with modulus $k' \in [0,1]$. The previous solution (4.1.21) is the monotonically increasing function, while this solution is the oscillating function. Then the thermodynamic potential takes the form,

$$\Omega = \Omega_0 - \left|\alpha_1 m + \alpha_3 m^3\right| C_1^{\rm os}(k') + \frac{1}{2}\left(\alpha_2 + \frac{1}{2G}\right) m^2 + \frac{\alpha_4}{4} m^4, \tag{4.1.29}$$

with

$$C_1^{\rm os}(k') \equiv 3 - 2k'^2 - \frac{4E(k')}{K(k')}. \tag{4.1.30}$$

When $k' = 1$, the solution (4.1.28) corresponds to $\theta(z)|_{k=1}$ and the thermodynamic potential becomes the one in the homogeneous phase. However, we can see that the oscillating solution is never favored compared to the homogeneous solution because $C_1^{\rm os}(k') \leq C_1^{\rm os}(k'=1)$. Therefore, the phase with the oscillating solution does not appear in the present situation[2].

4.2 Spectral asymmetry with m_c

It may be worth mentioning that the $\tilde{\alpha}_3$ term is originated from the spectral asymmetry of the quark energy and proportional to the magnetic field. Note that the $\tilde{\alpha}_3$ term remarkably extends the DCDW phase in the presence of the magnetic field [46], while it cannot appear in the RKC phase because of the absence of the phase degree of freedom. The presence of such term has been shown in the chiral limit and a close relation to chiral anomaly has been demonstrated [46]. This argument can be easily generalized even if the current mass is taken into account. We show that the $\tilde{\alpha}_3$ term is derived from the spectral asymmetry and relevant to chiral anomaly when the inhomogeneous chiral condensate has the phase degree of freedom. Generally quark number density at the finite T is given as [46],

$$n = -\frac{1}{2}\eta_H + \int dE \rho(E) \left[\frac{\theta(E)}{1 + e^{\beta(E-\mu)}} - \frac{\theta(-E)}{1 + e^{-\beta(E+\mu)}}\right], \tag{4.2.1}$$

where $\rho(E)$ is the density of state. The first term, which is called the Atiyah-Patodi-Singer η-invariant represents the anomalous particle number [47, 48],

$$\eta_H = \lim_{s \to +0} \int dE \rho(E) \mathrm{sign}(E) |E|^{-s}, \tag{4.2.2}$$

[2]The oscillating solution may be relevant near the critical point in the absence of the magnetic field, where the similar equation is derived for θ [41].

and measures the extent of *spectral asymmetry* about zero. The second term ($n_{\rm nom}$) corresponds to the normal particle number and we rewrite it as the form including the summation of the Matsubara frequency,

$$n_{\rm nom} = \frac{1}{2}\eta_H - \int dE\rho(E)T\sum_k \frac{1}{E-\mu-i\omega_k}. \tag{4.2.3}$$

Here the first term in (4.2.3) apparently cancels out the anomalous particle number. However, the information of the η invariant is not washed away since the infinite series reproduces the anomalous particle number at $\mu = T = 0$.

The local density of state takes the form,

$$\begin{aligned}\rho(\boldsymbol{x}, E) &= \frac{1}{\pi}{\rm Im\,tr}_{D,f,c}[R(\boldsymbol{x}, E+i\epsilon)] \\ &= -\frac{N_c}{\pi}\sum_f \frac{\partial}{\partial E}{\rm Im\,tr}_D \left\langle \boldsymbol{x}\left|\ln(H-E-i\epsilon)\right|\boldsymbol{x}\right\rangle, \end{aligned}\tag{4.2.4}$$

with the resolvent: $R(\boldsymbol{x}, E) \equiv \left\langle \boldsymbol{x}\left|\frac{1}{H-E}\right|\boldsymbol{x}\right\rangle$. In the present model, Hamiltonian takes the form,

$$H = \vec{\alpha}\cdot\boldsymbol{P} + \gamma^0\left[m_c + me^{i\gamma^5\tau_3\theta(\boldsymbol{r})}\right], \tag{4.2.5}$$

where $\alpha_i = \gamma_0\gamma_i$ and $\boldsymbol{P}$ is the covariant derivative. After the Weinberg transformation: $\psi \to \psi_W = e^{i\gamma^5\tau_3\theta(\boldsymbol{r})/2}\psi$, Hamiltonian changes to $\tilde{H}$,

$$\tilde{H} = \tilde{H}_0 + \delta\tilde{H}, \tag{4.2.6}$$

$$\tilde{H}_0 \equiv \vec{\alpha}\cdot\boldsymbol{P} + \gamma_0 m, \tag{4.2.7}$$

$$\delta\tilde{H} \equiv \gamma^0\left[m_c e^{-i\gamma^5\tau_3\theta(\boldsymbol{r})} - \frac{1}{2}\gamma^5\tau_3\boldsymbol{\gamma}\cdot\boldsymbol{\nabla}\theta(\boldsymbol{r})\right]. \tag{4.2.8}$$

Therefore, $\rho(\boldsymbol{x}, E)$ can be expanded to the form,

$$\begin{aligned}\rho(\boldsymbol{x}, E) = \frac{N_c}{\pi}\sum_f {\rm Im\,tr}\left\langle \boldsymbol{x}\left|\frac{1}{\tilde{H}_0 - E}\right|\boldsymbol{x}\right\rangle - \frac{N_c}{\pi}\sum_f \frac{\partial}{\partial E}{\rm Im\,tr}\left\langle \boldsymbol{x}\left|\frac{1}{\tilde{H}_0 - E - i\epsilon}\right|\boldsymbol{x}\right\rangle \delta\tilde{H}(\boldsymbol{x}) \\ + \mathcal{O}\left(\partial(\delta\tilde{H}), (\delta\tilde{H})^2\right),\end{aligned}\tag{4.2.9}$$

where the first term does not depend on θ. Here, $\left\langle \boldsymbol{x}\left|\frac{1}{\tilde{H}_0-E-i\epsilon}\right|\boldsymbol{x}\right\rangle$ can be rewritten into the propagator decomposed over the Landau levels [46].

Then the leading term proportional to $\partial\theta$ takes the form,

$$\rho_{\partial\theta}(\boldsymbol{x}, E) = -\frac{N_c}{4\pi^2}\sum_f |e_f B|\partial_z\theta(\boldsymbol{x})\frac{\partial}{\partial E}\left[\frac{|E|}{\sqrt{E^2-m^2}}\theta\left(|E|-m\right)\right]. \tag{4.2.10}$$

From Eq. (4.2.3), the part of quark number generated by $\rho_{\partial\theta}$ takes the form,

$$n_{\partial\theta} = \frac{N_c}{4\pi^2}\sum_f |e_f B| \int d^3\boldsymbol{x}\partial_z\theta(\boldsymbol{x})\Bigg\{1 + T\sum_k \int_0^\infty dy \\ \times \left[\frac{1}{(\sqrt{y^2+m^2}-\mu-i\omega_k)^2} + \frac{1}{(\sqrt{y^2+m^2}+\mu+i\omega_k)^2}\right]\Bigg\}, \tag{4.2.11}$$

where the first term is derived from the surface term in the partial integral about E and we take $y = \sqrt{E^2-m^2}$. Then the second term can be expanded with respect to m^2. It can be seen that m^0 part of the second term cancels out the first term and the the remnant of $N_{\partial\theta}$ takes the form,

$$n_{\partial\theta} = -\frac{N_c}{16\pi^3 T}\sum_f |e_f B| \int d^3\boldsymbol{x}\partial_z\theta(\boldsymbol{x})\frac{\partial}{\partial\mu}\mathrm{Im}\psi^{(1)}\left(\frac{1}{2}+i\frac{\mu}{2\pi T}\right)m^2 + \mathcal{O}(m^4). \tag{4.2.12}$$

From the thermodynamic relation, $N/V = -\partial\Omega/\partial\mu$, we can see that the $\tilde{\alpha}_3$ term is generated [76].

On the other hand, the result from chiral anomaly [49] is recovered in the limit: $m \to \infty$. Then the second term in Eq. (4.2.11) vanishes and the first term is the very contribution of chiral anomaly. This limit is consistent with the case where there is no valence quarks argued in Ref. [51]. Furthermore, substituting the configuration of θ (4.1.21), the quark number takes the form,

$$n_{\partial\theta} \to \frac{N_c}{4\pi^2}\sum_f |e_f B|\frac{\pi m_\pi^*}{kK(k)}. \tag{4.2.13}$$

For investigating the derivation from the case of the chiral limit [46], we take $2m_\pi^*/k = q$, where q is the wave vector of the DCDW condensate. Then it can be expanded with respect to $(m_\pi^*/q)^2$,

$$n_{\partial\theta} = \frac{N_c}{4\pi^2}\sum_f |e_f B| q\left[1 - 2\frac{m_\pi^{*2}}{q^2} + \mathcal{O}\left(\frac{m_\pi^{*4}}{q^4}\right)\right]. \tag{4.2.14}$$

The second term represents the correction by the finite m_c because of $m_\pi^{*2} \propto m_c$. The result also implies that spectral asymmetry should have the correction $\mathcal{O}(m_c)$ although the exact energy spectrum cannot be obtained at the finite m_c.

4.3 Results and discussions

4.3.1 Phase diagram around the transition point

For obtaining the phase diagram, the order parameters are determined to minimize Eq. (4.1.25). In the following, Q is used as the order parameter characterizing the inhomogenity instead

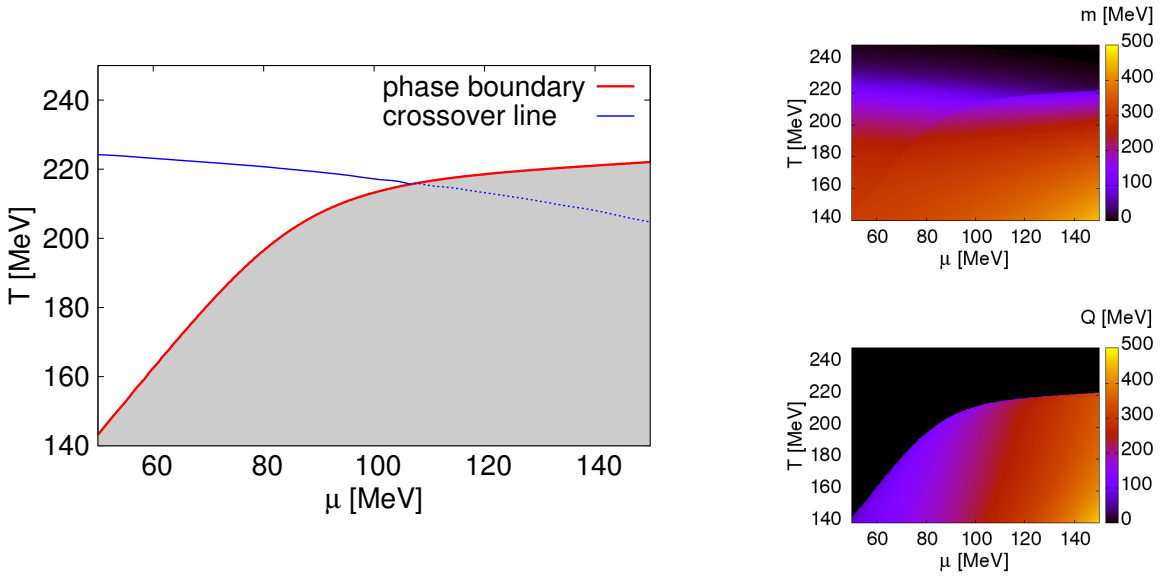

Figure 4.2: Phase diagram for $m_c = 5\text{MeV}, \sqrt{eB} = 1\text{GeV}$ (left panel). The red line describes the phase boundary between the massive DCDW phase (shaded area) and the homogeneous phase. The solid blue line describes the crossover line. The conventional crossover line without the massive DCDW phase corresponds to the dashed blue line. The right upper (lower) panel shows the value of m (Q) at the same range of $\mu - T$ as the left panel. (The figures are taken from Ref. [76].)

of k. In the present calculation, we use the parameter set in Ref. [18]: $\Lambda = 851\text{MeV}$ and $G\Lambda^2 = 2.87$, which reproduce pion decay constant $f_\pi = 93\text{MeV}$, pion mass $m_\pi = 135\text{MeV}$ and scalar condensate $\langle\bar{\psi}\psi\rangle = (-250\text{MeV})^3$ in the vacuum with $m_c = 5.2\text{MeV}$.

In Fig. 4.2, we show the phase diagram for $m_c = 5\text{MeV}, \sqrt{eB} = 1\text{GeV}$. There are the phase boundary between the massive DCDW phase and the homogeneous phase and the crossover line constituted by the pseudocritical temperature (T_{pc}) defined as the peak of the chiral susceptibility: $-\partial m/\partial T$ [76].

In Fig. 4.3, the change of the phase diagram is described when m_c or B changes. We can find that the massive DCDW phase is extended to the low μ region with the decrease of m_c. Then the result in Ref. [46] is recovered in the chiral limit: $m_c = 0$ and it is expected that the crossing point of the phase boundary and the crossover line agrees with LP in the chiral limit. On the other hand, the magnetic field increases the critical temperature in the phase transition, which is consistent with the magnetic catalysis [24]. In other words, the smaller m_c or the larger B becomes, the more widely the massive DCDW phase develops over the region: $\mu/T < 1$ [76].

The T dependence of the order parameters is shown in Fig. 4.4. A discontinuity in both order parameters can be found at the critical temperature (T_c). Therefore, it can be concluded that there is a first order phase transition between the massive DCDW phase (m is large and $Q \neq 0$) and the phase where chiral symmetry is approximately restored (m is

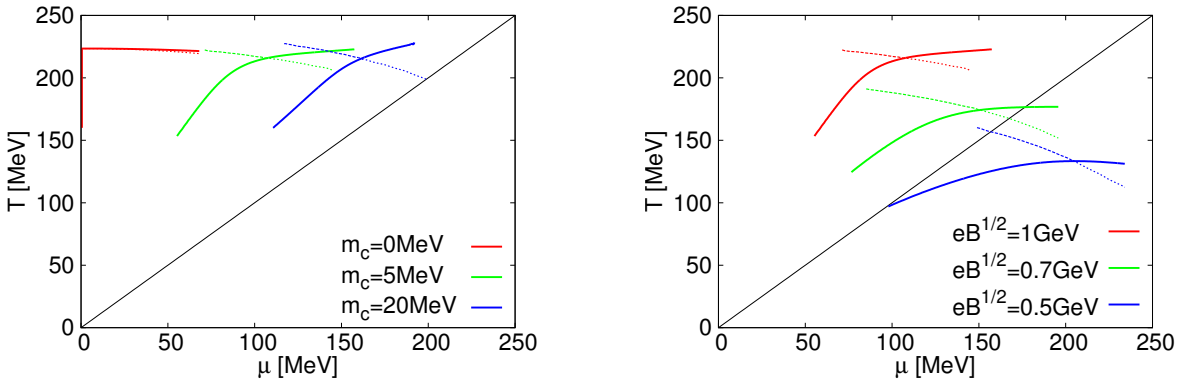

Figure 4.3: Change of the phase boundary. In the left panel, the red, green, blue lines describe the result at $m_c = 0$, 5, 20MeV and fixed $\sqrt{eB} = 1$GeV. In the right panel, the red, green, blue lines describe the result at $\sqrt{eB} = 1$, 0.7, 0.5GeV and fixed $m_c = 5$MeV. The solid lines describe each phase boundary between the massive DCDW phase and the homogeneous phase. The dashed lines describe each crossover line. (The figures are taken from Ref. [76].)

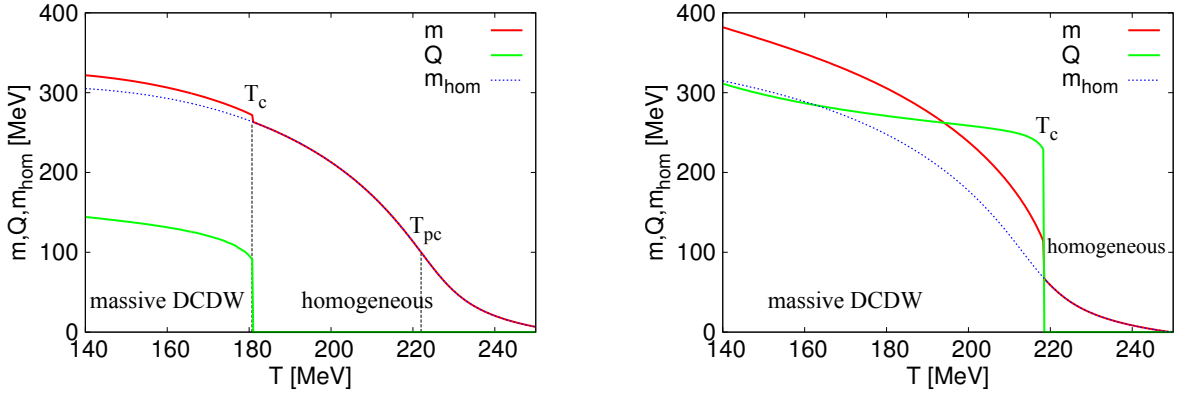

Figure 4.4: Dependence of the order parameters on T for the same parameter set in Fig. 4.2. The red or green line describes the amplitude m or the wave number Q respectively. The dashed blue line shows the conventional dynamical quark mass without the inhomogeneous chiral condensate. The left panel shows the result at $\mu = 70$MeV and there are the phase transition point between the homogeneous phase and the massive DCDW phase on $T_c = 181$MeV and the pseudocritical point on $T_{pc} = 222$MeV. The right panel shows the result at $\mu = 120$MeV and there is the phase transition point on $T_c = 219$MeV. (The figures are taken from Ref. [76].)

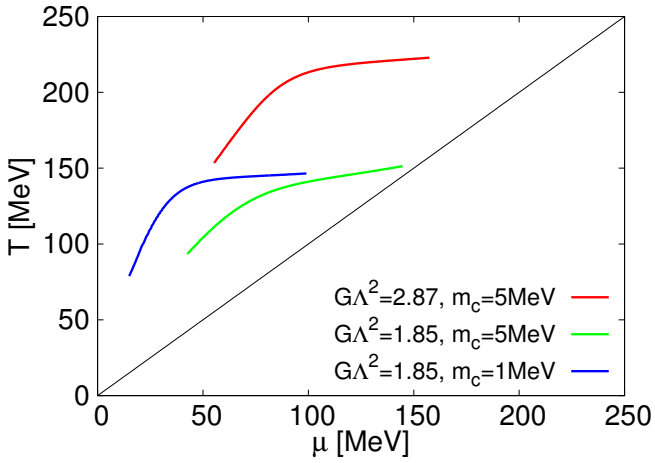

Figure 4.5: Phase boundary obtained including the inverse magnetic catalysis. The red line corresponds to the phase boundary in Fig. 4.2. On the other hand, the green and blue lines describe one at $m_c = 5$, 1MeV with the inverse magnetic catalysis. (The figure is taken from Ref. [76].)

small but finite and $Q = 0$) though there is the second order phase transition between the DCDW phase and the chiral-restored phase in the chiral limit [46]. The difference is caused by the finite m_c. In the chiral limit, Q can take any value in the chiral-restored phase since there is no condensate. On the other hand, the value of Q is uniquely determined in the case of the finite m_c because the condensate never vanishes there. In the right panel, we can see that the first order phase transition is strong while it becomes weaker for lower μ. The crossover between the usual SSB phase and the nearly-restored phase is also observed at the pseudocritical temperature $T = T_{\rm pc}$ in the left panel. The RKC or DCDW phase appears in the region: $\mu > 300$MeV and $T < 50$MeV with m_c and $B = 0$ [41, 28]. However we can see that B extends the massive DCDW phase over the low μ and high T region even if m_c is finite [76]. Furthermore the dynamical quark mass in the massive DCDW phase is larger than that in the case of the homogeneous condensate. In other words, the chiral symmetry breaking is enhanced in the massive DCDW phase. The fact may be consistent with the result in the chiral limit [46]; the chiral symmetry breaking is enhanced in the DCDW phase and the critical temperature is greater than the conventional one.

4.3.2 Effect of the inverse magnetic catalysis

From the lattice QCD calculation, it is known that the magnetic field makes chiral symmetry breaking weak at high T, called the inverse magnetic catalysis [25]. In this subsection, the effect of the inverse magnetic catalysis is discussed in the present model. There are still controversies about this phenomenon. Here, it is assumed that the effect is described by giving a dependence of the magnetic field to the coupling constant of the NJL model (G). According to Ref. [113], G is fitted to reproduce the result of the lattice simulation

[25, 114]. For the parameter set: $\Lambda = 851\text{MeV},\ G\Lambda^2 = 2.87,\ m_c = 5\text{MeV}$, the pseudocritical temperature can be obtained as $T_{pc}(eB = 0) = 173\text{MeV}$ at $\mu = B = 0$. In the following, we consider the case at $\sqrt{eB} = 1\text{GeV}$. The coupling constant is putted as $G\Lambda^2 = 1.85$, which gives the ratio: $T_{pc}/T_{pc}(eB = 0) = 0.86$ at $\mu = 0$. In Fig. 4.5, the change of the phase boundary by the inverse magnetic catalysis is shown. The region of the massive DCDW phase shrinks and the critical temperature decreases due to the effect [76]. However, the massive DCDW phase remains in the $\mu/T < 1$ region if m_c is sufficiently small.

4.4 Possibility of the observation of the inhomogeneous chiral phase

In Ref. [115], the possibility of the observation of the DCDW phase has been discussed in the case with the critical line, $\mu = 0$. Though the existence of the line is pointed out by the generalized GL expansion with the magnetic field in the chiral limit [46], the phase boundary is moved to $\mu \neq 0$ region due to the current quark mass. The discussion becomes somewhat simple in the present case. In the Taylor expansion method, some quantity is expanded around $\mu/T = 0$ for considering the effect of the finite μ. Therefore, this method cannot describe the singularity at $\mu \neq 0$ and the massive DCDW phase cannot be observed. For the same reason, the analytic continuation method from the imaginary chemical potential to the real one does not work either.

The reweighting method can overcome the difficulty of the singularity in principle. In this method, the importance sampling is carried out for some parameter choice, for example $\mathrm{Re}\,\mu = 0$, where there is no sign problem. However, the massive DCDW phase does not develop in that region. Therefore we need to find a special region with the massive DCDW phase and no sign problem there.

In the canonical approach, we also do not have a trouble of the singularity though the grand canonical potential with the real μ can be constructed from the one with the imaginary μ. If there is the massive DCDW phase in $\mu \neq 0$ region, it may be found that the quark number density has the discontinuity derived from some first order phase transition. However, the phase transition cannot be identified as one from the homogeneous phase to the massive DCDW phase. Therefore we need to find some specific order parameters on the phase transition. There is a similar difficulty in the Lee-Yang zero analysis in QCD. The behavior of zeros of the partition function indicates the existence of some phase transition. However, we cannot distinguish the phase transition including the massive DCDW phase by their distribution.

We also comment on the two color lattice QCD ($\mathrm{QC_2D}$). In the $\mathrm{QC_2D}$, there is no sign problem because the quark determinant is always real even if μ is real and finite [116]. Therefore, the existence of iCP may be investigated by the usual Monte Carlo simulation. It is also thought that this analysis works without sufficiently small m_c.

Chapter 5

Relation with the inhomogeneous chiral phase and the Fulde-Ferrel-Larkin-Ovchinnikov superconducting state through nesting and axial anomaly

In this chapter, we discuss the role of nesting and axial anomaly for the appearance of the inhomogeneous chiral phase (iCP) [83]. We consider iCP in 1+1 dimensions to clearly see their interplay. Manifestation of nesting or axial anomaly should be a common feature of iCP in any dimension, since these concepts are based on geometry of the Fermi surface and chiral symmetry itself. The duality between iCP and the Fulde-Ferrel-Larkin-Ovchinnikov (FFLO) superconducting state helps to accomplish our purpose. First, we discuss how axial anomaly is mapped by the duality transformation. Next we figure out the important role of nesting, which is one of the key mechanism for spatially inhomogeneous phases such as charge density wave (CDW), spin density wave (SDW) in quasi-one dimensional systems in condensed matter physics [33, 34, 35, 93], and pion condensation in nuclear matter [117]. It has been sometimes discussed that nesting is responsible for the appearance of dual chiral density wave (DCDW) or its one dimensional analog, chiral spiral, since the wave number q always takes 2μ. On the other hand, the wave number of real kink crystal (RKC) begins with $q = 0$. Since iCP may be regarded as a generation of a kind of density wave, we would like to look into nesting in the context of iCP in detail.

5.1 Axial anomaly in chiral spiral

Here we briefly review how axial anomaly plays a role in iCP by using the 1+1 dimensional Nambu-Jona-Lasinio (NJL_2) models. The Lagrangian of the NJL_2 model takes the form,

$$\mathcal{L}_{\mathrm{NJL}_2} = \bar{\psi} i \partial\!\!\!/ \psi + \frac{G}{2}\left[\left(\bar{\psi}\psi\right)^2 + \left(\bar{\psi} i\gamma_5 \psi\right)^2\right], \tag{5.1.1}$$

which is invariant under $U(1)_L \times U(1)_R$. This Lagrangian is one-flavor case, but easily extended to the N-flavor case endowed with $SU(N)_L \times SU(N)_R$ symmetry. For two-flavor case, it renders

$$\mathcal{L}_{\mathrm{2fNJL}_2} = \bar{\psi} i \partial\!\!\!/ \psi + \frac{G}{2}\left[\left(\bar{\psi}\psi\right)^2 + \left(\bar{\psi} i\gamma_5 \boldsymbol{\tau} \psi\right)^2\right], \tag{5.1.2}$$

which we call the $\mathrm{2fNJL}_2$ model.

Both models exhibit the spontaneous breaking of chiral symmetry. There have been many studies about iCP by using the NJL_2 model such as shown in Sec. 2.1 [90, 118], and little has used $\mathcal{L}_{\mathrm{2fNJL}_2}$ to study flavor asymmetric matter [43, 119, 120]. Chiral spiral is the most favorable phase on the $T-\mu$ plane within the NJL_2 model. The wave vector q then satisfies the relation, $q = 2\mu$, which looks to be the same for the nesting vector in SDW or CDW in quasi-one dimensional systems in condensed matter physics [33, 35, 93]. Accordingly it has been sometimes discussed that chiral spiral is caused by the nesting effect of the Fermi surface. When we consider DCDW in 1+3 dimensions, it appears with the wave vector to be $\mathcal{O}(\mu)$ as shown in Fig. 2.3 [29]. This phenomenon may be understood as a reminiscence of the nesting effect.

It is to be noted that the effect of axial anomaly should plays an important role in 1+1 dimensions, without any gauge field. Introducing a fictious gauge field B_μ, $B_\mu = (\mu, 0)$, we can consider QCD in the background of B_μ. It has been shown that axial-vector current $j_5^\mu = \bar{\psi}\gamma^\mu\gamma_5\psi$ is not conserved by anomaly,

$$\partial_\mu j_5^\mu = \frac{1}{2\pi}\epsilon^{\mu\nu} B_{\mu\nu}, \tag{5.1.3}$$

for one-flavor case, where $B_{\mu\nu} = \partial_\mu B_\nu - \partial_\nu B_\mu$ is the field tensor. This anomaly is an analog of axial anomaly in the presence of the electromagnetic field [49], and it is easily extended for the 1+3 dimensional case, e.g. in the presence of the magnetic field.

Adding a proper term for chemical potential μ, we have an effective Lagrangian,

$$\mathcal{L}_{\mathrm{MF}} = \bar{\psi} i \partial\!\!\!/ \psi - m\bar{\psi}\exp(-i\gamma_5 q x)\psi + \mu\bar{\psi}\gamma_0\psi, \tag{5.1.4}$$

within the mean-field approximation, where chiral spiral is asummed. Using the Weinberg transformation such that $\psi_W = \exp(-i\gamma_5 q x/2)\psi$, we have

$$\tilde{\mathcal{L}}_{\mathrm{MF}} = \bar{\psi}_W i \partial\!\!\!/ \psi_W - \bar{\psi}_W \left[m + \gamma_0 q/2\right]\psi_W + \mu\bar{\psi}_W\gamma_0\psi_W \tag{5.1.5}$$

Usually quark number becomes a finite value once μ is greater than the dynamical mass m at $T = 0$. However, it is known that the chiral spiral phase develops from $\mu = 0$ due

to axial anomaly: the single-particle energy is given by $\varepsilon_k = \pm(k^2+m^2)^{1/2} + q/2$ and the energy spectrum is shifted by $q/2$ from the free one. Anomalous quark number density, which coincides with Eq. (2.1.16) is then generated by the spectral asymmetry and is closely related to axial anomaly [47].

The quark number density is defined by using the Atiyah-Patodi-Singer η invariant, η_H,

$$\begin{aligned} n &= \frac{1}{2}\int \frac{dx}{L}\langle[\psi^\dagger,\psi]\rangle \\ &= -\frac{1}{2}\eta_H + \sum_k \left[\theta(\varepsilon_k) f_F(\varepsilon_k-\mu) - \theta(-\varepsilon_k) f_F(-\varepsilon_k+\mu)\right] \end{aligned} \tag{5.1.6}$$

with

$$\eta_H = \lim_{s\to+0}\sum_k \mathrm{sign}(\varepsilon_k)|\varepsilon_k|^{-s}, \tag{5.1.7}$$

where $f_F(\varepsilon) = (1+e^{\varepsilon})^{-1}$ is the Fermi-Dirac distribution function, η_H is proportional to q, and the particle number is not necessarily zero for any chemical potential [46]. That is why chiral spiral develops from $\mu = 0$.

It should be interesting to see that there is no anomaly for $\mathcal{L}_{\mathrm{2fNJL_2}}$. The anomaly relation (5.2.6) can be easily extended to the two flavor case: for the axial-vector current $j_5^\mu = \bar\psi(\tau_3/2)\gamma^\mu\gamma_5\psi$,

$$\partial_\mu j_5^\mu = \frac{1}{4\pi}\mathrm{tr}(\tau_3)\epsilon^{\mu\nu}B_{\mu\nu} = 0, \tag{5.1.8}$$

where the fictious gauge field B^μ should read $B^\mu = (\mu, 0)$ with $\mu_u = \mu_d = \mu$ in flavor symmetric matter. The chiral spiral is defined as $me^{iqx} = -G(\langle\bar\psi\psi\rangle - i\langle\bar\psi i\gamma^5\tau_3\psi\rangle)$ in this case and the effective Lagrangian renders

$$\mathcal{L}_{\mathrm{2fMF}} = \bar\psi i\partial\!\!\!/\psi - m\bar\psi\exp(-i\gamma_5\tau_3 qx)\psi + \mu\bar\psi\gamma_0\psi \tag{5.1.9}$$

under the mean-field approximation. Accordingly the Weinberg transformation is modified to $\psi_W = \exp(-i\gamma_5\tau_3 q/2)\psi$ and we find

$$\tilde{\mathcal{L}}_{\mathrm{2fMF}} = \bar\psi_W\left[i\partial\!\!\!/ - m - \gamma_0\tau_3 q/2\right]\psi_W + \mu\bar\psi_W\gamma_0\psi_W. \tag{5.1.10}$$

The single-particle energy is now flavor dependent: $\varepsilon_u = \pm(p^2+m^2)^{1/2} + q/2$ and $\varepsilon_d = \pm(p^2+m^2)^{1/2} - q/2$. Thus the energy spectrum of u quarks is shifted upward by $q/2$, while the one of d quarks is shifted downward by $q/2$ from the free case. Consequently, the spectral asymmetry of u and d quarks cancel each other and leave no anomalous quark number [83]. Since the wave number may be regarded as an "isospin chemical potential", $\mu_3 = -q/2$, in this case, we study the phase diagram for given μ by changing μ_3.

Thus chiral spiral appears above $\mu_c/m_0 \simeq 0.68$ in the 2fNJL$_2$ model [43], where m_0 denotes the dynamical mass at $T = \mu = 0$, in contrast with the NJL$_2$ model. It is interesting to see some similar feature to RKC, which also appears above the critical chemical potential $\mu_c/m_0 = 2/\pi$ in the NJL$_2$ model [90]. Since there is no axial anomaly for both RKC and chiral spiral within the 2fNJL$_2$ model, the phase boundaries between iCP and the chiral-restored phase are identical. Actually, it should be determined by the correlation function in the chiral-restored phase regardless of the detail of the inhomogeneous condensate [121].

5.2 Mapping of anomaly through the duality transformation

5.2.1 NJL_2 case

We now consider another manifestation of axial anomaly in the context of iCP. Thies have shown that there is a duality between chiral transition and a kind of superconducting models [77], using the NJL_2 model. Duality transformation is defined as, $\psi \to \chi = \frac{1}{2}(1-\gamma^5)\psi + \frac{1}{2}(1+\gamma^5)\psi^*$, where ${}^t\psi = (\psi_R, \psi_L)$. This is a canonical transformation and the Eq. (5.1.1) can be written as

$$\mathcal{L}_{1f} = \bar{\chi} i\partial\!\!\!/ \chi + \frac{G}{2}\left(\bar{\chi}^c\chi\right)\left(\bar{\chi}^c\chi\right)^\dagger \tag{5.2.1}$$

by introducing new fields, $\chi_L = \psi_L, \chi_R = \psi_R^*$, in terms of left-handed (L-) and right-handed (R-) Weyl fields, ${}^t\chi = (\chi_R, \chi_L)$. χ^c denotes the charge conjugation field, $\chi^c \equiv \gamma^5\chi^*$. The Lagrangian is called the Cooper pair model, which is a toy model of the color superconductivity [122]. For the chemical potential term, it is changed to,

$$\delta L = \mu\left(\chi_L^*\chi_L - \chi_R^*\chi_R\right), \tag{5.2.2}$$

which resembles the interaction term between "magnetic field" μ and "spin-up" (R-) and "spin-down" (L-) quarks, or μ may be regarded as "chiral chemical potential μ_5". In the following we use the notation h instead of $-\mu$. Considering the pairing between L- and R-quarks, the Hamiltonian within MFA renders,

$$\begin{aligned} H_{1f} &= \frac{1}{2}\int dx \left[\chi^\dagger(\gamma^5\hat{p} - \gamma^5 h)\chi + \chi^{c\dagger}(\gamma^5\hat{p} + \gamma^5 h)\chi^c + \Delta^*\bar{\chi}^c\chi + \Delta\bar{\chi}\chi^c + \frac{|\Delta|^2}{G}\right] \\ &= \int dx \left[\Psi^\dagger\left(\hat{p}\sigma_3 + h + \sigma_1 \mathrm{Re}\Delta + \sigma_2 \mathrm{Im}\Delta\right)\Psi + \frac{|\Delta|^2}{2G}\right], \end{aligned} \tag{5.2.3}$$

with the choice of the Dirac matrices as $\gamma_0 = \sigma_1, \gamma^1 = -i\sigma_2$ and $\gamma_5 = \sigma_3$, where $\Psi^\dagger = (\chi_R, \chi_L^*)$. The gap equation takes the form,

$$\Delta = -\frac{G}{2}\langle\bar{\chi}^c\chi\rangle. \tag{5.2.4}$$

Under the duality transformation the chiral condensate made of quark-anti-quark is transformed to the Cooper pair condensate in the context of superconductivity. Thus chiral transition on the T-μ plane is mapped into superconducting transition under the magnetic field h in the vacuum. If the Cooper pair condensate is spatially modulating, such phase can be described as the FFLO phase.

We can see how axial anomaly inherent in the Lagrangian (5.1.1) is mapped into the Lagrangian (5.2.1), following ref. [49]. Since the phase of the gap function defined in Eq. (5.2.4) represents the phonon degree of freedom φ, it transforms as $\varphi \to \varphi + 2\alpha$ under the $U(1)$ transformation, $\chi \to \exp(i\alpha)\chi$. In the presence of a fictious axial-vector gauge field, $C_\mu = (h, 0)$,

we have an anomaly relation for the vector current $j^\mu = \bar{\chi}\gamma^\mu\chi$ by way of the vacuum polarization,

$$\partial_\mu j^\mu = \frac{1}{2\pi}\epsilon_{\mu\nu}C^{\mu\nu}, \tag{5.2.5}$$

with the field strength, $C_{\mu\nu} = \partial_\mu C_\nu - \partial_\nu C_\mu$. This is an analog of Eq. (5.2.6). Accordingly the effective action changes,

$$\delta S = -\int dx \partial_\mu \alpha j^\mu. \tag{5.2.6}$$

Thus the effective Lagrangian must include the relevant term, $\mathcal{L}_{\rm ano} = \frac{1}{2\pi}\frac{d\varphi}{dx}h$, by way of anomaly matching, so that the coefficient of h may be regarded as magnetization [83].

As the case with anomaly in the superconducting states, we consider the FF state under the magnetic field in the vacuum by using the Eq. (5.2.3), where $\Delta = me^{-iqx}$ is assumed. The Hamiltonian can be rewritten by the Nambu-Gorkov formalism,

$$\begin{aligned} H_{1f} &= \frac{1}{2}\int dx \left[(\chi^\dagger, \chi^{c\dagger}) \begin{pmatrix} -i\gamma^5\partial_x - \gamma^5 h & \gamma^0 m e^{-iqx} \\ \gamma^0 m e^{iqx} & -i\gamma^5\partial_x + \gamma^5 h \end{pmatrix} \begin{pmatrix} \chi \\ \chi^c \end{pmatrix} + \frac{m^2}{G}\right] \\ &= \frac{1}{2}\int dx \left[(\chi'^\dagger, \chi'^{c\dagger}) \begin{pmatrix} -i\gamma^5\partial_x - \gamma^5(h-q/2) & \gamma^0 m \\ \gamma^0 m & -i\gamma^5\partial_x + \gamma^5(h-q/2) \end{pmatrix} \begin{pmatrix} \chi' \\ \chi'^c \end{pmatrix} + \frac{m^2}{G}\right], \end{aligned} \tag{5.2.7}$$

where $\chi' \equiv e^{-iqx/2}\chi$. The fermion fields are expanded as a series of the eigenstates,

$$\chi(x) = \int \frac{dp}{2\pi} e^{i(p+q/2)x} \frac{1}{\sqrt{2\epsilon_p}} \begin{pmatrix} \alpha_p\sqrt{\epsilon_p + p} + \beta_p^{c\dagger}\sqrt{\epsilon_p - p} \\ \beta_p\sqrt{\epsilon_p - p} - \alpha_p^{c\dagger}\sqrt{\epsilon_p + p} \end{pmatrix}, \tag{5.2.8}$$

$$\chi^c(x) = \int \frac{dp}{2\pi} e^{i(p-q/2)x} \frac{1}{\sqrt{2\epsilon_p}} \begin{pmatrix} \beta_p\sqrt{\epsilon_p + p} + \alpha_p^{c\dagger}\sqrt{\epsilon_p - p} \\ \alpha_p\sqrt{\epsilon_p - p} - \beta_p^{c\dagger}\sqrt{\epsilon_p + p} \end{pmatrix}, \tag{5.2.9}$$

where $\epsilon_p = \sqrt{p^2 + m^2}$, and, $\alpha_p, \beta_p, \alpha_p^c, \beta_p^c$, are the annihilation operators of the quasiparticles after the Bogoliubov transformation. However, the four annihilation operators are not independent; there is the relation, $\alpha_p(\beta_p) = \alpha_{-p}^c(\beta_{-p}^c)$, because they must satisfy the relation, $\chi^c = \gamma^5\chi^*$. Accordingly there appear four branches in the energy spectrum,

$$\begin{aligned} E_\alpha &= \epsilon_p - h + q/2, \\ E_\beta &= \epsilon_p + h - q/2, \\ E_\alpha^c &= -\epsilon_p + h - q/2, \\ E_\beta^c &= -\epsilon_p - h + q/2. \end{aligned} \tag{5.2.10}$$

The ground state $|\sigma\rangle$ is then defined by filling the negative energy states:

$$\begin{aligned} \alpha_p|\sigma\rangle &= 0 \ (E_\alpha > 0), \\ \beta_p|\sigma\rangle &= 0 \ (E_\beta > 0), \\ \alpha_p^\dagger|\sigma\rangle &= 0 \ (E_\alpha < 0), \\ \beta_p^\dagger|\sigma\rangle &= 0 \ (E_\beta < 0). \end{aligned} \tag{5.2.11}$$

Since the energies of the quasiparticles (5.2.10) exhibits spectral asymmetry, one may expect anomalous particle number as in Eq. (5.1.7). However, we can see that it never induces anomalous particle number, different from the Lagrangian (5.1.4). Note that the number of particles is not identical with that of quasiparticles due to the Bogoliubov transformation [123]. The particle number density can be evaluated in the same manner as in Eq. (5.1.6) and we find,

$$\begin{aligned} n &\equiv \frac{1}{2}\int \frac{dx}{L}\langle\sigma|[\chi^\dagger,\chi]|\sigma\rangle \\ &= \lim_{\Lambda\to\infty}\langle\sigma|\int_{-\Lambda-q/2}^{\Lambda-q/2}\frac{dp}{2\pi}\left[\left(\alpha_p^\dagger\alpha_p-\alpha_{-p}^\dagger\alpha_{-p}\right)\frac{\epsilon_p+p}{2\epsilon_p}+\left(\beta_p^\dagger\beta_p-\beta_{-p}^\dagger\beta_{-p}\right)\frac{\epsilon_p-p}{2\epsilon_p}\right]|\sigma\rangle \\ &= 0. \end{aligned} \tag{5.2.12}$$

In the above calculation, we have used the relation,

$$\langle\sigma|\alpha_p^\dagger\alpha_p|\sigma\rangle = \langle\sigma|\alpha_{-p}^\dagger\alpha_{-p}|\sigma\rangle = f_F(E_\alpha), \tag{5.2.13}$$

$$\langle\sigma|\beta_p^\dagger\beta_p|\sigma\rangle = \langle\sigma|\beta_{-p}^\dagger\beta_{-p}|\sigma\rangle = f_F(E_\beta). \tag{5.2.14}$$

Furthermore, in the limit: $m\to 0$, any physical quantity calculated from the fermion fields (5.2.8) and (5.2.9) should coincide with the one in the no interacting case even if q is still finite. This is because a physical quantity does not depend on q in the limit, $m\to 0$, where the wave number q becomes a redundant variable due to the amplitude m vanishing. To satisfy the requirement, we need to employ the asymmetric cutoff in the momentum integral, $[-\Lambda-q/2,\Lambda-q/2]$, for the χ field (see Appendix D for details).

As is inferred from Eq. (5.2.6), we shall see the appearance of the anomalous magnetization instead. By using the quasiparticle operators, the magnetization can be evaluated as,

$$\begin{aligned} M &\equiv \frac{1}{2}\int \frac{dx}{L}\langle\sigma|[\chi^\dagger,\gamma^5\chi]|\sigma\rangle \\ &= \lim_{\Lambda\to\infty}\langle\sigma|\int_{-\Lambda-q/2}^{\Lambda-q/2}\frac{dp}{2\pi}\left[\left(\alpha_p^\dagger\alpha_p+\alpha_{-p}^\dagger\alpha_{-p}-1\right)\frac{\epsilon_p+p}{2\epsilon_p}-\left(\beta_p^\dagger\beta_p+\beta_{-p}^\dagger\beta_{-p}-1\right)\frac{\epsilon_p-p}{2\epsilon_p}\right]|\sigma\rangle \\ &= \lim_{\Lambda\to\infty}\left[\int_{-\Lambda-q/2}^{\Lambda-q/2}\frac{dp}{2\pi}f_F(E_\alpha)\frac{\epsilon_p+p}{\epsilon_p}-\int_{-\Lambda-q/2}^{\Lambda-q/2}\frac{dp}{2\pi}f_F(E_\beta)\frac{\epsilon_p-p}{\epsilon_p}-\int_{-\Lambda-q/2}^{\Lambda-q/2}\frac{dp}{2\pi}\frac{p}{\sqrt{p^2+m^2}}\right] \\ &= \lim_{\Lambda\to\infty}\left\{\int_{-\Lambda-q/2}^{\Lambda-q/2}\frac{dp}{2\pi}\left[f_F(E_\alpha)-f_F(E_\beta)\right]+\int_{\sqrt{(\Lambda+q/2)^2+m^2}}^{\sqrt{(\Lambda-q/2)^2+m^2}}\frac{d\epsilon_p}{2\pi}\left[f_F(E_\alpha)-f_F(E_\beta)\right]\right. \\ &\quad \left.-\frac{m}{2\pi}\int_{\tan^{-1}(-\Lambda/m-q/2m)}^{\tan^{-1}(\Lambda/m-q/2m)}d\theta\frac{\tan\theta}{\cos\theta}\right\} \\ &= \lim_{\Lambda\to\infty}\int_{-\Lambda-q/2}^{\Lambda-q/2}\frac{dp}{2\pi}\left[f_F(E_\alpha)-f_F(E_\beta)\right]+\frac{q}{2\pi}. \end{aligned} \tag{5.2.15}$$

The first term represents the paramagnetic magnetization, which counts the difference of the number of the up- and down-spin particles and the second term means the anomalous

magnetization [83]. The anomalous magnetization corresponds to the coefficient of h in $\mathcal{L}_{\rm ano}$ by putting $\varphi = qx$ in Eq. (5.2.6). On the other hand, the LO state does not have the anomalous magnetization because there is no phase degree of freedom[1].

5.2.2 2fNJL$_2$ case

It is not evident whether the same features hold for other models such as the 2fNJL$_2$ model (5.1.2), which is an anomaly-free model. We shall see the different features for the 2fNJL$_2$ model and how anomaly is responsible to these differences. For this model, the duality transformation may be modified as $\psi \to \chi = \frac{1}{2}(1-\gamma^5\tau_3)\psi + \frac{1}{2}(1+\gamma^5\tau_3)\psi^*$ to include the flavor dependence[2], so that the Lagrangian (5.1.2) can be written as,

$$\mathcal{L} = \bar{\chi} i\partial\!\!\!/ \chi + \frac{G}{2}\left[\left(\bar{\chi}^c \tau_3 \chi\right)\left(\bar{\chi}^c \tau_3 \chi\right)^\dagger + \left(\bar{\chi} i\gamma^5 \tau_1 \chi\right)^2 + \left(\bar{\chi} i\gamma^5 \tau_2 \chi\right)^2 \right]. \tag{5.2.16}$$

For the chemical potential term, it is changed to,

$$\delta L = -h\left(\chi_L^{u*}\chi_L^u - \chi_R^{u*}\chi_R^u - \chi_L^{d*}\chi_L^d + \chi_R^{d*}\chi_R^d\right). \tag{5.2.17}$$

Accordingly we have the Hamiltonian within the mean-field approximation by assuming $\langle \bar{\chi} i\gamma^5 \tau_{1,2}\chi\rangle \equiv 0$ and

$$\Delta = -\frac{G}{2}\langle \bar{\chi}^c \tau_3 \chi\rangle (\neq 0), \tag{5.2.18}$$

for the charge-neutral system,

$$H_{2f} = \int dx \left[\tilde{\Psi}^\dagger \left(\hat{p}\sigma_3 + h + \sigma_1 {\rm Re}\Delta + \sigma_2 {\rm Im}\Delta\right)\tilde{\Psi} + \tilde{\Phi}^\dagger \left(\hat{p}\sigma_3 + h + \sigma_1 {\rm Re}\Delta - \sigma_2 {\rm Im}\Delta\right)\tilde{\Phi} + \frac{|\Delta|^2}{2G}\right], \tag{5.2.19}$$

where, $\tilde{\Psi}^\dagger = (\chi_R^u, \chi_L^{u*})$, $\tilde{\Phi}^\dagger = (\chi_R^{d*}, \chi_L^d)$.

If there is only the u-quark sector, the Hamiltonian is reduced to the one-flavor case (5.2.3). In the LO state or in the case of no phase factor in the gap function, two Hamiltonians of the $\tilde{\Phi}$ and $\tilde{\Psi}$ sectors become identical and the total Hamiltonian is reduced to the one-flavor case except the overall factor. Therefore the phase diagram of the LO state is not changed for any number of flavor.

However, for the FF state, the phase diagram is different between one- and two-flavor cases due to the existence of anomaly. Actually the Fig. 5.1 shows the difference of the appearing region of the FF phase between the one- and two-flavor cases. In the two-flavor case, the u-quark sector has the energy spectrum (5.2.10) while the d-quark sector has the

[1] It does not necessarily imply the absence of magnetization in the LO phase, where only paramagnetic effect gives rise to magnetization [124].

[2] One may consider the flavor independent transformation,$\psi \to \chi = \frac{1}{2}(1-\gamma^5)\psi + \frac{1}{2}(1+\gamma^5)\psi^*$, but the resultant Lagrangian explicitly violates particle number conservation. Therefore we treat only the flavor dependent transformation in the following.

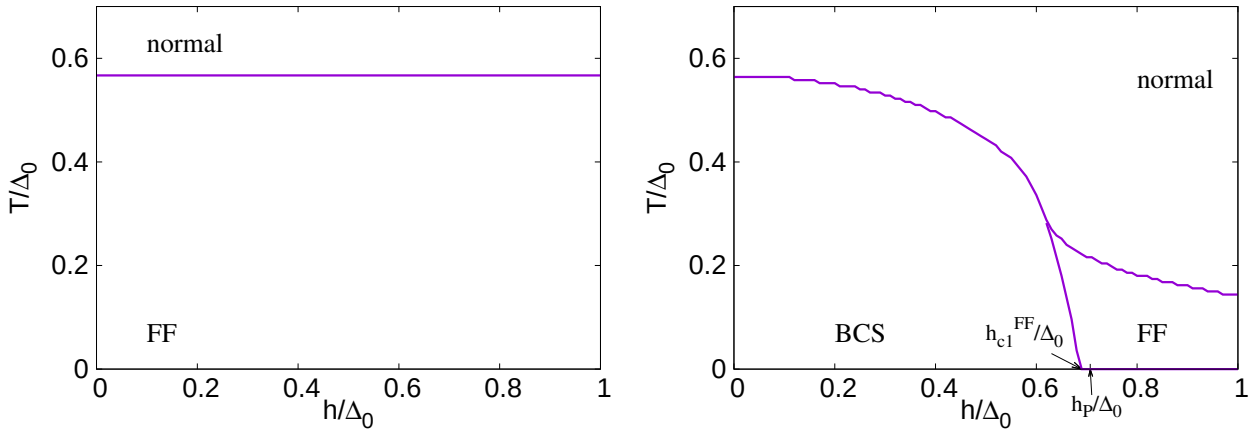

Figure 5.1: The difference of the regions of the FF phase between the one-flavor (left panel) and two-flavor (right panel) cases. Δ_0 denotes the magnitude of the gap function Δ at $T = h = 0$. h_P represents the Pauli paramagnetic limit, $h_P/\Delta_0 = 1/\sqrt{2}$, and h_{c1}^{FF} denotes the lower critical field at $T = 0$, where the first order phase transition occurs, $h_{c1}^{FF}/\Delta_0 \simeq 0.68$ in the 2fNJL$_2$ model, while $h_{c1}^{FF} = 0$ in the NJL$_2$ model. The higher critical field h_{c2}^{FF} diverges at $T = 0$ in both cases due to the perfect nesting (see the text). (The figures are taken from Ref. [83].)

similar energy spectrum with the opposite sign of q. Since the magnetization is given by summing up both contributions of the u- and d-sectors, they completely cancel each other. This may be also infered from the anomaly relation in the flavor-symmetric matter,

$$\partial_\mu j^\mu = \frac{1}{4\pi}\mathrm{tr}(\tau_3)\epsilon_{\mu\nu}C^{\mu\nu}, \tag{5.2.20}$$

for $j^\mu = \bar{\chi}\gamma^\mu\chi$ in the 2fNJL$_2$ model [83]. Consequently the phase diagram for RKC is the same as the one given by Machida and Nakanishi [124] for the LO state, once chemical potential is replaced by the magnetic field; they studied the possibility of the FFLO state in the quasi-one dimensional system by changing the strength of the magnetic field. They used the linear dispersion approximation near the Fermi surface, so that there appear Dirac electrons with definite motions, the light and right moving electrons for each spin state. Solving the Bogoliubov-de Gennes equation self-consistently within the mean-field approximation, they found the FFLO state above the critical magnetic field. They also found that the phase boundaries between the FF and LO states and the normal phase are identical as they should be. For the 2fNJL$_2$ model, the Hamiltonian (5.2.19) looks identical with the one argued by

Machida and Nakanishi with the following correspondence,

$$\begin{aligned} \chi_R^u &\leftrightarrow \psi_\downarrow, \\ \chi_L^u &\leftrightarrow \phi_\uparrow, \\ \chi_R^d &\leftrightarrow \psi_\uparrow, \\ \chi_L^d &\leftrightarrow \phi_\downarrow, \end{aligned} \tag{5.2.21}$$

where $\psi(\phi)$ represents the left(right) moving electron field and the up(down) arrow denotes the up(down) spin state.

5.3 Nesting for iCP

Nesting of the Fermi surface is one of the important concepts in condensed matter physics [33, 35, 38, 93]. As is already mentioned, the nesting effect is most prominent at $T = 0$. So we, in the following, concentrate on the low temperature case. Nesting may be also a driving mechanism for iCP. It has been sometimes discussed that chiral spiral appears due to nesting in 1+1 dimensions, because there is opened an energy gap m at the Fermi surface of massless quarks and the wave number q takes 2μ at the same time. On the other hand it looks rather difficult to interpret the onset of RKC by nesting, because the wave number takes zero at the threshold. We'd like to give some remarks about the relation between iCP and nesting.

First of all we point out that it is too naive for the onset of chiral spiral to be attributed to nesting. We have seen that axial anomaly plays an important role for the relation $q = 2\mu$. Moreover, chiral spiral develops for arbitrary chemical potential below the critical temperature. These are peculiar consequences within the NJL_2 model. Actually we have seen in the $\mathrm{2fNJL}_2$ model that there exists a critical chemical potential μ_c, above which chiral spiral develops. The phase transition is of the first order in this case, and the wave number takes a finite value of $\mathcal{O}(2\mu)$ at μ_c. Interestingly, the wave number takes the same order of magnitude as in the NJL_2 model. Note that the magical relation $q = 2k_F$ for nesting in 1+1 dimensions has been derived by the lowest-order perturbation; e.g., the Lindhard function, which is the lowest order density-density correlation function or susceptibility, logarithmically diverges at $q = 2k_F$ at $T = 0$ in 1+1 dimensions to lead to formation of density wave [125]. In the present model, k_F means the Fermi momentum of the no-interacting quarks, that is, $k_F = \mu$. In our case the energy gap is generated by the non-perturbative effect and the magical relation may not hold as it does. On the other hand, we can see that the number of the wave number approaches $2k_F$ at $T = 0$ around the critical chemical potential for the transition to the chiral-restored phase, where the non-perturbative effect becomes tiny and the perturbative result should hold. Thus we can see that nesting may play an important role for chiral spiral.

For RKC the phase transition is of the second order and the wave number takes $q = 0$ at the critical chemical potential $\mu_c^{\mathrm{RKC}}/m_0 = 2/\pi$ [28, 111, 126]. However, the number of the wave number rapidly increases in the RKC phase and immediately approaches $q = \mathcal{O}(2\mu)$. Thus one may say nesting works except a small region around μ_c^{RKC}.

It should be interesting to see how such nesting effect manifests after the duality transformation. Since the Hamiltonian describes a kind of superconducting phase, a different kind

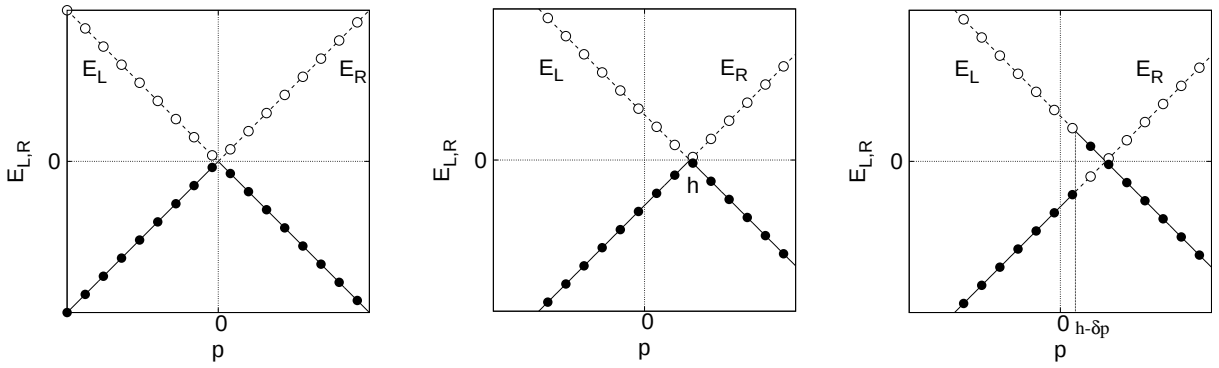

Figure 5.2: The vacua and an excited state with or without the magnetic field in the absence of the Cooper pairing. Filled(unfilled) circles denote the occupied(unoccupied) states. The left panel shows the normal vacuum in the absence of the magnetic field with the energy spectrum, $E_{R,L} = \pm p$. The midlle panel shows the h-vacuum to give the energy spectrum, $E_R = p - h, E_L = -p + h$. The right panel shows an excited state where the number density of L-particles is generated by $\frac{\delta p}{2\pi}$ and that of right-handed holes is generated by $\frac{\delta p}{2\pi}$ compared to the h-vacuum. (The figures are taken from ref. [83]).

of nesting should be seen. There are two kinds of nesting: one (type-I) is familiar as a driving mechanism of charge density wave or spin density wave in quasi-one dimensional system [33, 35, 93, 125]. The other one is responsible to the FFLO state (type-II). In the magnetic field, two Fermi spheres with different Fermi momenta p_F^i are created by the paramagnetic effect, if any interaction is absent. Nesting in the type-II case is a combination of the inversion and translation of one Fermi sphere by $\delta p_F \equiv |p_F^1 - p_F^2|$ to match with another one. In particular we shall see that RKC can be more easily understood by the type-II nesting.

Note that the FFLO state is not necessarily induced in the presence of the magnetic field. Instead there is a competition between the paramagnetic effect and the Cooper pairing effect; the paramagnetic effect favors a specific spin state and leads to the difference of the Fermi momenta of the two spin states, while the Cooper pairing effect becomes maximum for the equal Fermi momenta [79]. When the paramagnetic effect dominates over the Cooper pairing effect, the FFLO state is realized due to the type-II nesting. The landmark of the lower critical filed is then given by the Pauli paramagnetic (Chandrasekhar-Clogston) limit, $h_P/\Delta_0 = 1/\sqrt{2}$ [79].

We can see by two steps how the type-II nesting works by considering the change of the energy spectra given in Fig. 5.2. Normal vacuum is constructed by filling the negative energy states as given by the left panel in Fig. 5.2. In the first step we consider the paramagnetic effect. When the magnetic field is applied to the normal vacuum, the energy spectra are changed for L- and R-particles. The middle panel in Fig. 5.2 shows the vacuum in the presence of the magnetic field (h-vacuum), where all the negative energy states are occupied to make the total energy to be minimum. In the h-vacuum, there is an imbalance between the

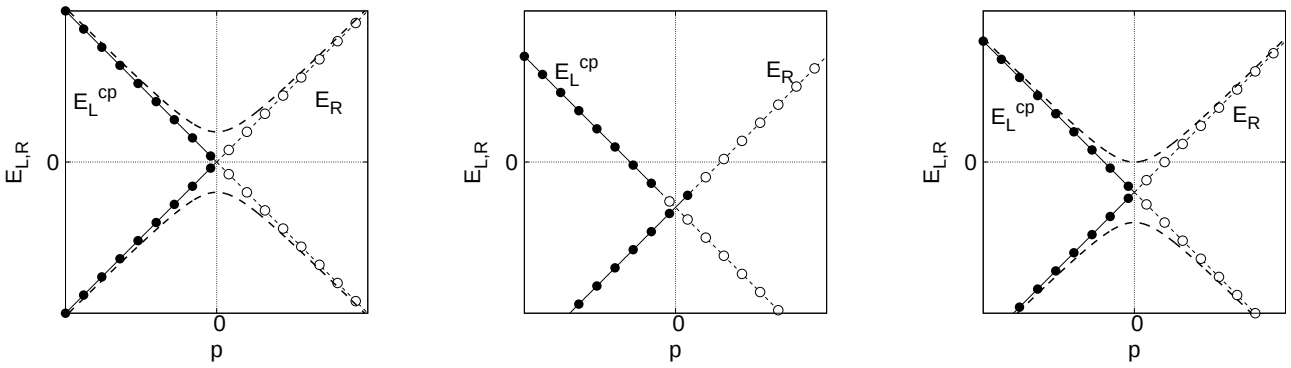

Figure 5.3: Configuration of the Fermi surface at the transition point from the normal phase to the superconducting phase. Filled(unfilled) circles denote the occupied(unoccupied) states. The left panel shows configuration of the BCS state in the absence of the magnetic field. E_L^{cp} denotes the inversion spectrum of E_L in the normal vacuum and the bold dashed lines describe the quasiparticle energy, $\pm\sqrt{m^2+p^2}$. The middle panel shows the inversion spectrum of E_L, E_L^{cp}, from the right panel in Fig. 5.2. The right panel shows the way of the pairing after the momentum shift $\pm(h-\delta p)$ to give the quasiparticle energy spectra (E_α and E_β^c) denoted by the bold dashed lines. (The figures are taken from Ref. [83]).

number of R- and L-particles due to the paramagnetic effect. Therefore magnetization can be evaluated to be $M_h = h/\pi$ because the number density of R-particles is increased by $\frac{h}{2\pi}$ and that of L-particles is inversely reduced by $\frac{h}{2\pi}$ compared to the normal vacuum. We can also consider the excited states where some particle-holes are generated from the h-vacuum. The right panel in Fig. 5.2 shows an excited state where the number density of particle-hole pairs is evaluated as $\frac{\delta p}{2\pi}$ by using the energy-level spacing $2\pi/L$. In the excited state, the number density of R-particles is reduced by $\frac{\delta p}{2\pi}$ and that of L-particles is increased by $\frac{\delta p}{2\pi}$ compared to the h-vacuum as shown in the middle panel in Fig. 5.2. Consequently, magnetization takes the finite value, $M = (h-\delta p)/\pi$. Note that we cannot choose the optimal one among them in this step, because the basic variational principle should be applied to the total energy after taking into account the Cooper pairing effect.

In the second step we consider the Cooper pairing effect. In Fig. 5.3 the construction of the quasi-particle energy is graphically explained. In the absence of the magnetic field, the BCS state is formed by the simple inversion of one energy spectrum from the normal vacuum as shown in the left panel. For the FFLO state, we arrive at the quasiparticle energy with the pairing gap at the Fermi surface by the inversion of one energy spectrum and the relative momentum shift with $q = 2(h-\delta p)$ for the excited state. Such momentum shift corresponds to the wave number of the spatial modulation of the gap function. When $q \neq 0$ takes the energy minimum, the FF state appears in the ground state in place of the BCS state. When $\delta p = h$, we can see the usual BCS gap at the Fermi surface $p_F = 0$ by inversion of one spectrum, so that the gap function is constant. On the other hand, when the same

manipulation is applied for the h-vacuum, we can see the momentum must be shifted by $q = 2h$ after inversion.

The h-vacuum is realized at the phase boundary between the FFLO state and the normal phase. The typical momentum $q = 2h$ can be also seen by considering the correlation function between the Cooper pairs in the normal phase: it depends on the dimensionality and logarithmically diverges at $q = 2h$ in 1+1 dimensions [127, 128, 129].

We consider how the type-I nesting is mapped to the type-Ⅱ nesting by the duality transformation [83]. As is discussed above axial anomaly sometimes conceals the nesting effect, we first discuss it by using an anomaly-free model, such as the 2fNJL$_2$ model. After applying the duality transformation, we consider the FFLO state under the magnetic field in the vacuum, described by the Hamiltonian (5.2.19). Our model then becomes the same one discussed by Machida and Nakanishi in the context of condensed matter physics. Accordingly the phase diagram becomes the same. For the LO state, the phase transition is of the second order from the BCS state at the lower critical field $h_{c1}^{\rm LO}$, $h_{c1}^{\rm LO}/\Delta_0 = 2/\pi$. The wave number increases from the zero value, which reflect the type-Ⅱ nesting. The excited state, $\delta p = h$, is realized at the phase boundary between the BCS state and the LO state. On the other hand, for the FF state, the phase transition is of the first order with finite wave number of $\mathcal{O}(2h)$. This feature looks somewhat different from the LO state, but one may see the type-Ⅱ nesting works except the small region of the lower critical field $h_{c1}^{\rm FF}$, $h_{c1}^{\rm FF}/\Delta_0 \simeq 0.68$. We can also see that the phase boundaries from the LO and FF phases to normal phase coincide with each other [83]. Thus we can say the type-Ⅱ nesting works for the FFLO state. It should be interesting to note that the upper critical field h_{c2} diverges for both phases as $T \to 0$ in 1+1 dimensions due to the perfect type-II nesting with $q = 2h$.

For the NJL$_2$ model, the argument about the LO state is unchanged, since the order parameter is real and the model Hamiltonian is reduced to (5.2.3), while that about the FF state is greatly modified. We shall discuss some surprising aspects of the FF state in the NJL$_2$ model. The FF state appears once a tiny magnetic field is applied due to anomaly inducing the anomalous term $\mathcal{L}_{\rm ano}$; the thermodynamic potential seems to include the linear term of q, To obtain the correct thermodynamic potential, the appropriate momentum cutoff,$[-\Lambda - q/2, \Lambda - q/2]$, should be used in the χ sector. From the relation, $\chi^c = \gamma^5\chi^*$, the asymmetric cutoff in the χ^c sector should be $[-\Lambda + q/2, \Lambda + q/2]$. From the Hamiltonian (5.2.7), the

thermodynamic potential at $T = 0$ renders,

$$
\begin{aligned}
\Omega &\equiv \frac{\langle\sigma|H_{1f}|\sigma\rangle}{L} \\
&= \frac{1}{2}\int\frac{dx}{L}\langle\sigma|(\chi'^{\dagger},\chi'^{c\dagger})\begin{pmatrix}-i\gamma^5\partial_x-\gamma^5(h-q/2) & \gamma^0 m\\ \gamma^0 m & -i\gamma^5\partial_x+\gamma^5(h-q/2)\end{pmatrix}\begin{pmatrix}\chi'\\ \chi'^c\end{pmatrix}|\sigma\rangle+\frac{m^2}{2G} \\
&= \frac{1}{2}\int_{-\Lambda-q/2}^{\Lambda-q/2}\frac{dp}{2\pi}\frac{1}{2\epsilon_p}\langle\sigma|\Big\{[p-h+q/2]\left[(\epsilon_p+p)\alpha_p^\dagger\alpha_p+(\epsilon_p-p)\beta_p^c\beta_p^{c\dagger}\right] \\
&\qquad -[p-h+q/2]\left[(\epsilon_p+p)\alpha_p^c\alpha_p^{c\dagger}+(\epsilon_p-p)\beta_p^\dagger\beta_p\sin^2\theta\right]\Big\}|\sigma\rangle \\
&\quad +\frac{1}{2}\int_{-\Lambda+q/2}^{\Lambda+q/2}\frac{dp}{2\pi}\frac{1}{2\epsilon_p}\langle\sigma|\Big\{[p+h-q/2]\left[(\epsilon_p+p)\beta_p^\dagger\beta_p+(\epsilon_p-p)\alpha_p^c\alpha_p^{c\dagger}\right] \\
&\qquad -[p+h-q/2]\left[(\epsilon_p+p)\beta_p^c\beta_p^{c\dagger}+(\epsilon_p-p)\alpha_p^\dagger\alpha_p\right]\Big\}|\sigma\rangle \\
&\quad +m^2\int_{-\Lambda+q/2}^{\Lambda-q/2}\frac{dp}{2\pi}\frac{1}{2\epsilon_p}\langle\sigma|\left(\alpha_p^\dagger\alpha_p-\beta_p^c\beta_p^{c\dagger}+\beta_p^\dagger\beta_p-\alpha_p^c\alpha_p^{c\dagger}\right)|\sigma\rangle+\frac{m^2}{2G}. \qquad (5.3.1)
\end{aligned}
$$

Assuming $|h-q/2|<m$, it can be reduced,

$$
\begin{aligned}
\Omega &= -\int_{-\Lambda-q/2}^{\Lambda-q/2}\frac{dp}{2\pi}\frac{p}{\epsilon_p}(p-h+q/2)-m^2\int_{-\Lambda+q/2}^{\Lambda-q/2}\frac{dp}{2\pi}\frac{1}{\epsilon_p}+\frac{m^2}{2G}. \\
&= -\frac{\Lambda^2}{2\pi}-\frac{m^2}{2\pi}\ln(2\Lambda/m)-\frac{m^2}{4\pi}+\frac{1}{2\pi}(h-q/2)^2-\frac{h^2}{2\pi}+\frac{m^2}{2G}. \qquad (5.3.2)
\end{aligned}
$$

The quadratic-divergence term is irrelevant and can be subtracted off. The logarithmic divergence can be removed by the appropriate renormalization scheme independent of q as in the GN model [130]. We can see that Ω includes the linear term of q, so that the minimum condition gives rise to the relation, $q = 2h$, even if the magnetic field is tiny [83]. In the case, $|h-q/2|>m$, the thermodynamic potential can be calculated in the same way. However its energy minimum is larger than that at $q = 2h$. Hence the lower critical field becomes zero and the perfect type-II nesting always holds with $q = 2h$.

Chapter 6

Effect of fluctuations in the inhomogeneous chiral phase

In this chapter, we analyze the effect of the fluctuations around the mean fields.

In the absence of the magnetic field, it has been shown that the Nambu-Goldstone (NG) mode excitations destroys the inhomogeneous chiral phase (iCP) at finite T [84, 85]. In these analysis, the dispersion of the NG mode is calculated by using the low-energy effective potential. As an important consequence, it has been shown that for one-dimensional modulations of the condensate the correlation functions of the quark-antiquark bilinear fields exhibit quasi-long-range order (QLRO) with algebraic decay at large distances at finite T in accord with the Landau-Peierls theorem [93, 131], while true long-range order is realized in the usual spontaneous symmetry breaking (SSB) phase. In addition, the thermal average of the quark condensate becomes zero for $T \neq 0$ due to thermal fluctuations. These results come from the spatially anisotropic dispersion relation of the NG modes.

We'd like to further elucidate the consequences of the anisotropic dispersion relation in the context of iCP. This chapter is composed of two parts. One is the analysis of the Brazovski-Dugaev effect in the absence of the magnetic field [121]. The other is the discussion about the stability of the dual chiral density wave (DCDW) phase in the presence of the magnetic field.

6.1 Effect of fluctuations to the inhomogeneous chiral phase transition in the absence of the magnetic field

In this section, we elucidate interesting aspect of the fluctuations near the phase boundary in the absence of the magnetic field [121]. Starting from the Lifshitz point (LP), iCP is enclosed by the two phase boundaries on the μ-T plane (see Fig. 6.1): one is the L-boundary separating the usual SSB phase and iCP at lower μ, and the other is the R-boundary in contact with the chiral-restored phase at larger μ. It has then been shown that the L-boundary has

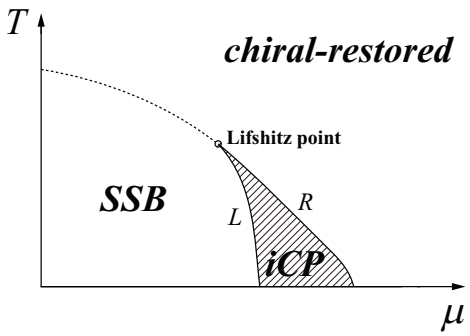

Figure 6.1: Schematic phase diagram for chiral symmetry breaking in the (μ, T) plane within the mean-field NJL model in the chiral limit. The shaded domain enclosed by the left- (L-) and right-hand-side (R-) boundaries represents iCP. The L-boundary is of first or second order, depending on the type of iCP [29, 28, 44], whereas the R-boundary is always of second order. The boundary between the SSB and chiral-restored phases is of second order in the chiral limit (dotted line). (The figure is taken from Ref. [121].)

different orders and properties of the phase transition, depending on the type of the condensates [29, 28, 44], while the R-boundary is determined independent of the condensate within the Nambu-Jona-Lasinio (NJL) model in the mean-field approximation (MFA)[1]. When we approach to the R-boundary from the chiral-restored phase, we may see a general feature: since the system is chiral-symmetric and isotropic in the chiral-restored phase, we cannot say what type of condensates is realized after the phase transition. Since the order parameter consists of the scalar and pseudoscalar condensates, the effective potential can be written by such condensates in a symmetric form in the chiral-restored phase. The R-boundary may be then found by the analysis of this effective potential. In the SSB phase, on the other hand, the effective potential may be written in terms of only the scalar condensate, so that the L-boundary can have different predictions. Within the MFA, it has been shown that the chiral-restored phase undergoes the second-order phase transition at the R-boundary. We study the nature of the inhomogeneous phase transition around the R-boundary by looking into both quantum and thermal fluctuations of quark-antiquark pairs or quark particle-hole pairs (hereafter collectively called "chiral pairs") in the chiral-restored phase.

A similar situation also arises in the context of pion condensation in nuclear matter, where nucleon particle-hole pairs are excited [117, 136]. In condensed matter physics, it corresponds to the Fulde-Ferrel-Larkin-Ovchinnikov (FFLO) state in superconductivity, where the electron Cooper pairs are excited [36, 37, 80, 81]. One important common feature prevailing in these phenomena can be seen through the dispersion relation of the fluctuations; it has a

[1] A similar result has been obtained in a Dyson-Schwinger type approximation to QCD [32]. However, in general, the character of the R-boundary depends on microscopic models and approximations. Actually, e.g., in the quark-meson model [28, 132, 133, 134] or nonlocal chiral quark models [135], it has been suggested that there is a high sensitivity of the existence of iCP (R-boundary) on model parameters.

minimum at a nonzero momentum $|\boldsymbol{q}| = q_c$ on the two-dimensional sphere[2] in isotropic systems [86, 87, 129, 137, 138], which suggests that the order parameter is spatially modulated after the phase transition. This is qualitatively different from the usual phase transitions, such as homogeneous transitions in superconductivity or those for chiral symmetry breaking, where the dispersion of the fluctuations has a minimum at $|\boldsymbol{q}| = 0$. In the context of superconductivity, the effect of the fluctuations has been studied in the vicinity of the critical point by Nozière and Schmitt-Rink [128] within the linear (Gaussian) approximation to clarify the BCS-BEC crossover problem. It has been further discussed in the context of a BEC of atoms [139], and also studied to understand a precursor of (color-)superconductivity, known as the pseudogap phenomenon [140, 141].

A general theory for the inhomogeneous phase transition has been first presented by Brazovskii [86] at finite T. A similar issue has been discussed by Dyugaev [87] at zero temperature in the context of pion condensation. They have taken into account the interactions among the fluctuations beyond the Gaussian approximation. Unlike the homogeneous phase transition, such a nonlinear effect is now essential. One of the remarkable findings is the change of the order of the phase transition stemming from the fluctuation effects; the second-order phase transition within the MFA is changed to the first-order one (sometimes termed the *fluctuation-induced first-order phase transition*). This subject has been further studied within the renormalization group approach [142]. Also, the Brazovskii theory has been applied to diblock coplymers [138, 137, 143], including its experimental verification [144]. However, it seems that the importance of such studies is not fully conceded, e.g., in the discussion of the FFLO state, while there are few works about the anomalous effect of the fluctuation [129]. A heuristic argument about the fluctuation-induced first-order phase transition for the inhomogeneous chiral transition have been presented [88]. The phenomenon is called the *Brazovskii-Dyugaev effect*. In this section, extending this work to the general case with $O(N)$ symmetry, we elucidate the particular roles of quantum and thermal fluctuations [121]. We also point out a continuity of the effects of both fluctuations across R-boundary, by analyzing the behavior of the correlation function attributed to the excitations of the (NG) modes in iCP.

Another purpose of this section is to draw one's attention again to the fluctuation-induced first-order phase transition. Throughout this section we emphasize some common features for inhomogeneous phase transitions, such as those into the FFLO state in superconductivity. We also discuss some observational implications peculiar to the fluctuation-induced first-order phase transition [121]. Recently, in a B20 compound MnSi which undergoes a fluctuation-induced first-order transition of the Brazovskii type[3] [86], an unequivocal experimental confirmation has been obtained via neutron scattering and thermodynamic observables [148]. The first-order character of such a transition may also be expected to be experimentally confirmed for the inhomogeneous chiral transition, e.g., in relativistic heavy-ion collisions.

[2] In this case, the fluctuations become soft on a finite manifold in momentum space, rather than at a single point [86].

[3] This type is relevant for the case with an $O(N)$ symmetric N-component order parameter, which differs from the case with an order parameter coupled to a fluctuating gauge field (e.g., for superconductors and smectic-A liquid crystals [145]) or with sufficiently large components $N \geq 4$ [146] (see also, e.g., Ref. [147]).

6.1.1 Framework

We use the two-flavor NJL model in 1+3 dimensions and the Lagrangian density takes the form,

$$\mathcal{L} = \bar{\psi} i \partial\!\!\!/ \psi + G \left[\left(\bar{\psi} \psi \right)^2 + \left(\bar{\psi} i \gamma_5 \boldsymbol{\tau} \psi \right)^2 \right]. \tag{6.1.1}$$

The partition function reads $Z = \int \mathcal{D}\psi \int \mathcal{D}\bar{\psi} e^{-S}$ with the Euclidean action in imaginary time ($t \to -i\tau$) being,

$$S = -\int_0^\beta d\tau \int d^3\boldsymbol{x} \left[\bar{\psi} \left(-\gamma^0 \frac{\partial}{\partial \tau} + i\boldsymbol{\gamma} \cdot \nabla + \mu \gamma^0 \right) \psi + G \left[\left(\bar{\psi} \psi \right)^2 + \left(\bar{\psi} i \gamma_5 \boldsymbol{\tau} \psi \right)^2 \right] \right], \tag{6.1.2}$$

where $\beta = 1/T$ is the inverse temperature. Introducing the auxiliary fields ϕ_a for $(-2G\bar{\psi}\psi, -2G\bar{\psi} i\gamma_5 \boldsymbol{\tau} \psi)$, one can rewrite the Euclidean partition function as

$$\begin{aligned} Z &= \int \mathcal{D}\psi \int \mathcal{D}\bar{\psi} \int \prod_a \mathcal{D}\phi_a \\ &\quad \times \exp\left\{ \int_0^\beta d\tau \int d^3\boldsymbol{x} \left[\bar{\psi} \left(-\gamma^0 \frac{\partial}{\partial \tau} + i\boldsymbol{\gamma} \cdot \nabla + \mu\gamma^0 - (\phi_0 + i\gamma_5 \boldsymbol{\tau} \cdot \boldsymbol{\phi}) \right) \psi - \frac{1}{4G} \phi_a^2 \right] \right\} \\ &= \int \prod_a \mathcal{D}\phi_a e^{-S_0}, \end{aligned} \tag{6.1.3}$$

where the effective action is

$$S_0 = \int_0^\beta d\tau \int d^3\boldsymbol{x} \left[\frac{1}{4G} \phi_a^2 \right] - \mathrm{Trlog}\left[-G_F^{-1} \right], \tag{6.1.4}$$

with

$$\begin{aligned} G_F^{-1} &= -\gamma^0 \frac{\partial}{\partial \tau} + i\boldsymbol{\gamma} \cdot \boldsymbol{\nabla} + \mu\gamma^0 - (\phi_0 + i\gamma_5 \boldsymbol{\tau} \cdot \boldsymbol{\phi}) \\ &\equiv S_\beta^{-1} - \Delta, \end{aligned} \tag{6.1.5}$$

and $\Delta \equiv (\phi_0 + i\gamma_5 \boldsymbol{\tau} \cdot \boldsymbol{\phi})$. The inverse of the thermal Green's function, S_β^{-1}, can be written as $S_\beta^{-1}(i\nu_m, \boldsymbol{p}) = \not{p}$ with $p_0 = i\nu_m + \mu$ in the frequency and momentum representation, where $\nu_m = (2m+1)\pi T$ is the Matsubara frequency for quarks. Thus we find

$$\begin{aligned} S_0(\phi) = &\int_0^\beta d\tau \int d^3\boldsymbol{x} \left[\frac{1}{4G} \phi_a^2 \right] - \mathrm{Trlog}[S_\beta^{-1}] - \frac{1}{2}\mathrm{Tr}[\Delta S_\beta]^2 - \frac{1}{4}\mathrm{Tr}[\Delta S_\beta]^4 + \cdots \\ =& S_f + \frac{1}{2} T \sum_{n_1} \int \frac{d^3\boldsymbol{q}_1}{(2\pi)^3} \Gamma^{(2)}_{\mathrm{ps}}(i\omega_{n_1}, \boldsymbol{q}_1) \phi_a(i\omega_{n_1}, \boldsymbol{q}_1) \phi_a(-i\omega_{n_1}, -\boldsymbol{q}_1) \\ &+ \frac{1}{4!} T^4 \prod_{i=1}^4 \sum_{n_i} \int \frac{d^3\boldsymbol{q}_i}{(2\pi)^3} \hat{\lambda}(\{i\omega_{n_i}\}, \{\boldsymbol{q}_i\}) \phi_a(i\omega_{n_1}, \boldsymbol{q}_1) \phi_a(i\omega_{n_2}, \boldsymbol{q}_2) \phi_b(i\omega_{n_3}, \boldsymbol{q}_3) \phi_b(i\omega_{n_4}, \boldsymbol{q}_4) \\ &+ \cdots, \end{aligned} \tag{6.1.6}$$

where $\omega_n = 2\pi nT$ is the Matsubara frequency for auxiliary fields and S_f is the action for free quarks. Since the component ($\omega_n = 0$, $|\boldsymbol{q}| = q_c$) is the most relevant degree of freedom, we here approximate the vertex function $\hat{\lambda}$ by the local four-point function $\hat{\lambda}(\{i\omega_{n_i}\}, \{\boldsymbol{q}_i\}) = \lambda(2\pi)^3\delta(\boldsymbol{q}_1 + \boldsymbol{q}_2 + \boldsymbol{q}_3 + \boldsymbol{q}_4)\delta(\omega_{n_1} + \omega_{n_2} + \omega_{n_3} + \omega_{n_4})$ with a coupling constant λ. As we shall see later, we must keep the frequency dependence of the composite fields ϕ_a to extract the correct behavior of the thermodynamic quantities at $T = 0$. The above effective action is obviously $SU(2) \times SU(2) \simeq O(4)$ symmetric in the chiral-restored phase. The $q\bar{q}$ polarization function $\Pi^0_{\rm ps}(i\omega_n, \boldsymbol{q})$ and the inverse two-point function $\Gamma^{(2)}_{\rm ps}(i\omega_n, \boldsymbol{q})$ are defined, respectively, by

$$\Pi^0_{\rm ps}(i\omega_n, \boldsymbol{q}) = -N_f N_c T \sum_m \int \frac{d^3\boldsymbol{p}}{(2\pi)^3} {\rm tr}\left[i\gamma_5\tau_3 S_\beta(i\omega_n + i\nu_m, \boldsymbol{q} + \boldsymbol{p}) i\gamma_5\tau_3 S_\beta(i\nu_m, \boldsymbol{p})\right], \quad (6.1.7)$$

and,

$$\Gamma^{(2)}_{\rm ps}(i\omega_n, \boldsymbol{q}) = \frac{1 - 2G\Pi^0_{\rm ps}(i\omega_n, \boldsymbol{q})}{2G}. \quad (6.1.8)$$

Within the linear approximation for the composite fields, only the first two terms are sufficient in Eq. (6.1.6), without other terms which give the nonlinear effects coming from the mutual interactions of fluctuations, such as the fourth-order term. In the following discussions, however, we must keep the terms up to fourth order in ϕ_a, as in a model *à la* Brazovskii [86, 137, 138].

6.1.2 Nonlinear effects of fluctuations

We first consider the thermodynamic potential $\Omega = -T\log Z$ within the linear approximation:

$$\Omega_{\rm LA} = \Omega_f + 2TV \sum_n \int \frac{d^3\boldsymbol{q}}{(2\pi)^3} \ln\left[1 - 2G\Pi^0_{\rm ps}(i\omega_n, \boldsymbol{q})\right], \quad (6.1.9)$$

where Ω_f is the thermodynamic potential for free quarks and V is the volume of the system. This thermodynamic potential corresponds to that obtained by Nozières and Schmitt-Rink [128] for superconductivity. Unlike the homogeneous phase transition, the polarization function has a minimum at $|\boldsymbol{q}| = q_c \neq 0$, i.e., $\frac{\partial\Pi^0_{\rm ps}(0,\boldsymbol{q})}{\partial|\boldsymbol{q}|}|_{|\boldsymbol{q}|=q_c} = 0$, for the case of the inhomogeneous transition in isotropic systems. Correspondingly, the criterion *à la* Thouless [127], $1 - 2G\Pi^0_{\rm ps}(i\omega_n = 0, q_c) = 0$, can be derived as the threshold condition within the MFA. This condition is equivalent to vanishing of the coefficient of the second-order term in Eq. (6.1.6).

Next we shall see that the nonlinear effects become essential for the inhomogeneous phase transition, which differs from the usual phase transition. Since the effective action is chiral symmetric, we can choose the thermal average of the pseudoscalar field to be $\beta\Phi(\boldsymbol{q})\delta_{n0} = \langle\phi_3\rangle$, as an appropriate order parameter for the inhomogeneous chiral transition. Then the thermodynamic potential can be expressed in powers of Φ, after putting $\phi_a = \beta\Phi(\boldsymbol{q})\delta_{n0}\delta_{a3} + \xi_a$

and integrating out the fluctuation fields ξ_a,

$$\begin{aligned}\Omega &= \Omega_0 + \frac{1}{2!}\prod_{i=1}^{2}\int\frac{d^3\boldsymbol{q}_i}{(2\pi)^3}\bar{\Gamma}^{(2)}_{\rm ps}(\{\boldsymbol{q}_i\})\Phi(\boldsymbol{q}_1)\Phi(\boldsymbol{q}_2)\\ &+\frac{1}{4!}\prod_{i=1}^{4}\int\frac{d^3\boldsymbol{q}_i}{(2\pi)^3}\bar{\Gamma}^{(4)}_{\rm ps}(\{\boldsymbol{q}_i\})\Phi(\boldsymbol{q}_1)\Phi(\boldsymbol{q}_2)\Phi(\boldsymbol{q}_3)\Phi(\boldsymbol{q}_4)\\ &+\frac{1}{6!}\prod_{i=1}^{6}\int\frac{d^3\boldsymbol{q}_i}{(2\pi)^3}\bar{\Gamma}^{(6)}_{\rm ps}(\{\boldsymbol{q}_i\})\Phi(\boldsymbol{q}_1)\Phi(\boldsymbol{q}_2)\Phi(\boldsymbol{q}_3)\Phi(\boldsymbol{q}_4)\Phi(\boldsymbol{q}_5)\Phi(\boldsymbol{q}_6)+\cdots, \quad (6.1.10)\end{aligned}$$

where each coefficient includes the effects of fluctuations described by up to fourth-order term in Eq. (6.1.6). The first term represents the ring diagrams (bubbles), while the quantities of $\Pi^0_{\rm ps}$ are modified by the fluctuations, as we will see below.

Next, we calculate the propagator of a chiral pair fluctuation field. By using the polarization function, we can construct the propagator within the random-phase approximation (RPA). The polarization function defined in Eq. (6.1.7) can be written in an apparent form [149, 150], with the Fermi-Dirac distribution function $f_F(\epsilon) = (1+e^{\beta\varepsilon})^{-1}$,

$$\begin{aligned}\Pi^0_{\rm ps}(i\omega_n,\boldsymbol{q}) &= N_f N_c\sum_{\boldsymbol{p}}\Bigg[(f_F(|\boldsymbol{p}|+\mu)-f_F(|\boldsymbol{p}+\boldsymbol{q}|+\mu))\frac{1-\boldsymbol{p}\cdot(\boldsymbol{p}+\boldsymbol{q})/|\boldsymbol{p}||\boldsymbol{p}+\boldsymbol{q}|}{i\omega_n+|\boldsymbol{p}+\boldsymbol{q}|-|\boldsymbol{p}|}\\ &+(f_F(|\boldsymbol{p}+\boldsymbol{q}|-\mu)-1+f_F(|\boldsymbol{p}|+\mu))\frac{1+\boldsymbol{p}\cdot(\boldsymbol{p}+\boldsymbol{q})/|\boldsymbol{p}||\boldsymbol{p}+\boldsymbol{q}|}{i\omega_n-|\boldsymbol{p}+\boldsymbol{q}|-|\boldsymbol{p}|}\\ &+(1-f_F(|\boldsymbol{p}+\boldsymbol{q}|+\mu)-f_F(|\boldsymbol{p}|-\mu))\frac{1+\boldsymbol{p}\cdot(\boldsymbol{p}+\boldsymbol{q})/|\boldsymbol{p}||\boldsymbol{p}+\boldsymbol{q}|}{i\omega_n+|\boldsymbol{p}+\boldsymbol{q}|+|\boldsymbol{p}|}\\ &+(f_F(|\boldsymbol{p}+\boldsymbol{q}|-\mu)-f_F(|\boldsymbol{p}|-\mu))\frac{1-\boldsymbol{p}\cdot(\boldsymbol{p}+\boldsymbol{q})/|\boldsymbol{p}||\boldsymbol{p}+\boldsymbol{q}|}{i\omega_n-|\boldsymbol{p}+\boldsymbol{q}|+|\boldsymbol{p}|}\Bigg], \quad (6.1.11)\end{aligned}$$

which consists of the vacuum contribution, $\Pi^0_{\rm ps}(i\omega_n,\boldsymbol{q})|_{(\mu,T)\to 0}$, and the remaining medium contribution. Here the ultraviolet divergence of the vacuum contribution should be regularized by the proper time regularization (PTR), whose explicit form is described in Ref. [88]. Each term in Eq. (6.1.11) may be easily understood in terms of the particle-antiparticle and particle-hole excitations. Note here that the following properties hold: $\Pi^0_{\rm ps}(i\omega_n,\boldsymbol{q}) = \Pi^0_{\rm ps}(-i\omega_n,\boldsymbol{q})$ and $\Pi^0_{\rm ps}(i\omega_n,\boldsymbol{q}) = \Pi^0_{\rm ps}(i\omega_n,-\boldsymbol{q})$.

By the proper analytic continuation $\Pi^0_{\rm ps}(i\omega_n\to\omega+i\eta,\boldsymbol{q})$, the polarization function can be written as

$$\Pi^0_{\rm ps}(i\omega_n,\boldsymbol{q}) = {\rm Re}\Pi^0_{\rm ps}(\omega+i\eta,\boldsymbol{q})|_{\omega=i\omega_n} + i\,{\rm sign}(\omega_n){\rm Im}\Pi^0_{\rm ps}(\omega+i\eta,\boldsymbol{q})|_{\omega=i\omega_n}. \quad (6.1.12)$$

The imaginary part is given by,

$$\begin{aligned}
\mathrm{Im}\Pi^0_{\rm ps}(\boldsymbol{q},\omega+i\eta) = -N_f N_c \pi \int \frac{d^3\boldsymbol{p}}{(2\pi)^3} \\
\times \Bigg\{ & [f_F(|\boldsymbol{p}|+\mu) - f_F(|\boldsymbol{p}+\boldsymbol{q}|+\mu)] \left[1 - \frac{\boldsymbol{p}\cdot(\boldsymbol{p}+\boldsymbol{q})}{|\boldsymbol{p}||\boldsymbol{p}+\boldsymbol{q}|}\right] \delta(\omega + |\boldsymbol{p}+\boldsymbol{q}| - |\boldsymbol{p}|) \\
& + [f_F(|\boldsymbol{p}+\boldsymbol{q}|-\mu) - f_F(|\boldsymbol{p}|-\mu)] \left[1 - \frac{\boldsymbol{p}\cdot(\boldsymbol{p}+\boldsymbol{q})}{|\boldsymbol{p}||\boldsymbol{p}+\boldsymbol{q}|}\right] \delta(\omega - |\boldsymbol{p}+\boldsymbol{q}| + |\boldsymbol{p}|) \\
& + [f_F(|\boldsymbol{p}+\boldsymbol{q}|-\mu) - 1 + f_F(|\boldsymbol{p}|+\mu)] \left[1 + \frac{\boldsymbol{p}\cdot(\boldsymbol{p}+\boldsymbol{q})}{|\boldsymbol{p}||\boldsymbol{p}+\boldsymbol{q}|}\right] \delta(\omega - |\boldsymbol{p}+\boldsymbol{q}| - |\boldsymbol{p}|) \\
& + [1 - f_F(|\boldsymbol{p}+\boldsymbol{q}|+\mu) - f_F(|\boldsymbol{p}|-\mu)] \left[1 + \frac{\boldsymbol{p}\cdot(\boldsymbol{p}+\boldsymbol{q})}{|\boldsymbol{p}||\boldsymbol{p}+\boldsymbol{q}|}\right] \delta(\omega + |\boldsymbol{p}+\boldsymbol{q}| + |\boldsymbol{p}|) \Bigg\}.
\end{aligned} \tag{6.1.13}$$

Each delta function is evaluated as

$$\delta(\omega + |\boldsymbol{p}+\boldsymbol{q}| - |\boldsymbol{p}|) = \frac{p-\omega}{pq}\delta\left(x - \frac{\omega^2 - 2p\omega - q^2}{2pq}\right)\theta(p-\omega), \tag{6.1.14}$$

$$\delta(\omega - |\boldsymbol{p}+\boldsymbol{q}| + |\boldsymbol{p}|) = \frac{p+\omega}{pq}\delta\left(x - \frac{\omega^2 + 2p\omega - q^2}{2pq}\right)\theta(p+\omega), \tag{6.1.15}$$

$$\delta(\omega - |\boldsymbol{p}+\boldsymbol{q}| - |\boldsymbol{p}|) = \frac{-p+\omega}{pq}\delta\left(x - \frac{\omega^2 - 2p\omega - q^2}{2pq}\right)\theta(-p+\omega), \tag{6.1.16}$$

$$\delta(\omega + |\boldsymbol{p}+\boldsymbol{q}| + |\boldsymbol{p}|) = \frac{-p-\omega}{pq}\delta\left(x - \frac{\omega^2 + 2p\omega - q^2}{2pq}\right)\theta(-p-\omega), \tag{6.1.17}$$

where $x = \cos\theta$. Considering the argument of the delta function, we find,

$$\begin{aligned}
\mathrm{Im}\Pi^0_{\rm ps}(\omega+i\eta,\boldsymbol{q}) = N_f N_c T \frac{\omega^2 - q^2}{8\pi q} \Big\{ & \ln\left[1 + e^{-\beta(q/2+\mu+\omega/2)}\right] - \ln\left[1 + e^{-\beta(q/2+\mu-\omega/2)}\right] \\
& + \ln\left[1 + e^{-\beta(q/2-\mu+\omega/2)}\right] - \ln\left[1 + e^{-\beta(q/2-\mu-\omega/2)}\right] + \beta\omega\theta(|\omega|-q) \Big\},
\end{aligned} \tag{6.1.18}$$

while it have been numerically found in Ref. [88].

Introducing an effective coupling constant $g_{\phi qq}$ between quarks and a fluctuation field [18], we define the chiral pair fluctuation fields as $g^{-1}_{\phi qq}\phi_a$. Then the Green's function of chiral pair fluctuation fields, $G_{\rm ps}(i\omega_n,\boldsymbol{q})$, can be then defined by the use of the two-point function (6.1.8):

$$G_{\rm ps}(i\omega_n,\boldsymbol{q}) \equiv g^{-2}_{\phi qq}[\Gamma^{(2)}_{\rm ps}(i\omega_n,\boldsymbol{q})]^{-1}, \tag{6.1.19}$$

where $g_{\phi qq}$ is an effective coupling constant between quarks and a fluctuation field [18]. Since the behavior around $|\boldsymbol{q}| = q_c$ and $\omega_n = 0$ is important in the vicinity of the phase boundary, we expand it as

$$G^{-1}_{\rm ps}(i\omega_n,\boldsymbol{q}) \sim \tau + \gamma\left(|\boldsymbol{q}|^2 - q_c^2\right)^2 + \alpha|\omega_n|, \tag{6.1.20}$$

where $\tau = G_{\rm ps}^{-1}(0, |\boldsymbol{q}| = q_c)$, $\gamma = \frac{1}{2} d^2 G_{\rm ps}^{-1}(0, |\boldsymbol{q}| = q_c)/(d|\boldsymbol{q}|^2)^2$, and $\alpha = g_{\phi qq}^2 d{\rm Im}\Pi_{\rm ps}^0(\omega = 0, |\boldsymbol{q}| = q_c)/d\omega$.

Using the effective action with the background field method, we can evaluate the fluctuation effects[4]. Inserting $\phi_a = \beta\Phi(\boldsymbol{q})\delta_{n0}\delta_{a3} + \xi_a$ into Eq. (6.1.6), the effective action can be written as

$$S_0(\phi_a) = S_0(\Phi) + S_1(\Phi, \xi_a). \tag{6.1.21}$$

Accordingly, the thermodynamic potential is given by the functional integral:

$$\Omega(\Phi) = TS_0(\Phi) - T{\rm log}\int \prod_a \mathcal{D}\xi_a {\rm exp}[-S_1(\Phi, \xi_a)]. \tag{6.1.22}$$

Each vertex function in Eq. (6.1.10) is then given by

$$\bar{\Gamma}^{(n)}(\boldsymbol{q}_1, \boldsymbol{q}_2, \cdots, \boldsymbol{q}_n) = (2\pi)^{3n} \left.\frac{\delta^n \Omega}{\delta\Phi(-\boldsymbol{q}_1)\delta\Phi(-\boldsymbol{q}_2)\cdots\delta\Phi(-\boldsymbol{q}_n)}\right|_{\Phi=0}. \tag{6.1.23}$$

The key equation is the first functional derivative,

$$\begin{aligned}(2\pi)^3 \frac{\delta\Omega}{\delta\Phi\left(-\boldsymbol{q}_1\right)} &= G_{\rm ps}^{-1}\left(0, \boldsymbol{q}_1\right)\Phi\left(\boldsymbol{q}_1\right) + \frac{\lambda}{3!}\int \frac{d^3\boldsymbol{q}_2\, d^3\boldsymbol{q}_3}{(2\pi)^6}\Phi\left(\boldsymbol{q}_2\right)\Phi\left(\boldsymbol{q}_3\right)\Phi\left(\boldsymbol{q}_1 - \boldsymbol{q}_2 - \boldsymbol{q}_3\right) \\ &+ \frac{\lambda}{2!}T^2\sum_n \int \frac{d^3\boldsymbol{q}_2\, d^3\boldsymbol{q}_3}{(2\pi)^6} \\ &\times \left[\left\langle\xi_3\left(i\omega_n, \boldsymbol{q}_2\right)\xi_3\left(-i\omega_n, \boldsymbol{q}_3\right)\right\rangle_\xi + \left\langle\xi_0\left(i\omega_n, \boldsymbol{q}_2\right)\xi_0\left(-i\omega_n, \boldsymbol{q}_3\right)\right\rangle_\xi\right]\Phi\left(\boldsymbol{q}_1 - \boldsymbol{q}_2 - \boldsymbol{q}_3\right),\end{aligned} \tag{6.1.24}$$

where the symbol $\langle\cdots\rangle_\xi$ denotes the thermal average, and we have used the following relation: $\left\langle\xi_0\left(i\omega_n, \boldsymbol{q}_2\right)\xi_0\left(-i\omega_n, \boldsymbol{q}_3\right)\right\rangle_\xi = \left\langle\xi_1\left(i\omega_n, \boldsymbol{q}_2\right)\xi_1\left(-i\omega_n, \boldsymbol{q}_3\right)\right\rangle_\xi = \left\langle\xi_2\left(i\omega_n, \boldsymbol{q}_2\right)\xi_2\left(-i\omega_n, \boldsymbol{q}_3\right)\right\rangle_\xi$. In general, the thermal average $\langle\xi(i\omega_n, \boldsymbol{q}_2)\xi(-i\omega_n, \boldsymbol{q}_3)\rangle_\xi$ has the off-diagonal momentum components, but we can neglect such components as long as the loop integrals are concerned [86]. Thus,

$$\langle\xi_a(i\omega_n, \boldsymbol{q}_2)\xi_a(-i\omega_n, \boldsymbol{q}_3)\rangle_\xi = \beta(2\pi)^3\delta(\boldsymbol{q}_2 + \boldsymbol{q}_3)\bar{G}_a(i\omega_n, \boldsymbol{q}_2). \tag{6.1.25}$$

where $\bar{G}_a(i\omega_n, \boldsymbol{q})$ is the self-consistent Green's function, given by $\bar{G}_a(i\omega_n, \boldsymbol{q}) = [r_a + \gamma(|\boldsymbol{q}|^2 - q_c^2)^2 + \alpha|\omega_n|]^{-1}$ with,

$$\begin{aligned} r_3 &= \tau + V^{-1}\frac{\lambda}{2}\int \frac{d^3\boldsymbol{q}}{(2\pi)^3}\Phi\left(\boldsymbol{q}\right)\Phi\left(-\boldsymbol{q}\right) + \frac{\lambda}{2}T\sum_n \int \frac{d^3\boldsymbol{q}}{(2\pi)^3}\left[\bar{G}_3(i\omega_n, \boldsymbol{q}) + \bar{G}_0(i\omega_n, \boldsymbol{q})\right] \\ &\equiv \tau + V^{-1}\frac{\lambda}{2}\int \frac{d^3\boldsymbol{q}}{(2\pi)^3}\Phi\left(\boldsymbol{q}\right)\Phi\left(-\boldsymbol{q}\right) + \frac{\lambda}{2}\left(I_1(r_3) + I_1(r_0)\right). \end{aligned} \tag{6.1.26}$$

The integrals I_n are defined by,

$$I_n(r) = T\sum_k \int \frac{d^3\boldsymbol{q}}{(2\pi)^3}\left(\frac{\partial^{(n-1)}}{\partial r^{n-1}}\right)\frac{1}{r + \gamma(|\boldsymbol{q}|^2 - q_c^2)^2 + \alpha|\omega_k|}, \tag{6.1.27}$$

[4]We evaluate the thermodynamic potential in an $O(4)$ symmetric way, while other ϕ_a (except for ϕ_3) has been discarded in Ref. [88].

where the integrals with $n \leq 2$ should be regularized by some regularization methods (see Appendix E for details). Similarly, $r_0 (= r_1 = r_2)$ reads,

$$r_0 = \tau + V^{-1} \frac{\lambda}{6} \int \frac{d^3 \boldsymbol{q}}{(2\pi)^3} \Phi(\boldsymbol{q}) \Phi(-\boldsymbol{q}) + \frac{\lambda}{2} \left(I_1(r_3) + I_1(r_0) \right). \tag{6.1.28}$$

While, strictly speaking, there are other two diagrams contributing to r_3 and r_0, their contribution can be neglected in the region $r_{3,0}^{1/2} \ll q_c$ [86]. Using r_3, Eq. (6.1.24) can be rewritten as,

$$\begin{aligned}(2\pi)^3 \frac{\delta \Omega}{\delta \Phi(-\boldsymbol{q}_1)} = &\left[r_3 + \gamma \left(|\boldsymbol{q}_1|^2 - q_c^2 \right)^2 \right] \Phi(\boldsymbol{q}_1) - V^{-1} \frac{\lambda}{2!} \Phi(\boldsymbol{q}_1) \int \frac{d^3 \boldsymbol{q}_2}{(2\pi)^3} \Phi(\boldsymbol{q}_2) \Phi(-\boldsymbol{q}_2) \\ &+ \frac{\lambda}{3!} \int \frac{d^3 \boldsymbol{q}_2 \, d^3 \boldsymbol{q}_3}{(2\pi)^6} \Phi(\boldsymbol{q}_2) \Phi(\boldsymbol{q}_3) \Phi(\boldsymbol{q}_1 - \boldsymbol{q}_2 - \boldsymbol{q}_3). \end{aligned} \tag{6.1.29}$$

Thus, $\Gamma^{(1)}$ is obviously vanished as should be expected. Subsequent derivatives of Ω give the even-order vertex functions. Note here that r_a is a functional of Φ and their derivatives satisfy the following equations:

$$\frac{\delta r_3}{\delta \Phi(-\boldsymbol{q}_2)} = \frac{(2\pi)^{-3} V^{-1} \lambda \Phi(\boldsymbol{q}_2)}{1 - \frac{\lambda}{2} I_2(r_3)} + \frac{\frac{\lambda}{2} I_2(r_0)}{1 - \frac{\lambda}{2} I_2(r_3)} \cdot \frac{\delta r_0}{\delta \Phi(-\boldsymbol{q}_2)}, \tag{6.1.30}$$

$$\frac{\delta r_0}{\delta \Phi(-\boldsymbol{q}_2)} = \frac{(2\pi)^{-3} V^{-1} \frac{\lambda}{3} \Phi(\boldsymbol{q}_2)}{1 - \frac{\lambda}{2} I_2(r_0)} + \frac{\frac{\lambda}{2} I_2(r_3)}{1 - \frac{\lambda}{2} I_2(r_0)} \cdot \frac{\delta r_3}{\delta \Phi(-\boldsymbol{q}_2)}. \tag{6.1.31}$$

The second-order vertex function thus reads,

$$\bar{\Gamma}^{(2)}(\boldsymbol{q}_1, \boldsymbol{q}_2) = (2\pi)^3 \delta(\boldsymbol{q}_1 + \boldsymbol{q}_2)(\tau_R + \gamma(|\boldsymbol{q}|^2 - q_c^2)^2), \tag{6.1.32}$$

where $\tau_R = r_3(\Phi = 0) = r_0(\Phi = 0)$. Likewise, the fourth-order vertex function renders,

$$\begin{aligned}\bar{\Gamma}^{(4)}(\{\boldsymbol{q}_i\}) = &(2\pi)^3 \lambda \Bigg[\delta(\boldsymbol{q}_1 + \boldsymbol{q}_2 + \boldsymbol{q}_3 + \boldsymbol{q}_4) \\ &+ (2\pi)^3 V^{-1} \frac{\frac{2\lambda}{3} I_2(\tau_R)}{1 - \lambda I_2(\tau_R)} \left[\delta(\boldsymbol{q}_1 + \boldsymbol{q}_2) \delta(\boldsymbol{q}_3 + \boldsymbol{q}_4) + 2 \text{ permutations} \right] \Bigg]. \end{aligned} \tag{6.1.33}$$

6.1.3 Brazovskii-Dyugaev effect

In this section, we discuss the fluctuation-induced first-order phase transition for the inhomogeneous chiral phase transition. First, we consider the second-order term (6.1.32). If τ_R becomes zero, it should be a signal of the second-order phase transition. From Eq. (6.1.26), τ_R satisfies,

$$\tau_R = \tau + \lambda I_1(\tau_R), \tag{6.1.34}$$

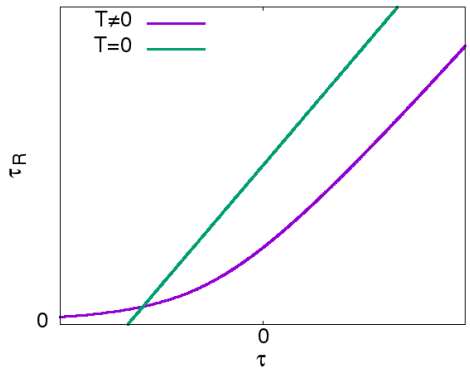

Figure 6.2: The τ dependences of τ_R at $T \neq 0$ (purple curve) and $T = 0$ (green line). τ_R always takes positive values when $T \neq 0$, while, when $T = 0$, it vanishes at $\tau = -\frac{\lambda\Lambda^3}{48\alpha\pi^{5/2}\gamma^{3/2}q_c^3}$. (The figure is taken from Ref.[121].)

with,

$$\tau = \tau_R - \frac{\lambda T}{2\pi^2}\int_{\tau_R/\Lambda^2}^{\infty} ds \left[\frac{\tau_R^{1/2}}{2}\left(\frac{\pi}{(4\gamma q_c^2 s)^3}\right)^{1/2} + \tau_R^{-1/2}\left(\frac{\pi q_c^2}{4\gamma s}\right)\right] e^{-s}\coth\left(\frac{\alpha\pi T s}{\tau_R}\right). \quad (6.1.35)$$

Looking into the behavior around $\tau_R = 0$, we find that,

$$\tau \simeq \tau_R - \frac{\lambda T q_c}{4\pi\gamma^{1/2}\tau_R^{1/2}} \quad \text{for} \quad T \neq 0, \quad (6.1.36)$$

while

$$\tau \simeq \tau_R - \frac{\lambda\Lambda^3}{48\alpha\pi^{5/2}\gamma^{3/2}q_c^3} \quad \text{for} \quad T = 0. \quad (6.1.37)$$

This is due to the singularity of $G^R_{\rm ps}(i\omega_n, \boldsymbol{q})$ on the sphere $|\boldsymbol{q}| = q_c$, which is a common feature for inhomogeneous phase transitions in isotropic systems [86, 87, 129, 137, 138]. From Eq. (6.1.36) and Fig. 6.2, we can see that τ diverges at $\tau_R = 0$ and τ_R is always positive for all range of τ, which implies that the phase transition is prohibited at finite T. On the other hand, there is no divergence at zero temperature [121]. In addition, the point $\tau_R = 0$ at $T = 0$ is somewhat shifted from the point $\tau = 0$. The difference of $T \neq 0$ and $T = 0$ can be easily understood from the fact that the lowest Matsubara frequency is dominant and the leading behavior (6.1.36) can be obtained by putting $\omega_n = 0$ into the integral I_1. Thus we can observe that there takes place a kind of dimensional reduction from $1 + 3$ to $0 + 3$ dimensions at $T \neq 0$. It would be interesting to see a similarity to the Coleman-Mermin-Wagner theorem [151, 152], which claims that the lower critical dimension is $1+2$ for thermal fluctuations [153]. In the case of $T = 0$, the imaginary part in $\bar{G}_{\rm ps}$ becomes important to lead to no divergent behavior; quantum fluctuations are gentle and only shifts the critical point.

The above considerations are insufficient for the possibility of the phase transition due to the only consideration for the second-order phase transition. Next, we shall introduce the fourth-order and sixth-order vertex functions to see whether the system undergoes the first-order phase transition. The sign change of the fourth-order vertex function by fluctuations has been first shown by Brazovskii at $T \neq 0$ and Dyugaev at $T = 0$. The integral $I_2(\tau_R)$ in $\bar{\Gamma}^{(4)}$ which will be seen in Eq. (6.1.43) can be evaluated as,

$$I_2(\tau_R) = -\frac{T}{2\pi^2}\int_0^\infty ds \left[\frac{1}{2}\left(\frac{\pi}{(4\gamma q_c^2)^3 s}\right)^{1/2}\tau_R^{-1/2} + \left(\frac{\pi q_c^2 s}{4\gamma}\right)^{1/2}\tau_R^{-3/2}\right] e^{-s}\coth\left(\frac{\alpha\pi T s}{\tau_R}\right). \tag{6.1.38}$$

Looking into the behavior around $\tau_R = 0$, we find that,

$$I_2(\tau_R) \simeq -\frac{T q_c}{8\pi\gamma^{1/2}}\tau_R^{-3/2} \quad \text{for} \quad T \neq 0, \tag{6.1.39}$$

while,

$$I_2(\tau_R) \simeq -\frac{q_c}{4\alpha\pi^2\gamma^{1/2}}\tau_R^{-1/2} \quad \text{for} \quad T = 0. \tag{6.1.40}$$

This result shows that the effects of fluctuations lead to the divergence of the integral I_2 near the phase boundary. Unlike τ_R, quantum fluctuations also give rise to a singular behavior, while it is less drastic than thermal fluctuations. These features can be understood as for the case of τ_R. The expression (6.1.33) is physically given by summing up the "dangerous diagrams," which are composed of bubbles of the renormalized propagator in the chiral-restored phase,

$$\begin{aligned} G^R_{\rm ps}(i\omega_n, \boldsymbol{q}) &= \bar{G}_{\rm ps}(i\omega_n, \boldsymbol{q}; \tau = \tau_R) \\ &= \frac{1}{\tau_R + \gamma(|\boldsymbol{q}|^2 - q_c^2)^2 + \alpha|\omega_n|}, \end{aligned} \tag{6.1.41}$$

and also represent the long-range interaction among chiral pair fluctuations,

$$L(\boldsymbol{k}) = T\sum_n \int \frac{d^3\boldsymbol{q}}{(2\pi)^3} G^R_{\rm ps}(i\omega_n, \boldsymbol{q}) G^R_{\rm ps}(-i\omega_n, \boldsymbol{k} - \boldsymbol{q}). \tag{6.1.42}$$

We can easily see that $L(\boldsymbol{k})$ becomes the most singular and $L(\boldsymbol{k}) \to -I_2(\tau_R)$ as $k \to 0$: the singularities in $G^R_{\rm ps}(i\omega_n, \boldsymbol{q})$ and $G^R_{\rm ps}(-i\omega_n, \boldsymbol{k} - \boldsymbol{q})$ come closer as $k \to 0$ to make the integral divergent. Finally, we find,

$$\bar{\Gamma}^{(4)} = (2\pi)^3\lambda\frac{1 + \frac{\lambda}{3}I_2(\tau_R)}{1 - \lambda I_2(\tau_R)}\delta(\boldsymbol{q}_1 + \boldsymbol{q}_2 + \boldsymbol{q}_3 + \boldsymbol{q}_4), \tag{6.1.43}$$

assuming the form of the condensate as $\Phi = \Delta\sin(q_c z)$. Hence, the sign of $\bar{\Gamma}^{(4)}$ is changed at the point, $1 + \frac{\lambda}{3}I_2(\tau_R) = 0$, which suggests that the phase transition is of first order, i.e., the fluctuation-induced first-order phase transition.

In the above discussion, the $O(4)$ model including four fluctuation fields is considered. We next extend the discussion to the $O(N)$ model. For arbitrary N, Eqs. (6.1.26) and (6.1.28) are recast into,

$$r_3 = \tau + V^{-1}\frac{\lambda}{2}\int\frac{d^3\boldsymbol{q}}{(2\pi)^3}\Phi(\boldsymbol{q})\Phi(-\boldsymbol{q}) + \frac{\lambda}{2}\left(I_1(r_3)+\frac{N-1}{3}I_1(r_0)\right), \tag{6.1.44}$$

$$r_0 = \tau + V^{-1}\frac{\lambda}{6}\int\frac{d^3\boldsymbol{q}}{(2\pi)^3}\Phi(\boldsymbol{q})\Phi(-\boldsymbol{q}) + \frac{\lambda}{2}\left(I_1(r_3)+\frac{N-1}{3}I_1(r_0)\right). \tag{6.1.45}$$

Consequently, $\bar{\Gamma}^{(4)}$ is modified as follows:

$$\bar{\Gamma}^{(4)} = (2\pi)^3\lambda\frac{1+\frac{10-N}{18}\lambda I_2(\tau_R)}{1-\frac{N+2}{6}\lambda I_2(\tau_R)}\delta(\boldsymbol{q}_1+\boldsymbol{q}_2+\boldsymbol{q}_3+\boldsymbol{q}_4). \tag{6.1.46}$$

In the case of $N=1$, the result obtained in [88] is reproduced, and the result for $N=4$ coincides with Eq. (6.1.43). In the case of $N \geq 10$, on the other hand, the fluctuation-induced first-order phase transition does not occur because $\bar{\Gamma}^{(4)}$ never becomes negative.

Next, we consider the continuity of the roles of fluctuations across the R-boundary. We have found that the effects of fluctuations are remarkable for the phase transition, and the role of thermal fluctuations is more profound than that of quantum fluctuations. On the other hand, it has been shown that the fluctuations in iCP[5] are important to cause the instability of one-dimensional structures at finite T [84]: the scalar or pseudoscalar correlation function, $f_a(\boldsymbol{r}) = \langle\phi_a(\boldsymbol{r})\phi_a(0)\rangle$ where ϕ_a denote the quark bilinear fields in scalar or pseudoscalar channel (i.e., $\phi_0 = \bar{\psi}\psi$ and $\phi_i = \bar{\psi}i\gamma_5\tau_i\psi$), algebraically decays at large distances due to the low-energy NG excitations. It is in accord with the Landau-Peierls theorem [93, 131]. For definiteness, we here consider the DCDW condensate. There appear three NG modes (β_i) with the anisotropic dispersion $\omega_i^2 = A_i k_z^2 + B_i k_\perp^4$. In the case of $T=0$, we find

$$\langle\beta_i(\boldsymbol{r})^2\rangle_{T=0} = c_i\int\frac{d^4k}{(2\pi)^4}\frac{1}{k_0^2+A_ik_z^2+B_ik_\perp^4}, \tag{6.1.47}$$

where k_z is the momentum in the direction parallel to the wave vector of the modulation, while $k_\perp$ is that in the directions perpendicular to the modulation. Here the coefficients c_i, A_i, and B_i can be evaluated within chiral effective models [28]. The above integral is convergent in the infrared region. In the case of $T \neq 0$, on the other hand, we find

$$\begin{aligned}\langle\beta_i(\boldsymbol{r})^2\rangle_{T\neq0} &= c_iT\sum_{\omega_n}\int_{-\infty}^{\infty}\frac{dk_z}{2\pi}\int_{l_\perp^{-1}}^{\Lambda_\perp}\frac{d^2\boldsymbol{k}_\perp}{(2\pi)^2}\frac{1}{\omega_n^2+A_ik_z^2+B_ik_\perp^4}, \\ &\sim \frac{c_iT}{8\pi\sqrt{A_iB_i}}\ln(\Lambda_\perp l_\perp),\end{aligned} \tag{6.1.48}$$

which is divergent in the infrared region ($l_\perp^{-1}\to 0$). The most dominant contribution comes from the lowest Matsubara frequency $\omega_n = 0$,

$$\langle\beta_i(\boldsymbol{r})^2\rangle_{T\neq0} \sim c_iT\int_{-\infty}^{\infty}\frac{dk_z}{2\pi}\int_{l_\perp^{-1}}^{\Lambda_\perp}\frac{d^2\boldsymbol{k}_\perp}{(2\pi)^2}\frac{1}{A_ik_z^2+B_ik_\perp^4}, \tag{6.1.49}$$

[5] A similar argument has been given for the LO-type liquid-crystal states [154].

and exhibits an infrared singularity due to the effective *dimensional reduction*. This implies that thermal fluctuations play a more important role in the infrared singularity than quantum ones. In this way, we can see the similar features to our results obtained in the previous subsection.

The stability of the DCDW phase an also be understood in the same way. Here the correlation function of the order parameter ϕ_3 takes the form [84, 85],

$$\langle \phi_3(z)\phi_3(0)\rangle \sim e^{-\frac{1}{2}\langle[\beta_3(z)-\beta_3(0)]^2\rangle}. \tag{6.1.50}$$

We find that for $T=0$,

$$\begin{aligned}\langle[\beta_3(z)-\beta_3(0)]^2\rangle_{T=0} &= c_3\int\frac{d^4k}{(2\pi)^4}\frac{1-e^{ik_z z}}{k_0^2+A_3k_z^2+B_3k_\perp^4}\\ &= \frac{c_3}{16\pi^3\sqrt{B_3}}\int_{-\infty}^{\infty}dk_0\int_{-\infty}^{\infty}dk_z\int_0^{\infty}dx\frac{1-e^{ik_z z}}{k_0^2+A_3k_z^2+x^2},\end{aligned} \tag{6.1.51}$$

where $x=\sqrt{B_i}k_\perp^2$. Furthermore, putting $y=\sqrt{x^2+k_0^2}$, we can obtain.

$$\begin{aligned}\langle[\beta_3(z)-\beta_3(0)]^2\rangle_{T=0} &= \frac{c_3}{16\pi^2\sqrt{B_3}}\int_{-\infty}^{\infty}dk_z\int_0^{\infty}ydy\frac{1-e^{ik_z z}}{y^2+A_3k_z^2}\\ &= \frac{c_3}{16\pi^2\sqrt{A_3B_3}}\int_0^{\Lambda}dy\left(1-e^{-A_3^{-1/2}y|z|}\right)\\ &\sim \frac{c_3}{16\pi\sqrt{A_3B_3}}\Lambda \quad \text{for large } |z|,\end{aligned} \tag{6.1.52}$$

where the ultraviolet cutoff Λ is inserted. In the case of $T\neq 0$, on the other hand, the leading contribution comes from the lowest Matsubara frequency,

$$\begin{aligned}\langle[\beta_3(z)-\beta_3(0)]^2\rangle_{T\neq 0} &\sim c_3T\int\frac{d^3\boldsymbol{k}}{(2\pi)^3}\frac{1-e^{ik_z z}}{A_3k_z^2+B_3k_\perp^4}\\ &= \frac{c_3T}{8\pi^2\sqrt{B_3}}\int_{-\infty}^{\infty}dk_z\int_0^{\infty}dx\frac{1-e^{ik_z z}}{A_3k_z^2+x^2}\\ &= \frac{c_3T}{8\pi\sqrt{A_3B_3}}\int_0^{\Lambda}dx\frac{1-e^{-A_3^{-1/2}x|z|}}{x}.\end{aligned} \tag{6.1.53}$$

Here we insert the regulator,

$$\begin{aligned}\langle[\beta_3(z)-\beta_3(0)]^2\rangle_{T\neq 0} &\sim \lim_{\epsilon\to+0}\frac{c_3T}{8\pi\sqrt{A_3B_3}}\int_0^{A_3^{-1/2}\Lambda|z|}dx\frac{1-e^{-x}}{x^{1-\epsilon}}\\ &= \lim_{\epsilon\to+0}\frac{c_3T}{8\pi\sqrt{A_3B_3}}\left[\frac{1}{\epsilon}\left(A_3^{-1/2}\Lambda|z|\right)^{\epsilon}-\Gamma(\epsilon)+\Gamma(\epsilon,A_3^{-1/2}\Lambda|z|)\right]\\ &\sim \frac{c_3T}{8\pi\sqrt{A_3B_3}}\ln\left(A_3^{-1/2}\Lambda|z|\right) \quad \text{for large } |z|,\end{aligned} \tag{6.1.54}$$

which logarithmically diverges in the limit $|z| \to \infty$, Similarly, the same results can be obtained for other order parameters. Here thermal fluctuations are still important for the same reason. Therefore, we can conclude that the correlation function algebraically decays only for $T \neq 0$ and the DCDW phase exhibits the feature of quasi-long range order [84] (see also [85] for real kink crystal). These results may suggest some continuity of the roles of fluctuations before and after the phase transition, as far as the one-dimensional modulation is concerned.

6.1.4 Singularlity in the thermodynamic quantities

It is well-known that fluctuations affect the thermodynamic quantities around the phase boundary. Singular behavior in various susceptibilities (the second derivatives of the thermodynamic potential) are characteristic features near the critical point of the second-order phase transition; the specific-heat sigularity, $C_v \sim (T - T_c)^{-1/2}$, has been shown due to fluctuations at the critical temperature T_c of superconductivity, while there is generated a finite discontinuity within the MFA. In the context of the usual chiral transition, the divergence of the quark number susceptibility, $\partial N/\partial\mu$, has been discussed [155].

The singular behavior of the propagator gives rise to new types of sigularities in the thermodynamic quantities for the inhomogeneous phase transition. In the context of the FFLO state in superconductivity, Ohashi have indicated the divergence of the electron number due to the fluctuation [129], where $N \sim \tau^{-1/2}$ within the linear approximation, which means that the first derivative of the thermodynamic potential becomes singular. As we have seen in the previous section, τ is renormalized to keep it to be positive definite by the non-linear effects, and the singularity mentioned above can not be observed. However, its remnant should be observed. Thus, the fluctuation-induced first-order transition is characterized by the discontinuity and singular behavior of the first derivative.

In the following, we shall discuss the quark number and the entropy for the inhomogeneous chiral transition. In the chiral-restored phase ($\Phi = 0$), the thermodynamic potential is given by,

$$\Omega(\Phi = 0) = \Omega_f - 2TV \sum_n \int \frac{d^3\boldsymbol{q}}{(2\pi)^3} \ln\left(G^R_{\rm ps}(i\omega_n, \boldsymbol{q})\right), \tag{6.1.55}$$

which is a simple generalization of Eq. (6.1.9) with a replacement of τ by τ_R. The quark number density can be written as,

$$n = n_f + 2T \sum_n \int \frac{d^3\boldsymbol{q}}{(2\pi)^3} G^R_{\rm ps}(i\omega_n, \boldsymbol{q}) \frac{\partial}{\partial\mu} \bar{\Pi}^0_{\rm ps}(i\omega_n, \boldsymbol{q}), \tag{6.1.56}$$

where,

$$n_f = \frac{N_c N_f}{\pi^2} \int_0^\infty p^2 dp \left(f(p-\mu) - f(p+\mu)\right). \tag{6.1.57}$$

Using Eq. (6.1.41) and I_1 derived from Appendix E, the fluctuation effects then can be seen

separately:

$$n \sim n_f + \frac{1}{\tau_R^{1/2}} \frac{N_f N_c q_c}{8\pi^3 \gamma^{1/2}} \int_{-\infty}^{\infty} pdp \frac{1}{[e^{\beta(p+\mu)/2} + e^{-\beta(p+\mu)/2}]^2} \left(4 + \frac{q_c}{p} \ln \left|\frac{2p - q_c}{2p + q_c}\right|\right) \quad \text{for} \quad T \neq 0, \tag{6.1.58}$$

while,

$$n \sim n_f - \frac{N_f N_c \Lambda^3}{96\pi^{9/2} \alpha \gamma^{3/2} q_c^3} \left(4\mu + q_c \ln \left|\frac{2\mu - q_c}{2\mu + q_c}\right|\right) \quad \text{for} \quad T = 0, \tag{6.1.59}$$

as the leading contribution. Thus we can see a singular behavior at $T \neq 0$, while at $T = 0$ only a finite gap is produced. A similar divergence ($\propto \tau_R^{-1/2}$) is also observed in the entropy. The entropy density is given by,

$$s = s_f - 2\sum_n \int \frac{d^3\boldsymbol{q}}{(2\pi)^3} \ln G_{\rm ps}^R(i\omega, \boldsymbol{q}) + 2T \sum_n \int \frac{d^3\boldsymbol{q}}{(2\pi)^3} G_{\rm ps}^R(i\omega, \boldsymbol{q}) \frac{\partial}{\partial T} \bar{\Pi}_{\rm ps}^0(i\omega_n, \boldsymbol{q}), \tag{6.1.60}$$

where,

$$s_f = \frac{2N_f N_c}{\pi^2} \int_0^{\infty} pdp \left[(2p - \mu) \ln(1 + e^{-\beta(p-\mu)}) + (2p + \mu) \ln(1 + e^{-\beta(p-\mu)})\right]. \tag{6.1.61}$$

The second term gives a minor contribution ($\propto \ln \tau_R$), while the leading contribution comes from the third term,

$$s \sim s_f - \frac{1}{\tau_R^{1/2}} \frac{N_f N_c q_c}{8\pi^3 \gamma^{1/2} T} \int_{-\infty}^{\infty} dp \frac{p(p+\mu)}{\left[e^{\beta(p+\mu)/2} + e^{-\beta(p+\mu)/2}\right]^2} \left(4 + \frac{q_c}{p} \ln \left|\frac{2p - q_c}{2p + q_c}\right|\right), \tag{6.1.62}$$

around the phase boundary. Such a singular behavior may be reflected in the particle production during relativistic heavy-ion collisions, if the system crosses the phase boundary. Here it would be worth mentioning that the entropy anomaly may also be a signal of the FFLO state.

6.2 Stability of the DCDW phase against the fluctuation in the presence of the magnetic field

In this section, we calculate the effect of the NG modes by using the low-energy effective potential described by the order parameter in the presence of the magnetic field while the NG mode excitations destroy iCP at the finite T in the absence of the magnetic field [84, 85].

To this end, we introduce an effective potential, which is composed by some low order terms with respect to the order parameter $\Delta(\boldsymbol{x})$, to approximately describe the original effective potential, $V(\Delta(\boldsymbol{x}))$, around the minimum point, $\Delta(\boldsymbol{x}) = \Delta_0(\boldsymbol{x})$. The form of the low-energy effective potential is determined only by the symmetry of the system. In the

following, we consider only the one-flavor case for simplicity. By the symmetry of the NJL model in the presence of the magnetic field, the effective potential renders,

$$\begin{aligned}\tilde{V}(\Delta(\boldsymbol{x})) = {} & \alpha_2|\Delta(\boldsymbol{x})|^2 + \alpha_3 B_i \,\mathrm{Im}[\Delta(\boldsymbol{x})\partial_i\Delta^*(\boldsymbol{x})] + \alpha_{4a}|\Delta(\boldsymbol{x})|^4 + \alpha_{4b}|\partial_i\Delta(\boldsymbol{x})|^2 \\ & + \alpha_{5a} B_i \,\mathrm{Im}[\partial^2\Delta(\boldsymbol{x})\partial_i\Delta^*(\boldsymbol{x})] + \alpha_{5b} B_i \,\mathrm{Im}\big[|\Delta(\boldsymbol{x})|^2\Delta(\boldsymbol{x})\partial_i\Delta^*(\boldsymbol{x})\big] \\ & + \alpha_{6a}|\Delta(\boldsymbol{x})|^6 + \alpha_{6b}|\partial_i\Delta(\boldsymbol{x})|^2|\Delta(\boldsymbol{x})|^2 + \alpha_{6c}\mathrm{Re}[\partial_i\Delta(\boldsymbol{x})\Delta^*(\boldsymbol{x})]^2 + \alpha_{6d}|\partial_i^2\Delta(\boldsymbol{x})|^2,\end{aligned} \tag{6.2.1}$$

up to the sixth-order terms. Here we can not obtain the explicit form of the coefficients but the details of the coefficients are not important in the present analysis. Note that, in the presence of the magnetic field, the form of the odd order terms is restricted as in Eq. (6.2.1) due to the peculiarity of the NJL model (for detail see the Appendix C). In Eq. (6.2.1), we explicitly write the magnetic field dependence in the coefficients of the odd order terms because they should vanish in the absence of the magnetic field. When only the second derivative of the time is considered, the effective Lagrangian takes the form,

$$\mathcal{L} = d_2|\partial_t\Delta(\boldsymbol{x})|^2 - \tilde{V}. \tag{6.2.2}$$

For simplicity, the direction of the magnetic field is taken along the z direction, $\boldsymbol{B} = B\hat{\boldsymbol{z}}$. If we consider DCDW as the ground state, $\Delta_0(\boldsymbol{x}) = me^{iqz}$, where the wave vector $\boldsymbol{q}$ is taken parallel to the magnetic field [45], the effective potential can be written as,

$$\begin{aligned}\tilde{V}(\Delta_0) = {} & \alpha_2 m^2 - \alpha_3 B m^2 q + \alpha_{4a} m^4 + \alpha_{4b} m^2 q^2 + \alpha_{5a} B q^3 m^2 \\ & - \alpha_{5b} B m^4 q + \alpha_{6a} m^6 + \alpha_{6b} m^4 q^2 + \alpha_{6c} m^2 q^4.\end{aligned} \tag{6.2.3}$$

The extremum conditions can be obtained as,

$$\begin{aligned}0 = {} & \frac{\partial\tilde{V}(\Delta_0)}{\partial m} \\ = {} & 2m\big(\alpha_2 - \alpha_3 B q + 2\alpha_{4a} m^2 + \alpha_{4b} q^2 + \alpha_{5a} B q^3 - 2\alpha_{5b} B m^2 q + 3\alpha_{6a} m^4 + 2\alpha_{6b} m^2 q^2 + \alpha_{6c} q^4\big),\end{aligned} \tag{6.2.4}$$

$$\begin{aligned}0 = {} & \frac{\partial\tilde{V}(\Delta_0)}{\partial q} \\ = {} & m^2\big(- \alpha_3 B + 2\alpha_{4b} q + 3\alpha_{5a} B q^2 - \alpha_{5b} B m^2 + 2\alpha_{6b} m^2 q + 4\alpha_{6c} q^3\big).\end{aligned} \tag{6.2.5}$$

Then we introduce the fluctuations $\delta(\boldsymbol{x})$, $\theta(\boldsymbol{x})$ around the ground state. Δ is represented as,

$$\Delta(\boldsymbol{x}) = (m + \delta(\boldsymbol{x}))e^{iqz + i\theta(\boldsymbol{x})}, \tag{6.2.6}$$

including the fluctuations. If the second order terms about the fluctuations are kept, the effective potential renders,

$$\begin{aligned}\tilde{V}(\Delta) = {} & \tilde{V}(\Delta_0) + C_1\delta^2 + 2C_2\delta\partial_z\theta + C_3(\partial_i\theta)^2 + C_4(\partial_i\delta)^2 + C_5\left[(\partial_z\delta)^2 + (\partial_z\theta)^2\right] \\ & + 2C_6\partial_z\delta\partial^2\theta + \alpha_{6c}\left[(\partial_i^2\delta)^2 + (\partial_i^2\theta)^2\right],\end{aligned} \tag{6.2.7}$$

where we redefine as $m\theta(\boldsymbol{x}) \to \theta(\boldsymbol{x})$. By using the extremum conditions (6.2.4), (6.2.5), the coefficients are obtained as,

$$C_1 \equiv 4\alpha_{4a}m^2 - 4\alpha_{5a}Bm^2q + 12\alpha_{6a}m^4 + 4\alpha_{6b}m^2q^2, \tag{6.2.8}$$
$$C_2 \equiv -\alpha_{5b}Bm^2 + 2\alpha_{6b}m^2q, \tag{6.2.9}$$
$$C_3 \equiv \frac{B}{2q}(-\alpha_{5b}Bm^2 + 2\alpha_{6b}m^2q)(\alpha_3 + \alpha_{5a}q^2 + \alpha_{5b}m^2), \tag{6.2.10}$$
$$C_4 \equiv \alpha_{4b} + \alpha_{5a}Bq + \alpha_{6b}m^2 + 4\alpha_{6d}m^2 + 2\alpha_{6c}q^2, \tag{6.2.11}$$
$$C_5 \equiv 2\alpha_{5b}Bq + 4\alpha_{6c}q^2, \tag{6.2.12}$$
$$C_6 \equiv \alpha_{5a}B + 4\alpha_{6c}q. \tag{6.2.13}$$

Furthermore, the equations of motion about the fluctuations, $\frac{\delta\mathcal{V}}{\delta\,\delta(\boldsymbol{x}),\theta(\boldsymbol{x})} = 0$, take the form,

$$-d_2\partial_t^2\delta - C_1\delta - C_2\partial_z\theta + C_4\partial^2\delta + C_5\partial_z^2\delta + C_6\partial^2\partial_z\theta - \alpha_{6c}\partial^4\delta = 0, \tag{6.2.14}$$
$$-d_2\partial_t^2\theta + C_2\partial_z\delta + C_3\partial^2\theta + C_5\partial_z^2\theta - C_6\partial^2\partial_z\delta - \alpha_{6c}\partial^4\theta = 0, \tag{6.2.15}$$

By the Fourier transformation, the equations can be rewritten in the momentum space $(\omega, \boldsymbol{k})$ as,

$$\begin{pmatrix} d_2\omega^2 - C_1 - C_4\boldsymbol{k}^2 - C_5k_z^2 - \alpha_{6c}\boldsymbol{k}^4 & iC_2k_z + iC_6\boldsymbol{k}^2k_z \\ -iC_2k_z - iF\boldsymbol{k}^2k_z & d_2\omega^2 - C_3\boldsymbol{k}^2 - C_5k_z^2 - \alpha_{6c}\boldsymbol{k}^4 \end{pmatrix} \begin{pmatrix} \delta \\ \theta \end{pmatrix} = 0 \tag{6.2.16}$$

When the matrix is diagonalized, two dispersions are obtained as,

$$\omega_1^2 = \frac{1}{d_2}\left[C_1 + C_4\boldsymbol{k}^2 + \left(C_5 + \frac{C_2^2}{C_1}\right)k_z^2 + \mathcal{O}(\boldsymbol{k}^4)\right], \tag{6.2.17}$$
$$\omega_2^2 = \frac{1}{d_2}\left[C_3\boldsymbol{k}^2 + \left(C_5 - \frac{C_2^2}{C_1}\right)k_z^2 + \mathcal{O}(\boldsymbol{k}^4)\right], \tag{6.2.18}$$

where ω_1 represents the massive mode and ω_2 denotes the massless mode. It is the fluctuation of the massless mode to pay attention because the massless mode gives rise to the infrared divergence to destroy the spatial structure of the ground state. In the following, the massless mode (6.2.18) is represented as $u(\boldsymbol{x})$. From the dispersion, the free energy, F, about $u(\boldsymbol{x})$ renders,

$$F = \int d^3\boldsymbol{x}\left\{C_3\left[\nabla u(\boldsymbol{x})\right]^2 + \left(C_5 - \frac{C_2^2}{C_1}\right)\left[\partial_z u(\boldsymbol{x})\right]^2 + \mathcal{O}((\nabla^2 u)^2)\right\}. \tag{6.2.19}$$

Using the free energy, we can evaluate the correlation function of $u(\boldsymbol{x})$ as,

$$\begin{aligned}\langle u(\boldsymbol{x})^2\rangle &\sim \int [\mathcal{D}u]\, u(\boldsymbol{x})^2 e^{-F/T} \\ &\sim T\int_{L^{-1}}^{k_c} \frac{d^3\boldsymbol{k}}{C_3\boldsymbol{k}^2 + \left(C_5 - \frac{C_2^2}{C_1}\right)k_z^2 + \mathcal{O}(\boldsymbol{k}^4)} \\ &\sim T\left[k_c + \mathcal{O}(L^{-1})\right],\end{aligned} \tag{6.2.20}$$

L and k_c denote the length of the system and the ultraviolet cutoff, respectively. In the present case, if we consider the infinite system, $L \to \infty$, the correlation function remains finite and there is no infrared divergence. Therefore, it is found that the DCDW phase is stable against fluctuation. On the other hand, when $B = 0$, we can see that the distribution changes to $\omega_2^2 \sim k_z^2 + \mathcal{O}(k^4)$ for $C = 0$ from Eq. (6.2.10), which corresponds to the dispersion argued in Ref. [84]. In this case, the correlation function is evaluated as,

$$\begin{aligned} \langle u(\boldsymbol{x})^2 \rangle &\sim T \int_{L^{-1}}^{k_c} \frac{d^3\boldsymbol{k}}{k_z^2 + \mathcal{O}(\boldsymbol{k}^4)} \\ &\sim T \ln(k_c L), \end{aligned} \tag{6.2.21}$$

which has a logalithmic divergence for $L \to 0$. Therefore the DCDW phase is unstable against thermal fluctuations. From the above argument, we can conclude that the DCDW phase is stabilized against the fluctuations in the presence of the magnetic field.

Chapter 7

Summary and outlook

In this thesis, we have mainly discussed the various phenomena due to axial anomaly in iCP. In the presence of the magnetic field or in 1+1 dimensions, the energy spectrum may be asymmetric about zero with DCDW and spectral asymmetry gives rise to axial anomaly.

First, we have shown that quark matter has the spontaneous magnetization in the DCDW phase where the response to the external magnetic field changes from the one in the usual SSB ohase or the chiral-restored phase; the term linearly dependent on the magnetic field emerges in the thermodynamic potential. In Ref. [49], they have simply discussed the possibility of the spontaneous magnetization by using the WZW term in the effective meson Lagrangian. However, we have seen that $\Delta\Omega^{(1)}$ has not only the anomalous contribution closely related to the WZW term but also the contribution of valence quarks. In this sense, the fermion degrees of freedom and their dynamics are indispensable. Thus we can say that DCDW provides a realistic ground where the spontaneous magnetization is realized. Furthermore the spontaneous magnetization discussed here has an interesting feature different from the usual spin alignment [94]: the magnetization in the DCDW phase is caused by the different operators from the naive magnetic moment.

We have emphasized that spectral asymmetry is important for the mechanism of the spontaneous magnetization. Since the complex order parameter $\Delta(\boldsymbol{r})$ is necessary for the energy spectrum to be asymmetric [46], it is conceivable that there is no spontaneous magnetization in the RKC phase with the real order parameter $\Delta(\boldsymbol{r})$. On the other hand, the spontaneous magnetization should emerge in the similar way in the phase with hybrid chiral condensate [96].

For the ferromagnetic transition in the DCDW phase, the magnetic susceptibility does not diverge. This behavior is different from the ferromagnetic phase transition in the spin system. Furthermore, we have discussed the possible existence of the massless mode like magnon in the DCDW phase. By counting the number of the independent massless modes in the ground state, we found that there are only pions as the NG modes in this case. The result that the massless mode corresponding to magnon does not appear is also different from the spin system.

Secondly, we have discussed the effect of the finite current mass m_c on iCP at $B \neq 0$. The thermodynamic potential around the phase transition is obtained by the generalized GL

expansion based on the NJL model. It is found that the magnetic field extends the massive DCDW phase over the low density region similar to the DCDW phase in the chiral limit, while m_c tends to reduce this phase. Then, there is the first order phase transition between the massive DCDW phase and the homogeneously broken phase. Furthermore, chiral symmetry is strongly broken in this phase compared to the homogeneously broken phase.

Within our analysis, the magnetic field seems to increase the critical temperature. A mechanism similar to the magnetic catalysis should lead to this behavior. On the other hand, we have adjusted the coupling constant of the NJL model to estimate the qualitative influence of the inverse magnetic catalysis. As a consequence, the critical temperature decreases. However, the massive DCDW phase can develop in the region: $\mu/T < 1$ if m_c is sufficiently small. Therefore we suggest that iCP can be found by the lattice QCD simulations just by choosing some proper method, for example, the reweighting method or the canonical approach. Since there is few work where the local chiral condensate is discussed [156], it is a challenging work to directly confirm the existence of iCP by the lattice QCD simulations.

Thirdly, using the duality relation, we have discussed the roles of axial anomaly and nesting in the context of iCP. We have seen that the NJL_2 model has $U(1)_L \times U(1)_R$ symmetry in the classical level, but symmetry is broken due to axial anomaly in the presence of the gauge field, $U(1)_L \times U(1)_R \to U_V(1)$. Invoking the technique of the fictious gauge field, $B^\mu = (\mu, 0)$, such anomaly effect can be built in the thermodynamic potential in medium as anomalous quark number, which is given by spectral asymmetry of the quark field [46]. The NJL_2 model can be written as another form by way of the duality transformation. New Lagrangian has a suitable form to describe a kind of superconductivity in the presence of the magnetic field, which resembles the FFLO state in the condensed matter physics.

After the duality transformation we have seen a different manifestation of axial anomaly: spectral asymmetry of quasiparticles does not necessarily implies the anomalous number in this case. Instead, anomalous magnetization is generated for the complex order parameter. Existence of magnetization means the different numbers for L- and R-quarks and leads to the different sizes of the Dirac seas. Consequently, the FF state distinctively behaves in the magnetic field due to anomaly, and the phase diagram becomes much different from the one for the FF state in condensed matter physics. It develops, once the magnetic field is applied, i.e., the lower critical field $h_{c1}^{\mathrm{FF}} = 0$. We have confirmed this result by considering an anomaly free-model, two flavor NJL_2 model, where the FF state appears beyond the lower critical field as in condensed matter physics.

Based on these considerations we have discussed how nesting plays in the context of iCP. In the case of the anomaly free model we have first seen that the usual nesting (type-I nesting) works for both chiral spiral and RKC; the wave number becomes $\mathcal{O}(2\mu)$. After the duality transformation we have considered the different type of nesting (type-Ⅱ nesting) in the context of superconductivity. Using the concept of the type-Ⅱ nesting, we have shown that the type-Ⅱ nesting holds for both cases. Interestingly, we have observed an ideal type-Ⅱ nesting for the LO state, where the new phase is brought about by the second order phase transition, and the wave number smoothly increases from the zero value to the maximum value of 2μ. For the NJL_2 model, anomaly modifies these pictures, especially for chiral spiral. Sometimes one may attribute the relation $q = 2\mu$ to the type-I nesting, but we have

emphasized that axial anomaly may be mainly responsible to this relation to conceal the nesting effect: nesting effect should be really appreciated in anomaly-free models.

Besides, we would like to make a comment about a phenomenological perspective of our result. If there is the low dimensional system, where all right(left)-going electrons have up(down) spin, a new type of superconductivity, which corresponds to our FF state and reflects anomaly may be found. If it can be created, we can see the FF state for a tiny magnetic field.

Fourthly, we have discussed the effects of chiral pair fluctuations on the inhomogeneous chiral transition. We have taken into account the non-linear effects of chiral-pair fluctuations in a systematic way beyond the linear approximation. Eventually, we have elucidated the salient roles of quantum and thermal fluctuations separately; the latter is more drastic than the former due to the dimensional reduction, but both lead to the fluctuation-induced first-order phase transition. The curvature parameter τ is renormalized by the fluctuation effects to be positive definite at $T \neq 0$, while for $T = 0$ it is mildly shifted from the one within MFA. Thus, we have observed that the second-order phase transition is prohibited by thermal fluctuations. More importantly, the dangerous diagrams composed of the bubbles of two fluctuation Green's function become essential and change the sign of the fourth-order vertex function for both the $T = 0$ and $T \neq 0$ cases. The sign of the sixth-order vertex function can be shown to be positive definite, and thus we can clearly see the first-order phase transition. These features are brought about by the unique behavior of the dispersion of chiral pair fluctuations, and also common in any inhomogeneous phase transition.

The first derivative of the thermodynamic potential exhibits a singular behavior through the momentum integral, since the dispersion of chiral pair fluctuations has a minimum on the sphere $|\boldsymbol{q}| = q_c$. To figure out such a singular behavior, we have evaluated the number density and entropy density, with the result that the fluctuation-induced first-order phase transition can be characterized by the discontinuity and singular behavior of the first derivatives. It would be worth mentioning that our formalism to treat the non-linear effects of fluctuations may also be applied to other cases, such as the FFLO state in superconductivity; the effect of the Cooper pair fluctuations are composed of the particle-particle ladder diagrams instead, but the dispersion relation has a similar feature discussed here. Accordingly, the entropy anomaly may be a possible evidence for the phase transition.

Furthermore, we have considered the stability the DCDW phase against the fluctuations. While it has been known that the thermal fluctuation induces the logarithmic divergence in the correlation function of the NG modes, we have found that the quantum fluctuation does not give rise to any divergence in that. Therefore, the DCDW phase becomes stable and shows the long range order at $T = 0$. The result also implies that the effect of the thermal fluctuation is severer than the quantum fluctuation due to the dimensional reduction. On the other hand, when the magnetic field is switched on, the dispersion relation of the fluctuation changes and the DCDW phase is stabilized even at finite temperature.

Finally, we would like to present some outlooks of our works. From the phenomenological view, it is important to obtain the phase diagram of quark matter with the finite current quark mass. Since our analysis about the massive DCDW phase works only at high T, we need investigate the growth of the massive DCDW phase at zero or low T to be applied to

quark matter in neutron stars. In particular, in order to explain the strong magnetic field in neutron stars by the mechanism in Chapter 3, it is necessary to study the appearance of the massive DCDW phase in more realistic situations such as under charge neutrality or chemical equilibrium. Besides, it is thought that quark matter including s-quarks may exist with strong magnetic field in neutron stars. If the s-quark condensate is assumed to be homogeneous as in the previous works [42, 157], the analysis in this thesis may be easily extended to the three-flavor system. However, the relevant form and the properties of the inhomogeneous condensate including s-quarks are open questions.

From the theoretical view, it is interesting to analyze the behavior of the vertex functions by solving the flow equations within the renormalization group approach. The renormalization group is somewhat different from the usual treatment due to the existence of the special point q_c in momentum space, but can be formulated in the similar way to the work by Shankar [158] for fermion many-body systems, where the Fermi momentum corresponds to q_c. Since our formalism is very much similar to theirs, it is expected that our findings in Chapter 6 may be confirmed by the renormalization group approach.

Throughout Chapter 6, we have discussed the properties of the R-boundary. As for the L-boundary, it has been shown that it should be of first order in the case of DCDW, while of second order in the case of RKC. Therefore, it would be interesting to apply our argument to the L-boundary of RKC, where the number susceptibility has been suggested to be divergent within the MFA [44].

Lastly, we would like to make some comments in the light of recent development about topological materials, such as Weyl semimetal, in condensed matter physics [159, 160, 161, 162]. We can see that quarks in the DCDW phase exhibit the same dispersion as electrons in the Weyl semimetal [163], which suggests the DCDW phase can be regarded as a Weyl semimetal. For the Weyl semimetal, q is related to the spin polarization of electrons, while that denotes the wave number of the chiral condensate for DCDW. Therefore it is interesting to investigate the similarities between DCDW and the Weyl semimetal. It has been known that there is the anomalous Hall current and the Hall conductivity is approximately proportional to q [163]. Similarly, for DCDW, the Maxwell equations are modified and the anomalous Hall current appears due to axial anomaly [164]. It is expected that, for DCDW, the Hall conductivity has two parts, the anomalous contribution proportional to q and the contribution of valence quarks.

Acknolegement

I would like to thank my supervisor, Toshitaka Tatsumi for useful discussion and great guidance. I also thank to my collaborators, Tong-Gyu Lee and Kazuya Nishiyama in the works included by this thesis. I am grateful for all the member of the nuclear theory group in Kyoto University and Yukawa Institute for Theoretical Physics.

This work is supported by the Grant-in-Aid for JSPS fellows (No.15J01814).

Appendix A

Mermin-Wagner-Coleman theorem

In this appendix, we argue Mermin-Wagner-Coleman (MWC) theorem [151, 152], which claims the relation between SSB of a continuous symmetry and dimension of the system. Generally, if a continuous symmetry is spontaneously broken, the NG modes corresponding to the broken generators appear as low energy excitations. MWC theorem tells that if a symmetry is spontaneously broken in the 1+2 or less dimensional system, the broken phase is not stable against the thermal fluctuations of the NG mode. In other words, the symmetry can not always be broken.

Concretely, we consider the Heisenberg model, which is a model for describing ferromagnetic transition. In the Heisenberg model, the spins with the $O(n)$ symmetry are located on each lattice site separated by the lattice spacing λ. The Hamiltonian renders,

$$H = -J \sum_{\langle i,j \rangle} \sum_{a=1}^{n} \boldsymbol{S}_i^a \cdot \boldsymbol{S}_j^a, \tag{A.0.1}$$

where J denotes the coupling constant and the summation of i and j is taken about the neighboring sites. When the $O(n)$ symmetry is spontaneously broken, the spins are aligned in one direction. In the following, we consider the phase where the spins are aligned in the direction $a = 1$. The ground state is described as $\langle \boldsymbol{S}_0 \rangle = (1, 0, \cdots, 0)$. If the fluctuation of the direction, $\{\sigma_\alpha\}$, is introduced, the spin with the fluctuation takes the form,

$$\boldsymbol{S} = \left(\sqrt{1 - \sum_{\alpha=1}^{n-1} \sigma_\alpha^2}, \{\sigma_\alpha\} \right), \tag{A.0.2}$$

where $\sum_{\alpha=1}^{n-1} \sigma_\alpha^2 \ll 1$ is assumed. Then, the Hamiltonian is expanded as,

$$H = H_0 + \frac{J}{2} \sum_{\langle i,j \rangle} \sum_{\alpha=1}^{n-1} (\sigma_i^\alpha - \sigma_j^\alpha)^2 + \cdots . \tag{A.0.3}$$

If we consider the continuum limit, $a \to 0$ and ignore the constant term, The Hamiltonian is

calculated as,

$$H = \frac{J}{2}\int d^d x \sum_{\alpha=1}^{n-1} (\nabla\sigma^\alpha(x))^2 + \cdots , \tag{A.0.4}$$

where σ^α represent the $n-1$ NG bosons, which appear due to SSB, $O(n) \to O(n-1)$. From the partition function, $Z = e^{-H/T}$, the two-point correlation function in the d dimension can be calculated as,

$$\langle \sigma^\alpha(x)\sigma^\alpha(0)\rangle = \frac{T}{J}\int_0^{1/a} \frac{d^d k}{(2\pi)^d}\frac{e^{i\boldsymbol{k}\cdot\boldsymbol{x}}}{k^2}. \tag{A.0.5}$$

At $T \neq 0$, the correlation function on the same point renders,

$$\langle \sigma_\alpha^2(0)\rangle \sim \int_0^{1/\lambda} dk k^{d-3}. \tag{A.0.6}$$

This result means that the the expectation value of the fluctuation includes the ultraviolet divergence at $d \leq 2$. On the other hand, from Eq. $(A.0.2)$, the expectation value of the spin renders,

$$\langle S^{a=1}\rangle = 1 - \frac{1}{2}\sum_{\alpha=1}^{n-1}\langle\sigma_\alpha^2\rangle + \cdots . \tag{A.0.7}$$

Therefore, the divergence of the second term contradicts the spin alignement. In other words, when the number of spatial dimension is less than two, it is seen that the ordered state is destroyed by the thermal fluctuation. The result can be extended to the case of the general field theory.

Within the 1+3 dimensional NJL model, three pions appear as the NG modes in the two-flavor case when chiral symmetry is spontaneously broken. When the magnetic field is applied, the motion of quarks is limited to one direction. However the important is the number of the dimension where pions can move. The charged pions, $\pi^\pm$, are no longer NG modes because they combine have the effective mass due to the coupling with the magnetic field. On the other hand, the motion of the neutral pion π^0 is not limited due to no interaction with the magnetic field. Therefore it is 1+3 dimensional NG mode. From the above, it turns out that even if the magnetic field is applied in the 1+3 dimensions and the motion of quarks is limited, the chiral symmetry breaking do not conflict with MWC theorem.

Appendix B

Proper time regularization

In this appendix, we explain the way of the proper time regularization (PTR). "Proper time" has been considered by Schwinger for calculating the propagator of the fermion in the presence of the magnetic field [99]. The proper time τ is introduced in the way,

$$\frac{1}{A} = \int_0^\infty d\tau \, \exp\left(-\tau A\right), \tag{B.0.1}$$

where $A > 0$ is assumed. Furthermore, integrating that equation about A, we can obtain the relation,

$$\mathrm{lnA} = \mathrm{lnc} - \int_0^\infty \frac{\mathrm{d}\tau}{\tau} \, \exp\left(-\tau \mathrm{A}\right) + \int_0^\infty \frac{\mathrm{d}\tau}{\tau} \, \exp\left(-\tau \mathrm{c}\right), \tag{B.0.2}$$

where c denotes the arbitrary constant value and the constant terms are irrelevant in most cases. When this prescription is applied to the vacuum part in the thermodynamic potential (2.1.27), it renders

$$\begin{aligned}
\Omega_{\mathrm{vac}} =& - N_f N_c \int \frac{\mathrm{d}^3 p}{(2\pi)^3} \sum_{s=\pm} E_s(\boldsymbol{p}) \\
=& \lim_{\epsilon \to 0} i N_f N_c \int \frac{d^4 p}{(2\pi)^4} \sum_{s=\pm} \ln \left[p_0^2 - \left(E_s(\boldsymbol{p}) + i\epsilon \right)^2 \right] \\
=& \lim_{\epsilon \to 0} -i N_f N_c \int \frac{d^4 p}{(2\pi)^4} \sum_{s=\pm} \int_0^\infty \frac{d\tau}{\tau} e^{i\tau \left[p_0^2 - \left(E_s(\boldsymbol{p}) \right)^2 + i\epsilon \right]} \\
=& N_f N_c \int \frac{d^4 p_E}{(2\pi)^4} \sum_{s=\pm} \int_0^\infty \frac{d\tau}{\tau} e^{\tau \left[-p_0^2 - p_\perp^2 - (\sqrt{p_z^2 + m^2} + sq/2)^2 \right]} \\
=& \frac{N_f N_c}{8\pi^{3/2}} \int \frac{dp_z}{2\pi} \sum_{s=\pm} \int_0^\infty \frac{d\tau}{\tau^{5/2}} e^{-\tau (\sqrt{p_z^2 + m^2} + sq/2)^2}
\end{aligned} \tag{B.0.3}$$

After taking the momentum integral, the ultraviolet divergence appears on $\tau \to 0$. Therefore, introducing the cutoff in the lower limit of τ integral to regularize the divergence, we can

obtained the vacuum part with PTR as,

$$\Omega_{\rm vac} = \frac{N_f N_c}{8\pi^{3/2}} \int \frac{dp_z}{2\pi} \int_{1/\Lambda^2}^{\infty} \frac{d\tau}{\tau^{5/2}} \left[e^{-\tau\left(\sqrt{p_z^2+m^2}+q/2\right)^2} + e^{-\tau\left(\sqrt{p_z^2+m^2}-q/2\right)^2} \right]. \tag{B.0.4}$$

PTR may be appropriate for the regularization in the anisotropic system compared to the three or four momentum cutoff.

Appendix C

Generalized Ginzburg-Landau expansion

In this appendix, the thermodynamic potential is expanded about the order parameter and its derivative with $m_c \neq 0$. We also expand it around the external magnetic field (B) along the z axis, based on Nickel's work [89]. We use the 2-flavor NJL model and the Lagrangian within MFA renders,

$$\mathcal{L}_{\rm MF} = \bar{\psi}[S_B^{-1} - {\rm Re}\tilde{\Delta}(z) - i\gamma^5\tau^3{\rm Im}\tilde{\Delta}(z)]\psi - \frac{|\Delta(z)|^2}{4G}, \tag{C.0.1}$$

with $\tilde{\Delta} \equiv m_c + \Delta(z)$, where $\Delta(z)$ is given in Eq. (4.1.2) and Ω_0 is independent of the order parameters. S_B corresponds to the propagator in the chiral limit,

$$S_B = \frac{1}{i\not{D} + \mu\gamma^0}, \tag{C.0.2}$$

where D_μ represents the covariant derivative, $D_\mu = \partial_\mu + ieA_\mu$. From the Lagrangian, the thermodynamic potential takes the form,

$$\begin{aligned}\Omega(\mu,T,B) &= -\frac{T}{V}{\rm Tr}_{D,c,f,\mathcal{V}}\,{\rm Ln}\left[S_B^{-1} - \left({\rm Re}\tilde{\Delta} + i\gamma^5\tau^3{\rm Im}\tilde{\Delta}\right)\right] + \int\frac{d^3\boldsymbol{x}}{V}\frac{|\Delta|^2}{4G} \\ &= \Omega_0 - \frac{T}{V}\sum_{j\geq 1}\frac{1}{j}{\rm Tr}_{D,c,f,\mathcal{V}}\left[S_B\left({\rm Re}\tilde{\Delta} + i\gamma^5\tau^3{\rm Im}\tilde{\Delta}\right)\right]^j + \int\frac{d^3\boldsymbol{x}}{V}\frac{|\Delta|^2}{4G},\end{aligned} \tag{C.0.3}$$

where the trace is taken about the Dirac space, color, flavor, volume and imaginary time. Then odd j terms always vanish by the Dirac trace. We need the expansion up to the fifth order about $\tilde{\Delta}$ and its derivative to obtain the thermodynamic potential constituted by the terms up to the fourth order about Δ and its derivative and the first order in m_c. The

thermodynamic potential is expanded into the form in $B = 0$ [85],

$$\begin{aligned}\Omega =&\Omega_0 + \int \frac{d^3\boldsymbol{x}}{V}\left\{\frac{\alpha_2}{2}|\tilde{\Delta}|^2 + \frac{\alpha_4}{4}\left[|\tilde{\Delta}|^4 - \mathrm{Re}\left(\tilde{\Delta}\tilde{\Delta}''\right)\right] + \frac{|\Delta|^2}{4G}\right\}\\ =&\Omega_0 + \int \frac{d^3\boldsymbol{x}}{V}\left[\frac{\alpha_2}{2}\left(|\Delta|^2 + 2m_c\mathrm{Re}\Delta\right) + \frac{\alpha_4}{4}\left(|\Delta|^4 + 4m_c|\Delta|^2\mathrm{Re}\Delta + |\Delta'|^2 - m_c\mathrm{Re}\Delta''\right)\right.\\ &\left. + \frac{|\Delta|^2}{4G}\right] + \mathcal{O}(m_c^2), \end{aligned} \tag{C.0.4}$$

with the GL coefficients,

$$\alpha_{2j} = (-1)^j 4N_c N_f T\sum_k \int \frac{d^3\boldsymbol{p}}{(2\pi)^3}\frac{1}{[(\omega_k + i\mu)^2 + \boldsymbol{p}^2]^j}. \tag{C.0.5}$$

Switching on B, the energy spectrum in α_{2j} should change the follows,

$$4N_c N_f \int \frac{d^3\boldsymbol{p}}{(2\pi)^3} \to 2N_c \sum_f \frac{|e_f B|}{2\pi}\sum_n \int \frac{dp_z}{2\pi}(2 - \delta_{n,0}), \tag{C.0.6}$$

$$\boldsymbol{p}^2 \to p_z^2 + 2|e_f B|n, \tag{C.0.7}$$

where n denontes the Landau levels. Furthermore some odd order terms are added from the derivative expansion. The third order term is derived from a part of $j = 2$ in Eq. (C.0.3),

$$\begin{aligned}&-\frac{T}{V}\frac{1}{2}\mathrm{Tr}_{D,c,f,\mathcal{V}}\left[S_B\left(\mathrm{Re}\tilde{\Delta} + i\gamma^5\tau^3\mathrm{Im}\tilde{\Delta}\right)\right]^2\\ \to&-\frac{T}{V}\frac{1}{2}N_c\sum_f\int d^4x d^4x'\mathrm{tr}\big\{[\mathrm{Re}\tilde{\Delta}(x_3) + i\gamma_5\sigma_f\mathrm{Im}\tilde{\Delta}(x_3)]S_B(x,x')\\ &\times[\mathrm{Re}\tilde{\Delta}'(x_3) + i\gamma_5\sigma_f\mathrm{Im}\tilde{\Delta}'(x_3)](x_3' - x_3)S_B(x',x)\big\}\\ =&N_c\sum_f\frac{|e_f B|}{16\pi^3 T}\mathrm{Im}\psi^{(1)}\left(\frac{1}{2} + i\frac{\mu}{2\pi T}\right)\int\frac{d^3\boldsymbol{x}}{V}\mathrm{Im}\left(\tilde{\Delta}^*\tilde{\Delta}'\right)\\ =&\tilde{\alpha}_3\int\frac{d^3\boldsymbol{x}}{V}\left[\mathrm{Im}\left(\Delta^*\Delta'\right) + m_c\mathrm{Im}\Delta'\right], \end{aligned} \tag{C.0.8}$$

with $\sigma_u = +1, \sigma_d = -1$. It is convenient to use S_B in the momentum representation [99, 122].

The fifth order terms are derived from a part of $j=2$ in Eq. (C.0.3),

$$
\begin{aligned}
&-\frac{T}{V}\frac{1}{2}\mathrm{Tr}_{D,c,f,\mathcal{V}}\left[S_B\left(\mathrm{Re}\tilde{\Delta}+i\gamma^5\tau^3\mathrm{Im}\tilde{\Delta}\right)\right]^2\\
\to&-\frac{T}{V}\frac{1}{2}N_c\sum_f\int d^4xd^4x'\mathrm{tr}\Big\{[\mathrm{Re}\tilde{\Delta}(x_3)+i\gamma_5\sigma_f\mathrm{Im}\tilde{\Delta}(x_3)]S_B(x,x')\\
&\times\frac{1}{6}[\mathrm{Re}\tilde{\Delta}'''(x_3)+i\gamma_5\sigma_f\mathrm{Im}\tilde{\Delta}'''(x_3)](x_3'-x_3)^3S_B(x',x)\Big\}\\
=&N_c\sum_f\frac{|e_fB|}{1536\pi^5T^3}\mathrm{Im}\psi^{(3)}\left(\frac{1}{2}+i\frac{\mu}{2\pi T}\right)\int\frac{d^3\boldsymbol{x}}{V}\mathrm{Im}\left(\tilde{\Delta}^*\tilde{\Delta}'''\right)\\
=&\tilde{\alpha}_{4b}\int\frac{d^3\boldsymbol{x}}{V}\mathrm{Im}\Delta'''+\mathcal{O}(\Delta\Delta'''). \qquad \text{(C.0.9)}
\end{aligned}
$$

From a part of $j=4$,

$$
\begin{aligned}
&-\frac{T}{V}\frac{1}{4}\mathrm{Tr}_{D,c,f,\mathcal{V}}\left[S_B\left(\mathrm{Re}\tilde{\Delta}+i\gamma^5\tau^3\mathrm{Im}\tilde{\Delta}\right)\right]^4\\
\to&-\frac{T}{\mathcal{V}}\frac{3}{4}N_c\sum_f\int d^4xd^4x'd^4x''d^4x'''\mathrm{tr}\Big\{[\mathrm{Re}\tilde{\Delta}(x_3)+i\gamma_5\sigma_f\mathrm{Im}\tilde{\Delta}(x_3)]S_B(x,x')\\
&\times[\mathrm{Re}\tilde{\Delta}(x_3)+i\gamma_5\sigma_f\mathrm{Im}\tilde{\Delta}(x_3))]S_B(x',x'')[\mathrm{Re}\tilde{\Delta}(x_3)+i\gamma_5\sigma_f\mathrm{Im}\tilde{\Delta}(x_3)]S_B(x'',x''')\\
&\times[\mathrm{Re}\tilde{\Delta}'(x_3)+i\gamma_5\sigma_f\mathrm{Im}\tilde{\Delta}'(x_3)](x_3'''-x_3)S_B(x''',x)\Big\}. \qquad \text{(C.0.10)}
\end{aligned}
$$

Here we can see that only $|\tilde{\Delta}|^2\mathrm{Im}(\tilde{\Delta}^*\tilde{\Delta}')\sim m_c|\Delta|^2\mathrm{Im}\Delta'+2m_c\mathrm{Re}\Delta\mathrm{Im}(\Delta^*\Delta')$ term survives after taking the Dirac trace and integrating. Therefore this term can be described as,

$$
\tilde{\alpha}_{4a}\int\frac{d^3\boldsymbol{x}}{V}\left[|\Delta|^2\mathrm{Im}\Delta'+2\mathrm{Re}\Delta\mathrm{Im}(\Delta^*\Delta')\right], \qquad \text{(C.0.11)}
$$

where the coefficient is written as $\tilde{\alpha}_{4a}$ for convenience. In summary, the thermodynamic potential takes the form (4.1.4) up to fourth-order.

Appendix D

Consistent UV regularization

We explain the UV cutoff procedure in the calculation of the physical quantities such as quark number density or magnetization. In the free theory without the magnetic field h, the fermion field renders,

$$\chi^{(0)}(x) = \int \frac{dp}{2\pi} e^{ipx} \begin{pmatrix} a_p^{(0)}\theta(p) + b_{-p}^{(0)\dagger}\theta(-p) \\ a_p^{(0)}\theta(-p) - b_{-p}^{(0)\dagger}\theta(p) \end{pmatrix}, \tag{D.0.1}$$

where $a_p^{(0)}(b_p^{(0)})$ denotes the annihilation operator of the (anti-)particle with the energy $E = |p|$. When h is switched on, we define the creation and annihilation operators,

$$\chi(x) = \int \frac{dp}{2\pi} e^{ipx} \begin{pmatrix} a_p\theta(p) + b_{-p}^{\dagger}\theta(-p) \\ a_p\theta(-p) - b_{-p}^{\dagger}\theta(p) \end{pmatrix}, \tag{D.0.2}$$

where $a_p(b_p)$ denotes the annihilation operator of the (anti-)particle with $E = (p-h)\mathrm{sign}(p)$. It seems that the energy spectrum of R(L)-particles and anti-particles is just shifted by $-h(h)$ from no magnetic field case. The h-vacuum $|0\rangle$ is defined by filling all the "negative energy states",

$$a_p|0\rangle = 0 \quad (p > h,\, p < 0), \tag{D.0.3}$$
$$a_p^{\dagger}|0\rangle = 0 \quad (0 < p < h), \tag{D.0.4}$$
$$b_{-p}|0\rangle = 0 \quad (p > h,\, p < 0), \tag{D.0.5}$$
$$b_{-p}^{\dagger}|0\rangle = 0 \quad (0 < p < h). \tag{D.0.6}$$

In this case, the quark number density can be calculated as,

$$\begin{aligned} n_0 &\equiv \frac{1}{2}\int \frac{dx}{L}\langle 0|[\chi^\dagger,\chi]|0\rangle \\ &= \lim_{\Lambda\to\infty}\langle 0|\left[\int_0^\Lambda \frac{dp}{2\pi}\left(a_p^\dagger a_p - \frac{1}{2}\right) - \int_{-\Lambda}^0 \frac{dp}{2\pi}\left(b_{-p}^\dagger b_{-p} - \frac{1}{2}\right)\right. \\ &\quad \left. + \int_{-\Lambda}^0 \frac{dp}{2\pi}\left(a_p^\dagger a_p - \frac{1}{2}\right) - \int_0^\Lambda \frac{dp}{2\pi}\left(b_{-p}^\dagger b_{-p} - \frac{1}{2}\right)\right]|0\rangle \\ &= \lim_{\Lambda\to\infty}\left[\int_0^h \frac{dp}{2\pi}\langle 0|a_p^\dagger a_p|0\rangle - \int_0^h \frac{dp}{2\pi}\langle 0|b_{-p}^\dagger b_{-p}|0\rangle\right] \\ &= 0, \end{aligned} \tag{D.0.7}$$

which means that the number density of R-particles is $\frac{h}{2\pi}$ and that of L-anti-particle is simultaneously produced by just $\frac{h}{2\pi}$ compared to the normal vacuum. Therefore the net quark number density vanishes but magnetization has the finite value, $\frac{h}{\pi}$. It corresponds to the right panel in Fig. 5.2. Furthermore, the momentum cutoff Λ is introduced to regularize the divergence.

Next we consider the quark number density in the FF state. By equating Eq. (D.0.2) with Eq. (5.2.8), the Bogoliubov transformation is obtained as,

$$\alpha_p = \frac{1}{\sqrt{2\epsilon_p}}\begin{cases} a_{p+q/2}\sqrt{\epsilon_p+p} - a_{-p+q/2}^\dagger\sqrt{\epsilon_p-p} & (p>q/2) \\ a_{p+q/2}\sqrt{\epsilon_p+p} + b_{p-q/2}\sqrt{\epsilon_p-p} & (-q/2<p<q/2) \\ b_{-p-q/2}^\dagger\sqrt{\epsilon_p+p} + b_{p-q/2}\sqrt{\epsilon_p-p} & (p<-q/2) \end{cases}, \tag{D.0.8}$$

$$\beta_p = \frac{1}{\sqrt{2\epsilon_p}}\begin{cases} b_{p-q/2}\sqrt{\epsilon_p+p} - b_{-p-q/2}^\dagger\sqrt{\epsilon_p-p} & (p>q/2) \\ a_{-p+q/2}^\dagger\sqrt{\epsilon_p+p} - b_{-p-q/2}^\dagger\sqrt{\epsilon_p-p} & (-q/2<p<q/2) \\ a_{-p+q/2}^\dagger\sqrt{\epsilon_p+p} + a_{p+q/2}\sqrt{\epsilon_p-p} & (p<-q/2) \end{cases}. \tag{D.0.9}$$

Setting $m=0$ in Eq. (5.2.8), it should reproduce the free field theory with h even if q is still finite. Therefore the quark number density in the FF state becomes independent on q and coincides with Eq. (D.0.7) at $m=0$. At $m=0$, the transformation renders,

$$\alpha_p = \begin{cases} a_{p+q/2} & (p>0) \\ b_{p-q/2} & (p<0) \end{cases}, \tag{D.0.10}$$

$$\beta_p = \begin{cases} b_{p-q/2} & (p>q/2) \\ a_{-p+q/2}^\dagger & (0<p<q/2) \\ -b_{-p-q/2}^\dagger & (-q/2<p<0) \\ a_{p+q/2} & (p<-q/2) \end{cases}. \tag{D.0.11}$$

Once we introduce the lower and upper momentum cutoffs independently, $[\Lambda_{\min},\Lambda_{\max}]$, to determine the appropriate one in the FF state, the quark number density renders from

Eq. (5.2.8),

$$
\begin{aligned}
n &\equiv \frac{1}{2}\int \frac{dx}{L}\langle\sigma|[\chi^\dagger,\chi]|\sigma\rangle \\
&= \lim_{\substack{\Lambda_{\max}\to\infty \\ \Lambda_{\min}\to-\infty}} \langle\sigma|\int_{\Lambda_{\min}}^{\Lambda_{\max}} \frac{dp}{2\pi}\left[\left(\alpha_p^\dagger\alpha_p - \alpha_{-p}^\dagger\alpha_{-p}\right)\frac{\epsilon_p+p}{2\epsilon_p} + \left(\beta_p^\dagger\beta_p - \beta_{-p}^\dagger\beta_{-p}\right)\frac{\epsilon_p-p}{2\epsilon_p}\right]|\sigma\rangle.
\end{aligned}
\tag{D.0.12}
$$

Setting $m=0$, the ground state becomes $|0\rangle$ and the quark number density can be calculated as,

$$
\begin{aligned}
n &= \lim_{\substack{\Lambda_{\max}\to\infty \\ \Lambda_{\min}\to-\infty}} \langle 0|\int_{\Lambda_{\min}}^{\Lambda_{\max}} \frac{dp}{2\pi}\left[\left(\alpha_p^\dagger\alpha_p - \alpha_{-p}^\dagger\alpha_{-p}\right)\theta(p) + \left(\beta_p^\dagger\beta_p - \beta_{-p}^\dagger\beta_{-p}\right)\theta(-p)\right]|0\rangle \\
&= \lim_{\substack{\Lambda_{\max}\to\infty \\ \Lambda_{\min}\to-\infty}} \langle 0|\left[\int_0^{\Lambda_{\max}+q/2} \frac{dp}{2\pi}\left(a_p^\dagger a_p - b_{-p}^\dagger b_{-p}\right) + \int_{\Lambda_{\min}+q/2}^{0} \frac{dp}{2\pi}\left(a_p^\dagger a_p - b_{-p}^\dagger b_{-p}\right)\right]|0\rangle,
\end{aligned}
\tag{D.0.13}
$$

where the transformation (D.0.10), (D.0.11) is used. Therefore we can see that quark number density in the FF state reproduces Eq. (D.0.7) at $m=0$ when the momentum cutoff is put to be asymmetric, $\Lambda_{\max}=\Lambda-q/2, \Lambda_{\min}=-\Lambda-q/2$. It can be also confirmed that magnetization is consistently calculated in the same way by using that asymmetric momentum cutoff.

Appendix E

Integrals I_n

We evaluate the integrals I_n by using the proper time formalism,

$$I_n(r) = (-1)^{n-1} T \sum_m \int \frac{d^3\boldsymbol{q}}{(2\pi)^3} \int_0^\infty ds\, s^{n-1} e^{-s\left[r+\gamma\left(|\boldsymbol{q}|^2-q_c^2\right)^2+\alpha|\omega_m|\right]}. \tag{E.0.1}$$

The Matsubara frequency can be summed up as follows:

$$I_n(r) = (-1)^{n-1} T \int \frac{d^3\boldsymbol{q}}{(2\pi)^3} \int_0^\infty ds\, s^{n-1} e^{-s\left[r+\gamma\left(|\boldsymbol{q}|^2-q_c^2\right)^2\right]} \coth(\alpha\pi T s). \tag{E.0.2}$$

If r is sufficiently small, the main contribution to the integral comes from $|\boldsymbol{q}| \sim q_c$. Therefore, the integral can be approximated as

$$\begin{aligned} I_n(r) &\simeq \frac{(-1)^{n-1}T}{4\pi^2} \int_{-\infty}^\infty q^2 dq \int_0^\infty ds\, s^{n-1} \left\{ e^{-s\left[r+4\gamma q_c^2 (q-q_c)^2\right]} + e^{-s\left[r+4\gamma q_c^2 (q+q_c)^2\right]} \right\} \coth(\alpha\pi T s) \\ &= \frac{(-1)^{n-1}T}{2\pi^2} \int_0^\infty ds \left(\frac{1}{2}\sqrt{\frac{\pi}{(4\gamma q_c^2 s)^3}} + \sqrt{\frac{\pi q_c^2}{4\gamma s}} \right) s^{n-1} e^{-sr} \coth(a_1 \pi T s). \end{aligned} \tag{E.0.3}$$

When $n = 1, 2$, the proper time regularization should be introduced because the integrals have an ultraviolet divergence. However, the leading contribution is not affected by the cutoff at $r \sim 0$, except for $n = 1$ at $T = 0$.

Bibliography

[1] Y. Nambu, Preludes In Theoretical Physics , 133 (1966).

[2] D. J. Gross and F. Wilczek, Phys. Rev. Lett. **30**, 1343 (1973).

[3] H. D. Politzer, Phys. Rev. Lett. **30**, 1346 (1973).

[4] K. Fukushima and T. Hatsuda, Rep. Prog. Phys. **74**, 014001 (2011).

[5] M. Gyulassy and L. McLerran, Nucl. Phys. **A750**, 30 (2005).

[6] S. L. Shapiro and S. A. Teukolsky, Black Holes, White Dwarfs and Neutron Stars (Wiley, 1983).

[7] P. Haensel, A. Y. Potekhin, and D. G. Yakovlev, Neutron Stars 1 (Springer, 2007).

[8] P. B. Demorest, T. Pennucci, S. M. Ransom, M. S. E. Roberts, and J. W. T. Hessels, Nature **467**, 1081 (2010).

[9] J. Antoniadis and et al., Science **340**, 6131 (2013).

[10] A. Schmitt, Lect. Notes Phys. **811**, 1 (2010).

[11] N. K. Glendenning, Compact Stars (Springer, 2000).

[12] K. G. Wilson, Phys Rev. **D10**, 2445 (1974).

[13] M. Creutz, Phys. Rev. **D21**, 2308 (1980).

[14] S. Muroya, A. Nakamura, C. Nonaka, and T. Takahashi, Prog. Theor. Phys. **110**, 615 (2003).

[15] F. Karsch, Prog. Theor. Phys. Suppl. **153**, 106 (2004).

[16] Y. Nambu and G. Jona-Lasinio, Phys. Rev. **122**, 345 (1961).

[17] T. Hatsuda and T. Kunihiro, Phys. Rept. **247**, 221 (1994).

[18] S. P. Klevansky, Rev. Mod. Phys. **64**, 649 (1992).

[19] V. V. Skokov, A. Y. Illarinov, and V. D. Toneev, Int. J. Mod. Phys. **A24**, 5925 (2009).

[20] S. A. Olausen and V. M. Kaspi, Astrophys. J. Suppl. **212**, 6 (2014).

[21] C. Thompson and R. C. Duncan, MNRAS **275**, 255 (1995).

[22] H. Suganuma and T. Tatsumi, Ann. Phys. **208**, 470 (1991).

[23] S. P. Klevansky and R. H. Lemmer, Phys. Rev. **D39**, 3478 (1989).

[24] V. Gusynin, V. Miransky, and I. Shovkovy, Nucl. Phys. **B462**, 249 (1996).

[25] G. S. Bali, F. Bruckmann, G. Endrődi, Z. Fodor, S. D. Katz, and A. Schäfer, Phys. Rev. **D86**, 071502 (2012).

[26] K. Fukushima and Y. Hidaka, Phys. Rev. Lett. **110**, 031601 (2013).

[27] K. Fukushima, D. E. Kharzeev, and H. J. Warringa, Phys. Rev. **D78**, 074033 (2008).

[28] D. Nickel, Phys. Rev. **D80**, 074025 (2009).

[29] E. Nakano and T. Tatsumi, Phys. Rev. **D71**, 114006 (2005).

[30] G. Basar, G. V. Dunne, and M. Thies, Phys. Rev. **D79**, 105012 (2009).

[31] M. Buballa and S. Carignano, Prog. Part. Nucl. Phys. **81**, 39 (2015).

[32] D. Muller, M. Buballa, and J. Wambach, Phys. Lett. **B727**, 240 (2013).

[33] A. W. Overhauser, Phys. Rev. **128**, 1437 (1962).

[34] G. Grüner, Rev. Mod. Phys. **60**, 1129 (1988).

[35] G. Gruner, Rev. Mod. Phys. **66**, 1 (1994).

[36] P. Fulde and R. A. Ferrell, Phys. Rev. **A135**, 550 (1964).

[37] A. I. Larkin and Y. N. Ovchinnikov, Zh. Eksp. Teor. Fiz. **47**, 1136 (1964).

[38] H. Shimahara, Phys. Rev. **B50**, 12760 (1994).

[39] D. Nickel and M. Buballa, Phys. Rev. **D79**, 054009 (2009).

[40] T. Kojo, Y. Hidaka, L. McLerran, and R. D. Pisarski, Nucl. Phys. **A843**, 37 (2010).

[41] S. Karasawa and T. Tatsumi, Phys. Rev. **D92**, 116004 (2015).

[42] J. Moreira, B. Hiller, W. Broniowski, A. A. Osipov, and A. H. Blin, Phys. Rev. **D89**, 036009 (2014).

[43] D. Ebert, N. V. Gubina, K. G. Klimenko, S. G. Kurbanov, and V. C. Zhukovsky, Phys. Rev. **D84**, 025004 (2011).

[44] S. Carignano, D. Nickel, and M. Buballa, Phys. Rev. **D82**, 054009 (2010).

[45] I. E. Frolov, V. C. Zhukovsky, and K. G. Klimenko, Phys. Rev. **D82**, 076002 (2010).

[46] T. Tatsumi, K. Nishiyama, and S. Karasawa, Phys. Lett. **B743**, 66 (2015).

[47] A. J. Niemi and G. W. Semenoff, Phys. Rep. **135**, 99 (1986).

[48] A. J. Niemi, Ndcl. Phys. **B251**, 155 (1985).

[49] D. T. Son and M. A. Stephanov, Phys. Rev. **D77**, 014021 (2008).

[50] M. Eto, K. Hashimoto, and T. Hatsuda, Phys. Rev. **D88**, 081701 (2013).

[51] R. Yoshiike, K. Nishiyama, and T. Tatsumi, Phys. Lett. **B751**, 123 (2015).

[52] C. Allton, M. Doring, S. Ejiri, S. Hands, O. Kaczmarek, and et al., Phys. Rev. **D71**, 054508 (2005).

[53] R. V. Gavai and S. Gupta, Phys. Rev. **D78**, 114503 (2008).

[54] Z. Fodor and S. Katz, Phys. Lett. **B534**, 87 (2002).

[55] Z. Fodor, S. Katz, and K. Szabo, Phys. Lett. **B568**, 73 (2003).

[56] Z. Fodor and S. Katz, JHEP **0203**, 014 (2002).

[57] Z. Fodor and S. Katz, JHEP **0404**, 050 (2004).

[58] A. Alexandru, M. Faber, I. Horvath, and K.-F. Liu, Phys.Rev. **D72**, 114513 (2005).

[59] S. Kratochvila and P. de Forcrand, Phys.Rev. **D73**, 114512 (2006).

[60] P. de Forcrand and S. Kratochvila, Nucl.Phys.Proc.Suppl. **153**, 62 (2006).

[61] A. Li, A. Alexandru, K.-F. Liu, and X. Meng, Phys. Rev. **D82**, 054502 (2010).

[62] I. Barbour and A. Bell, Nucl.Phys. **B372**, 385 (1992).

[63] A. Nakamura and K. Nagata, PTEP **2016**, 033D01 (2016).

[64] K. Nagata, K. Kashiwa, A. Nakamura, and S. M. Nishigaki, Phys. Rev. **D91**, 094507 (2015).

[65] P. de Forcrand and O. Philipsen, Nucl.Phys. **B642**, 290 (2002).

[66] P. de Forcrand and O. Philipsen, Nucl.Phys. **B673**, 170 (2003).

[67] M. D'Elia and M.-P. Lombardo, Phys.Rev. **D67**, 014505 (2003).

[68] M. D'Elia and M. P. Lombardo, Phys.Rev. **D70**, 074509 (2004).

[69] H.-S. Chen and X.-Q. Luo, Phys.Rev. **D72**, 034504 (2005).

[70] Y.-S. W. G. Parisi, Sci. Sin. **24**, 483 (1981).

[71] G. Parisi, Phys. Lett. **B131**, 393 (1983).

[72] G. Aarts, E. Seiler, and I.-O. Stamatescu, Phys. Rev. D **81**, 054508 (2010).

[73] E. Witten, AMS/IP Stud. Adv. Math. **50**, 347 (2011).

[74] M. Cristoforetti, F. Di Renzo, and L. Scorzato (AuroraScience Collaboration), Phys. Rev. D **86**, 074506 (2012).

[75] H. Fujii, D. Honda, M. Kato, Y. Kikukawa, S. Komatsu, and et al., JHEP **1310**, 147 (2002).

[76] R. Yoshiike and T. Tatsumi, Phys. Rev. **D92**, 116009 (2015).

[77] M. Thies, Phys. Rev. **D68**, 047703 (2003).

[78] M. Thies, J. Phys. **A39**, 12707 (2006).

[79] D. Saint-James, G. Sarma, and E. Thomas, Type II Superconductivity (Elsevier, 1969).

[80] Y. Liao and et al., Nature **467**, 567 (2010).

[81] R. Casalbuoni and G. Nardulli, Rev. Mod. Phys. **76**, 263 (2004).

[82] H. Mayaffre and et al., Nat. Phys. **10**, 926 (2014).

[83] R. Yoshiike and T. Tatsumi, (2017), arXiv:1711.11425 [hep-ph] .

[84] T.-G. Lee, E. Nakano, Y. Tsue, T. Tatsumi, and B. Friman, Phys. Rev. **D92**, 034024 (2015).

[85] Y. Hidaka, K. Kamikado, T. Kanazawa, and T. Noumi, Phys. Rev. **D92**, 034003 (2015).

[86] S. A. Brazovskii, Sov. Phys. JETP **41**, 85 (1975).

[87] A. M. Dyugaev, Sov. Phys. JETP Lett. **22**, 83 (1975).

[88] S. Karasawa, T.-G. Lee, and T. Tatsumi, Prog. Theor. Exp. Phys. **2016**, 043D02 (2016).

[89] D. Nickel, Phys. Rev. Lett. **103**, 072301 (2009).

[90] G. Basar and G. V. Dunne, Phys. Rev. **D78**, 065022 (2008).

[91] P. G. de Gennes, Superconductivity of Metals and Alloys (Addison-Wesley, 1989).

[92] I. Kosztin, S. Kos, M. Stone, and A. J. Leggett, Phys. Rev. **B58**, 9365 (1999).

[93] R. E. Peierls, Quantum Theory of Solids (Clarendon Press, 1955).

[94] T. Tatsumi, Phys. Lett. **B489**, 280 (2000).

[95] W. J. de Haas and P. M. van Alphen, Proc. Am. Acad. Arts Sci. **33**, 1106 (1936).

[96] K. Nishiyama, S. Karasawa, and T. Tatsumi, Phys. Rev. **D92**, 036008 (2015).

[97] J. Goldstone and R. L. Jaffe, Phys. Rev. Lett. **51**, 1518 (1983).

[98] P. J. Mulders, Phys. Rev. **D30**, 1073 (1984).

[99] J. Schwinger, Phys. Rev. **82**, 664 (1951).

[100] S. Scherer and M. R. Schindler, A Primer for Chiral Perturbation Theory (Springer, 2011).

[101] J. Wess and B. Zumino, Phys. Lett. **B37**, 95 (1971).

[102] E. Witten, Nucl. Phys. **B223**, 422 (1983).

[103] J. F. Donohue, E. Golowich, and B. R. Holstein, Dynamics of the Standard Model (Cambridge Universiry Press, 1992).

[104] J. Goldstone and F. Wilczek, Phys. Rev. Lett. **47**, 986 (1981).

[105] H. Nielsen and V. Soni, Phys. Lett. **B726**, 41 (2013).

[106] J. W. Negele and H. Orland, Quantum Many-Particle System (Addison Wesley, 1988).

[107] T. Holstein and H. Primakoff, Phys. Rev. **58**, 1098 (1940).

[108] I. Low and A. V. Manohar, Phys. Rev. Lett. **88**, 101602 (2002).

[109] H. Watanabe and H. Murayama, Phys. Rev. Lett. **110**, 181601 (2013).

[110] T. Hayata and Y. Hidaka, Phys. Rev. **D91**, 056006 (2015).

[111] O. Schnetz, M. Thies, and K. Urlichs, Ann. Phys. **321**, 2604 (2006).

[112] S. Maedan, Prog. Theor. Phys. **123**, 285 (2010).

[113] M. Ferreira, P. Costa, O. Lourenço, T. Frederico, and C. Providência, Phys. Rev. **D89**, 116011 (2014).

[114] G. Endrodi, JHEP **1507**, 173 (2015).

[115] K. Kashiwa, T.-G. Lee, K. Nishiyama, and R. Yoshiike, (2015), arXiv:1507.08382 [hep-ph] .

[116] J. B. Kogut, D. K. Sinclair, S. J. Hands, and S. E. Morrison, Phys. Rev. **D64**, 094505 (2001).

[117] A. Migdal, Rev. Mod. Phys. **50**, 107 (1978).

[118] K. Ohwa, Phys. Rev. **D65**, 085040 (2002).

[119] D. Ebert and K. Klimenko, Phys. Rev. **D80**, 125013 (2009).

[120] M. Thies, Phys. Rev. **D93**, 085024 (2016).

[121] R. Yoshiike, T.-G. Lee, and T. Tatsumi, Phys. Rev. **D95**, 074010 (2017).

[122] A. Chodos, K. Everding, and D. A. Owen, Phys. Rev. **D42**, 2881 (1990).

[123] M. Tinkham, Introduction to superconductivity (McGraw-Hill Inc., 1996).

[124] K. Machida and H. Nakanishi, Phys. Rev. **B30**, 122 (1984).

[125] G. Gruner, Density Waves in Solids (Addison-Wesley, 1999).

[126] M. Thies and K. Urlichs, Phys. Rev. **D67**, 125015 (2003).

[127] D. Thouless, Ann. Phys. **10**, 553 (1960).

[128] P. Noziéres, S. Schmitt-Rink, and J. Low, Temp. Phys. **59**, 195 (1985).

[129] Y. Ohashi, J. Phys. Soc. Jpn. **71**, 2625 (2002).

[130] D. Gross and A. Neveu, Phys. Rev. **D10**, 3235 (1974).

[131] L. D. Landau and E. M. Lifshitz, Statistical Physics (Clarendon Press, 1968).

[132] S. Carignano, M. Buballa, and B.-J. Schaefer, Phys. Rev. **D90**, 014033 (2014).

[133] S. Carignano, M. Buballa, and W. Elkamhawy, Phys. Rev. **D94**, 034023 (2016).

[134] P. Adhikari, J. O. Andersen, and P. Kneschke, Phys. Rev. **D96**, 016013 (2017).

[135] J. P. Carlomagno, D. G. Dumm, and N. N. Scoccola, Phys. Rev. **D92**, 056007 (2015).

[136] A. B. Migdal, E. E. Saperstein, M. A. Troitsky, and D. N. Voskresensky, Phys. Rep. **192**, 179 (1990).

[137] P. C. Hohenberg and J. B. Swift, Phys. Rev. **E52**, 1828 (1995).

[138] G. H. Fredrickson and K. Binder, J. Chem. Phys. **91**, 7265 (1989).

[139] A. G. Y. Ohashi, Phys. Rev. Lett. **89**, 130402 (2013).

[140] V. M. Loktev, R. M. Quick, and S. G. Sharapov, Phys. Rep. **349**, 1 (2001).

[141] M. Kitazawa, T. Koide, T. Kunihiro, and Y. Nemoto, Phys. Rev. **D65**, 091504 (2002).

[142] D. D. Ling, B. Friman, and G. Grinstein, Phys. Rev. **B24**, 2718 (1981).

[143] L. Leibler, Macromolecules **13**, 1602 (1980).

[144] F. S. Bates, J. H. Rosedale, and G. H. Fredrickson, J. Chem. Phys. **92**, 6255 (1990).

[145] B. I. Halperin, T. C. Lubensky, and S. Ma, Phys. Rev. Lett. **32**, 292 (1974).

[146] P. Bak, S. Krinsky, and D. Mukamel, Phys. Rev. Lett. **36**, 52 (1976).

[147] K. Binder, Rep. Prog. Phys. **50**, 783 (1997).

[148] M. Janoschek, M. Garst, A. Bauer, P. Krautscheid, R. Georgii, P. Böni, and C. Pfleiderer, Phys. Rev. **B87**, 134407 (2013).

[149] A. A. Abrikosov, L. P. Gorkov, and I. E. Dzyaloshinskii, Methods of Quantum Field Theory in Statistical Physics (Prentice-Hall, Inc., 1963).

[150] A. L. Fetter and J. L. Walecka, Quantum Theory of Many-Particle Systems (McGraw-Hill, 1971).

[151] S. Coleman, Commun. math. Phys. **31**, 259 (1973).

[152] N. D. Mermin and H. Wagner, Phys. Rev. Lett. **17**, 1133 (1966).

[153] X.-G. Wen, Quantum Field Theory of Many-Body Systems (Oxford University Press, 2004).

[154] L. Radzihovsky, Phys. Rev. **A84**, 023611 (2011).

[155] H. Fujii and M. Ohtani, Phys. Rev. **D70**, 014016 (2004).

[156] T. Iritani, G. Cossu, and S. Hashimoto, Phys. Rev. **D91**, 094501 (2015).

[157] S. Carignano, E. J. Ferrer, V. de la Incera, and L. Paulucci, Phys. Rev. **D92**, 105018 (2015).

[158] R. Shankar, Rev. Mod. Phys. **66**, 129 (1994).

[159] S. Murakami, New Journal of Physics **9**, 356 (2007).

[160] X. Wan, A. M. Turner, A. Vishwanath, and S. Y. Savrasov, Phys. Rev. B **83**, 205101 (2011).

[161] K.-Y. Yang, Y.-M. Lu, and Y. Ran, Phys. Rev. B **84**, 075129 (2011).

[162] A. A. Burkov and L. Balents, Phys. Rev. Lett. **107**, 127205 (2011).

[163] D. Kurebayashi and K. Nomura, J. Phys. Soc. Jpn. **83**, 063709 (2014).

[164] E. J. Ferrer and V. de la Incera, Phys. Lett. **B769**, 208 (2017).